NUREG/CR-2821
ANL-82-66

NUREG/CR-2821
ANL-82-66

EBR-II IN-VESSEL NATURAL-CIRCULATION ANALYSIS

by

W. L. Baumann, H. M. Domanus, D. Mohr,
W. T. Sha, R. C. Schmitt, and J. E. Sullivan

ARGONNE
NATIONAL
LABORATORY

MASTER

ARGONNE NATIONAL LABORATORY, ARGONNE, ILLINOIS

Prepared for the Office of Nuclear Regulatory Research
U. S. NUCLEAR REGULATORY COMMISSION
under Interagency Agreement DOE 40-550-75

The facilities of Argonne National Laboratory are owned by the United States Government. Under the terms of a contract (W-31-109-Eng-38) among the U. S. Department of Energy, Argonne Universities Association and The University of Chicago, the University employs the staff and operates the Laboratory in accordance with policies and programs formulated, approved and reviewed by the Association.

MEMBERS OF ARGONNE UNIVERSITIES ASSOCIATION

The University of Arizona
Carnegie-Mellon University
Case Western Reserve University
The University of Chicago
University of Cincinnati
Illinois Institute of Technology
University of Illinois
Indiana University
The University of Iowa
Iowa State University
The University of Kansas
Kansas State University
Loyola University of Chicago
Marquette University
The University of Michigan
Michigan State University
University of Minnesota
University of Missouri
Northwestern University
University of Notre Dame
The Ohio State University
Ohio University
The Pennsylvania State University
Purdue University
Saint Louis University
Southern Illinois University
The University of Texas at Austin
Washington University
Wayne State University
The University of Wisconsin-Madison

Available from

GPO Sales Program
Division of Technical Information and Document Control
U. S. Nuclear Regulatory Commission
Washington, D.C. 20555

and

National Technical Information Service
Springfield, Virginia 22161

NUREG/CR-2821
ANL-82-66

(Distribution
Code: R7)

NUREG/CR--2821

DE83 005150

ARGONNE NATIONAL LABORATORY
9700 South Cass Avenue
Argonne, Illinois 60439

EBR-II IN-VESSEL NATURAL-CIRCULATION ANALYSIS

by

W. L. Baumann,* H. M. Domanus, D. Mohr, W. T. Sha,
R. C. Schmitt, and J. E. Sullivan

Components Technology Division

September 1982

Prepared for the

U. S. NUCLEAR REGULATORY COMMISSION
Office of Nuclear Regulatory Research
Washington, D.C. 20555

under Interagency Agreement DOE 40-550-75

NRC FIN No. A2045

*Visiting Scientist from KFK, West Germany

EBR-II IN-VESSEL NATURAL-CIRCULATION ANALYSIS

by

W. L. Baumann, H. M. Domanus, D. Mohr, W. T. Sha,
R. C. Schmitt, and J. E. Sullivan

ABSTRACT

The in-vessel thermal-hydraulic analysis of the EBR-II Pool Reactor for Transient Test No. 10, Phase 2, has been performed using the COMMIX-1A computer code. The analysis includes all reactor components inside the reactor vessel.

COMMIX-1A employs the porous-media formulation in which the concepts of volume porosity, surface permeability, and distributed resistance and heat source are used to model the internal structures. The governing equations of conservation of mass, momentum, and energy are solved as a boundary problem in space and as an initial-value problem in time.

This report presents the steady-state and transient in-vessel thermal-hydraulic results of the EBR-II natural-circulation simulation. Comparisons show close agreement between computational and experimental data. The phenomenon of reversed flow in the low-pressure plenum, which was observed during the EBR-II transient test, is confirmed by the simulation.

FIN No. A2045 — Title: 3-D Time-dependent Code Development

TABLE OF CONTENTS

LIST OF FIGURES

LIST OF FIGURES (CONTD.)

LIST OF FIGURES (CONTD.)

EXECUTIVE SUMMARY

A two-dimensional in-vessel thermal-hydraulic simulation of the EBR-II Pool Reactor Transient Test No. 10, Phase 2, has been performed using the implicit formulation of the COMMIX-1A computer code. This simulation includes all reactor components inside the reactor vessel. The test was initiated under reactor shut-down conditions, and consists of a severe flow and a minor power transient.

The geometry of the EBR-II components, including subassemblies, two lower plena, an upper plenum, and inlet and outlet pipes, was modeled in detail on the basis of volume porosity and surface permeability. Resistances due to the presence of structures and thermal interactions between coolant and structures are explicitly taken into account in the analysis.

The computational results presented here are steady-state and a 200-s transient. Comparisons of transient temperatures and flow measurements show a close agreement between the simulation and the experiment. The phenomenon of reversed flow in the low-pressure plenum, which was observed during the EBR-II transient test, is confirmed by the simulation. Further numerical investigations indicate that this reversed flow is caused by a buoyancy effect within the core region.

1. INTRODUCTION

This report describes the steady-state and transient in-vessel thermal-hydraulic simulation of the EBR-II* Pool Reactor for Transient Test No. 10, Phase 2, which was carried out at the EBR-II Project, Idaho Falls, Idaho.[1] The test was initiated under reactor shut-down conditions, the power level being about 1.5% of nominal power generation. During the test, the flow was reduced from 100% nominal value to less than 1% within 45 s, whereas the power slowly decreased due to fission-product decay. Experimental measurements, including flow and temperature data at various locations, were taken to verify and understand the transient system behavior.[2]

2. EXPERIMENTAL BACKGROUND

The test was done in an effort to verify that natural circulation in the reactor is capable of removing fission-product-decay heat following a complete loss of primary pumping power, which is of great importance in safety and licensing of liquid-metal fast breeder reactors (LMFBRs). In the course of the investigation, reversed flow in the low pressure plenum was observed.[2]

Sodium mass flow was always entering the reactor inlet pipes, which branch out into high- and low-pressure pipes. These pipes are feeding into the high-pressure plenum and driver zone, and into the low-pressure plenum, reflector, and blanket zones (Fig. 1). During a certain time of the experiment, it was observed that the flow was entering only the high-pressure plenum (HPP) and passing the driver subassemblies (Fig. 2). On the low pressure side, a stagnating or even reversed flow was observed, from the outer rows of subassemblies returning to the low-pressure plenum (LPP), moving back to the pipe junction and feeding into the HPP. The phenomenon of reversed flow observed in this experiment is somewhat surprising, but it is not completely unexpected.

Since the reactor core consists of three main regions, i.e., driver, reflector, and blanket, each region having a different power level, hydraulic resistance, and heat capacity, the local flow stagnation, flow reversal, or flow recirculation occurring in any part of these regions is possible.

Previous calculations employing a one-dimensional model indicated that the flow reversal in the blanket region is primarily caused by thermal-buoyancy forces. To provide more insight into this problem a two-dimensional simulation of the experiment using the COMMIX-1A computer code was performed.[3,4]

3. MODELING

With regard to the complexity of the EBR-II reactor (Fig. 3) and to the long transient time, efforts were made to create a computer-cost effective numerical model. This model will not lose details that are considered to be essential for the simulation.

---

*Experimental Breeder Reactor No. II

3.1 Geometry

3.1.1 Grid Arrangement

In the sense of saving computer running time, a two-dimensional approach was taken using a grid system of 24 axial x 14 radial cells (Fig. 4), the azimuthal section corresponding to 1/16th of the total circumference.

3.1.2 Components

The main components to be modeled are the subassemblies including driver, reflector and blanket region, the lower plena (HPP and LPP), the upper plenum, and the inlet and outlet pipes.

3.1.2.1 Subassemblies

In total, the EBR-II reactor consists of 127 driver, 144 reflector, and 366 blanket subassemblies; control and safety rods are not being taken into consideration (Fig. 4). The center subassembly and the six adjacent rods of the driver region were lumped together into one radial grid element. The remaining five rows of driver subassemblies were modeled using one radial grid element for each.

The reflector and blanket regions with three and six rows of rods, respectively, were modeled using two radial grid elements for each zone (Fig. 4).

Detailed axial subassembly flow cross sections were modeled by using the appropriate porosities and permeabilities in different axial levels (Fig. 5, App. A.6).

3.1.2.2 Lower Plena and Inlet

The geometry of the EBR-II lower plena is very complicated because high- and low-pressure mass flows enter separate lower plena in the radial direction and flow through a mixing region before entering the subassemblies, however, remaining separated by adapter tubes (Fig. 6).

Modeling this complex geometry in two dimensions according to its physical design would not have been possible. Therefore, the geometry for numerical simulation was set up in a slightly different way. The inlet mass flow was changed from the -R to the +R direction, allowing high-pressure flow to enter the HPP, and low-pressure flow to pass into the LPP, without having to model the high pressure piping that passes through the LPP (Fig. 4). The various baffles and grid plates of the HPP and LPP were taken into account using the appropriate values of volume porosity and surface permeability within the numerical model (Figs. 5 and 6). To tune mass flow and velocities, inlet surface areas and inlet cell volumes were adjusted to the physical cross-sections of HPP and LPP inlet pipes (Fig. 5 and 6). A junction between high- and low-pressure flow was established at the boundary between the two inlet cells representing the throttle valve between the high-pressure and low-pressure piping which connects the primary pump and the inlet plena. This provides the possiblity of flow redistribution within the configuration.

3.1.2.3 Upper Plenum and Outlet

The main features of the upper plenum that affect flow and flow velocities are the top end fixtures of the subassemblies pointing into the upper plenum, the finger holders to keep HPP subassemblies in place, and the flow-distribution baffle (skirt), which is designed to eliminate the effect of asymmetric flow conditions being induced by the outlet pipe. Both top end fixtures and finger holders were modeled by setting the equivalent volume porosities (not shown in Fig. 5). In the flow-distribution-baffle, an averaged permeability of the total circumference was used for the simulation. The surface areas and volumes of the outlet cells were adjusted to the physical outlet pipe cross sections and to the mass flow of the 1/16th size of the model.

3.2 Structures

Both the resistance due to the presence of structure and the thermal interactions between coolant and structures were modeled and have a profound effect on the system behavior. For simplicity, these two effects are denoted as force structures and thermal structures.

3.2.1 Force Structures

The coolant mass flow of the EBR-II reactor, which is separated into high- and low-pressure flow, is based on the pressure-drop scheme shown in Fig. 7. These pressures and pressure drops were verified in the numerical model using the equations presented below.

Axial Direction, Subassemblies:

$$F = K \times Re^{-m}, \tag{1}$$

where F is the friction factor, Re is the Reynolds number based on the hydraulic diameter, and K and m have the following values:[5]

	K	m
Driver	0.1922	0.072
Reflector	6.48	0.03
Blanket	2.574	0.269
Driver Re < 557.5	26.33	0.85

Pressure Loss at Baffles:

$$\Delta P = \frac{1}{2} \rho \, w^2 \cdot \zeta, \tag{2}$$

where ρ is the fluid density, w is the velocity normal to the baffle, and ζ is the loss coefficient

$$\zeta = \varepsilon(\varepsilon - 1)^2 \times 7, \tag{3}$$

based on the average permeability of the baffle:

$$\varepsilon = 1 - \text{avg. permeability} \tag{4}$$

Equation 3 is a modified correlation originally developed from measurements in rod bundles with grid spacers.[6] This modification was done because COMMIX uses the local velocity instead of the undisturbed flow velocity which was used to evaluate the original equation.

Inlet of HPP[5]

$$\zeta = \frac{61.75}{Re^{0.2}}. \tag{5}$$

Inlet of LPP[5]

$$\zeta = 27.0. \tag{6}$$

Transverse Direction:

Flow resistance in the transverse direction caused by the lower adapter tubes in the HPP, and by the finger holders and top end fixtures in the upper plenum, was simulated using

$$F = \frac{180}{Re}, \qquad Re \leq 202.5, \tag{7}$$

for laminar flow, and

$$F = \frac{1.92}{Re^{.145}}, \qquad Re > 202.5, \tag{8}$$

for turbulent flow.[7]

3.2.2 Thermal Structures

To account for the interaction between coolant flow and solid structures (especially during a transient), so-called thermal structures were introduced into the simulation. Thermal structures are cylindrical elements dimensioned to have the same volumes and surface areas as the simulated solid structures. A total of 32 thermal structures were used to model density, heat capacity, and heat conductivity of the EBR-II subassemblies including driver fuel, blanket fuel, cladding, and shroud. For each of the radial grid elements of the subassembly regions, two thermal structures representing pins and shrouds were used. The core zone, however, was modeled separately. The subassembly regions were the driver (Fig. 8), reflector (Fig. 9), and blanket zone (Fig. 10). The properties used for modeling the thermal structures are

listed in Fig. 11.

The power and local power distribution are simulated by using volumetric heat sources, which are given in Appendices A.4 and A.5.

The axial power shapes of driver, reflector, and blanket regions are not identical with each other (Appendix A5). The power shape of the driver region was used to calculate the normalized axial power distribution QK (Appendix A5). The factor QK is obtained from the equation

$$QK = \frac{Q_{dloc}}{Q_{dtot}} \times \frac{L}{DZ}, \tag{9}$$

where

Q_{dloc} = local power-generation rate in one node of the driver region,

Q_{dtot} = total power of the driver region,

L = total length of the subassemblies = 1.6695 ,

and

DZ = local node length in the axial direction.

The following equations were used to model thermal structure heat transfer:

$$h = 10{,}000 \frac{W}{m^2K} \tag{10}$$

accounting for the interaction in the gap between fuel and cladding,[8] and

$$Nu = 4.5 + 0.0052 \times Re^{0.3}, \tag{11}$$

which is a modified equation accounting for the interaction between subassemblies and coolant.[9] Here, h is the heat-transfer coefficient, Nu is the Nusselt number, and Re is the Reynolds number based on the hydraulic-flow channel diameter.

3.3 Operating Conditions

3.3.1 Steady State

The EBR-II Natural Circulation Test No. 10, Phase 2, was initiated under reactor shut-down conditions, the total decay power level being about 1.5% of nominal power generation. The power distribution within each of the radial subassembly regions, driver, reflector, and blanket, respectively, was specified at an appropriate value and assumed to be uniform over each region. The operating conditions at the beginning of the test (steady state) are presented in Appendix A.2; a detailed pressure drop scheme for the initial test values is shown in Fig. 7.

3.3.2 Transient

Two transient functions were used for the simulation, a flow transient providing the total reactor inlet mass flow, and a power transient providing the total reactor power generation (Fig. 12). During the transient calculation, inlet temperature and outlet pressure were kept constant.

4. SOLUTION PROCEDURE

The simulation was performed using COMMIX-1A, Version 8.0, with the capability of a new implemented implicit formulation. COMMIX-1A is a steady/unsteady, three-dimensional single-phase computer code developed for thermal-hydraulic analysis of reactor components.[3,4] The solution procedure is a cell-by-cell iterative procedure with mass rebalancing (Fig. 13). The conservation equations of mass, momentum, and energy were solved as a boundary-value problem in space, and as an initial-value problem in time. The forward marching in time was continued until an asymptotic steady-state solution was obtained, i.e., when maximum local changes in velocity and temperature fields are less than the present convergence criterion (1.E-5). The computer running time to achieve steady state was 43 s. The transient calculation using the implicit formulation was carried on up to 200 s of transient time, the time-step size being 2s. The computer time to complete the transient calculation was 57 min.

5. RESULTS

5.1 Steady-State Solution

The steady-state results of the simulation are shown in the form of a velocity vector and an isotherm plot (Figs. 14 and 15). As can be seen from Fig. 14, both inlet vectors are pointing in a horizontal direction, which means that the mass flow splits off correctly according to the boundary conditions. The flow velocity within the driver region is observed to be much higher than within the reflector and blanket subassemblies, and there is flow recirculation in the upper plenum. The isotherm plot (Fig. 15) shows that the highest temperature rise is in the reflector subassemblies, a fact that had been expected from analyzing the power-to-flow ratios across the reactor subassemblies (Appendix A.2).

5.2 Transient Solution

Velocity vector and isotherm plots have been generated to display the 200-s transient in time intervals of 10 s. These plots, which give insight into transient changes of flow pattern and temperature fields, are presented in Figs. 20-61.

Low-pressure flow is moving upwards in both the reflector and blanket region until about 40s (Figs. 20-24). At that time the blanket flow reverses, which means it enters the blanket region from the upper plenum, moves down toward the LPP and passes through the junction to the HPP and the core region. This flow pattern is maintained up to 160s (Figs. 25-36). After that time the reversed flow disappears (Figs. 37-40). The isotherm plots show that the transient mass flow rundown causes a high temperature rise within the core region and parts of the reflector while the temperatures of the outlet

blanket remain comparatively unchanged (Figs. 46-61). Due to these high core temperatures a strong buoyancy effect is observed in the core region.

Computational and experimental results are compared using coolant temperatures and mass flow rates. The temperatures were measured in the instrumented driver subassembly XX08 (Fig. 16) at the outlet (OTC) and at the top-of-core (TTC) positions; the mass flow rates were evaluated from flow meters at the inlet of the LPP. The comparisons shown in Figs. 17-19 indicate a close agreement when thermal structure is used for the simulation. The decay heat data available from the test is not a measured quantity, and its uncertainty is estimated to be of the order of 10%.

In the same figures, results are also shown from additional simulations that have been performed one by not using the thermal-structure option (this basically means that the heat capacity of the reactor structures was not taken into account), and another one by by-passing the energy equations (isothermal run). As can be seen from Figs. 17 and 18, the temperatures calculated without using thermal structures show a large discrepancy from the experimental data, and the reversed flow of the LPP turns out to be more severe (Fig. 19), but covers a shorter range of transient time. In the isothermal calculation, no reversed flow is observed at all (Fig. 19).

6. CONCLUSION

The natural-circulation simulation of EBR-II reveals that a strong interaction is taking place between the reactor components of the EBR-II primary system, i.e., the inlet and outlet plena and the various reactor subassembly types. This means that the components cannot be modeled separately from each other. In fact, a multicomponent analysis is required to simulate this natural-circulation problem. Though the heat-source input is not based on direct measurements in the reactor, and may include an error of the order of 10%, the results appear in close agreement with the experimental data. From detailed investigations in the course of the simulation, it is concluded that the reversed flow in the LPP is caused by a considerable buoyancy effect within the core region and sustained by the heat capacity of the reactor structures.

APPENDIX

EBR-II Geometric and Operating Characteristics

A.1 Dimensions

Vessel Radius	1.164 m
Vessel Height	3.071 m
Inlet Flow Cross Section	
- HPP	2 x 510 cm^2
- LPP	2 x 82.2 cm^2
Outlet Flow Cross Section	856.3 cm^2
Number of Subassemblies	
- Driver	127
- Reflector	144
- Blanket	366
Subassembly Details	
- Driver	91 pins, 0.442 cm ϕ
- Reflector	no pins, annular hex geometry
- Blanket	19 pins, 1.252 cm ϕ

A.2 Initial Operating Conditions

Total Power	0.895 MW
Total Inlet Flow	0.507 m^3/s
Inlet Velocity	4.25 m/s
Inlet Temperature	365°C
Average Temperature Increase	~ 1°C
Inlet Pressure	4.265 bars
Outlet Pressure	1.709 bars

Power and Flow Distribution:

	DRIVER	REFLECTOR	BLANKET
Power (%)	76.5	7.8	15.7
Flow (%)	86.5	2	11.5
Power/Flow	0.88	3.9	1.36

A.3 Boundary Conditions

Inlet	Prescribed velocity and temperature
Outlet	Zero gradients on outlet velocity and temperature
Walls	Adiabatic

A.4 Reactor Region Power and Volumetric Heat Sources

Reactor Region	Power (Watts)	Power per Rod Length $\frac{W}{m}$	Structure Volume $\frac{m^3}{m}$	Volumetric Heat Sources W/m^3
Driver fuel	670405	401560	0.098847	4062440
struc	13682	8195	0.11762	69673.5
Reflector	69746	41776.6	0.3705	112757.35
Blanket fuel	139480	83546	0.66086	126420.12
struc	1409	844	0.26755	3154.55
TOTAL	894722			

A.5 Local Power Distribution

(QK = normalized axial power distribution)

Node #	DZ (m)	Power Distribution (Watts)					QK
		Driver		Refl.	Blanket		
		Fuel	Structure	Structure	Fuel	Structure	
7	0.0559	41.5	0.84	4.3	8.6	0.09	0.00185
8	0.2840	450.5	9.2	46.9	93.7	0.095	0.00395
9	0.2840	3444	70.3	358.3	716.5	0.95	0.0302
10	0.0857	158158	3227.7	16454	32905	332.4	4.596
11	0.1029	211735	4321	22028	44052	445	5.124
12	0.1029	202884	4140	21107	42211	426.4	4.910
13	0.1029	93165.4	1901	9692.5	19383	195.8	2.255
14	0.2178	35	0.7	3.6	7.3	0.07	0.0004
15	0.1793	439.2	0.9	45.7	91.4	0.92	0.0061
16	0.0485	41	0.8	4.3	8.5	0.09	0.0021
17	0.1508	4	0.08	4.2	0.8	0.09	0.000066
18	0.0548	1.3	0.03	0.14	0.3	0.03	0.000061

A.6 Flow Cross sections and Calculated Porosities of Reactor Subassemblies

Node	DZ (m)	Driver		Reflector		Blanket	
		A_f (cm^2)	Porosity	A_f (cm^2)	Porosity	A_f (cm^2)	Porosity
7	0.0559	10.89	0.3627	27.29	0.9090	27.29	0.9090
8	0.2840	10.89	0.3627	3.533	0.1177	3.280	0.1093
9	0.2840	10.89	0.3627	3.533	0.1177	3.280	0.1093
10	0.0857	10.20	0.3398	3.533	0.1177	3.280	0.1093
11	0.1029	10.20	0.3398	3.533	0.1177	3.280	0.1093
12	0.1029	10.20	0.3398	3.533	0.1177	3.280	0.1093
13	0.1029	10.20	0.3398	3.533	0.1177	3.280	0.1093
14	0.2178	10.20	0.3398	3.533	0.1177	3.280	0.1093
15	0.1793	9.935	0.3309	3.533	0.1177	3.280	0.1093
16	0.0485	11.774	0.3922	3.533	0.1177	3.280	0.1093
17	0.1508	11.774	0.3922	3.533	0.1177	27.29	0.9090
18	0.0548	27.29	0.9090	27.29	0.9090	27.29	0.9090

A. 7. Input Data

```
FILE: EBR2I2   DATA     A   ANL VM/CMS LEVEL 102

 &GEOM
  IFREB=1,
  ISTRUC=1, NADJCC=240, NMATRG=40, NPAR=40, NSTREL=240, NELPAR=288,
  NM1=257,  NL1=598,
  IFITEN=3,  ISYMCH=3,
  NFORCE=12,
  IGEOM=-1,
  IMAX=14, JMAX=1,  KMAX=24,
  NSURF=9, IFRES=1, LMPRNT=0,
  DX=.08179, 5*.053316, 2*.08026, 2*.13565, .0598, 3*.1619,
  DY=1*.3927,
  DZ=.165, .200, .100, 2*.138, .090, .0559, 2*.2840,
     .0857, 3*.1029, .2178,
     .1793, .0485, .1508, .0548, 2*.072, 4*.1065,
  XNORML= 0, 0, 1, 0, 0, 1,-1,-1, 1,
  YNORML= 0, 0, 0, 1,-1, 0, 0, 0, 0,
  ZNORML= 1,-1, 0, 0, 0, 0, 0, 0, 0,
  &END
REG         -1.   1   4   1   1   4   4   1    +Z
REG         -1.   4  11   1   1   1   1   1
REG         -1.  11  11   1   1  19  19   1
REG         -1.  12  13   1   1  17  17   1
REG         -1.  14  14   1   1  19  19   1
REG         -1.   1  13   1   1  24  24   2    -Z
REG         -1.  11  11   1   1   2   2   2
REG         -1.  14  14   1   1  21  21   2
REG         -1.   4   4   1   1   2   2   2
REG     .001028   4   4   1   1   1   1   3    +X  INLET
REG     .006375   4   4   1   1   2   2   3
REG         -1.   4  11   1   1   1   2   4    +Y
REG         -1.   1   4   1   1   4  24   4
REG         -1.   5  10   1   1   3  24   4
REG         -1.  11  11   1   1  19  24   4
REG         -1.  12  13   1   1  17  24   4
REG         -1.  14  14   1   1  19  21   4
REG         -1.   4  11   1   1   1   2   5    -Y
REG         -1.   1   4   1   1   4  24   5
REG         -1.   5  10   1   1   3  24   5
REG         -1.  11  11   1   1  19  24   5
REG         -1.  12  13   1   1  17  24   5
REG         -1.  14  14   1   1  19  21   5
REG         -1.   5   5   1   1   3   3   6    +X
REG         -1.  12  12   1   1  17  18   6
REG         -1.  11  11   1   1   1   2   7    -X
REG         -1.  10  10   1   1   3  18   7
REG         -1.  13  13   1   1  17  18   7
REG         -1.  13  13   1   1  22  24   7
REG     .001538  14  14   1   1  19  20   8    -X  OUTLET
REG     .002275  14  14   1   1  21  21   8
REG         -1.   1   1   1   1   4  24   9    +X  ORIGIN
END
 &DATA
  VELOC=2*0., 4.280, 6*0.,
  KFLOW=2*3, 1, 4*3, -5, -3,
  TEMP=9*365.0,
```

```
FILE: EBR2I2   DATA     A   ANL VM/CMS LEVEL 102

 ISTATE=0, IFENER=3,
 KTEMP=2*400, 1, 6*400,
 NTHCON=1,2,3,5,8,15,-20,
 IT=1, ITIBUG=0, TREST=20.,
  OMEGA=1.9,  OMEGAV=0.8,  ITMAXP=200,
 EPS1=1.E-5, IDTIME=1,  RDTIME=1000.0, DTENER=1.,
  EPS5=2.E-6, DDDHMX=0., OMEGAE=0.8, ITMAXE=100,
 TEMP0=365.0, PRES0=1.450E5, ZPRES0=2.6085,
 GRAVZ=-9.8,  NTPRNT=-9999,  NTMAX=10000,
 ISTPR=1201, 3201, 5201, 8201, 15201,
 NTHPR=1201, 3201, 5201, 8201, 15201, 90108, 90608,
 IREBIT=9,
 NMEATC=1,
 HEATC1=4.5,
 HEATC2=0.0052,
 HEATC3=0.3,
 NMATER=3,
 C0K=      23.36,       14.176,       31.15,
 C1K=        0.0,        0.0137,       0.0,
 C2K=        0.0,        0.0,          0.0,
 C0CP=    188.41,      504.4,        188.41,
 C1CP=       0.0,        0.1130,       0.0,
 C2CP=       0.0,        0.0,          0.0,
 C0RO=  15506.0,      8041.3,      17940.7,
 C1RO=       0.0,       -0.4634,       0.0,
 C2RO=       0.0,        0.0,          0.0,
 QK= 6*0, 0.00185, 0.00395, 0.00302, 4.596, 5.124, 4.910, 2.255,
     0.0004, 0.00615, 0.00207, 0.000066, 0.000061, 6*0,
   NREBRT=8,  NREBM=18, 44, 10, 2*30, 40, 66, 16,
 NREBX=1, 5*0, 5, 3,   NREBZ=6, 5*10, 2*0,
 CLENTH=  -1.,   -1.,   -1.,   -1., .0316,  .182,
        .0029, .0036, .0014,   -1.,   -1.,   -1.,
 REYLEN= .138, .1024, .1650, .5000, .1700,  .270,
        .0029, .0036, .0014, .2548, .1024, .0083,
 ICORR = 1,2,3,4,5,5,6,7,8,9,10,11,
 FORCEF=12*.5,
 NCORR =11,
 ACORRL=    0.,    0.,    0.,    0.,  180.,
          26.33,  6.48, 2.574, 61.75,    0.,    0.,
 BCORRL=    1.,    1.,    1.,    1.,   -1.,
           -.85,  -.03, -.269,   -.2,    1.,   -1.,
 CCORRL=   .370,  .312,  .164, .2500,    0.,
             0.,    0.,    0.,    0.,   27.,  1.46,
 ACORRT=    0.,    0.,    0.,    0.,  1.92,
          .1922,  6.48, 2.574, 61.75,    0.,    0.,
 BCORRT=    1.,    1.,    1.,    1., -.145,
          -.072,  -.03, -.269,   -.2,    1.,   -1.,
 CCORRT=   .370,  .312,  .164, .2500,    0.,
             0.,    0.,    0.,    0.,   27.,  1.46,
 REYTRN=  1.E9,  1.E9,  1.E9,  1.E9, 202.5,
          557.6,  1.E9,  1.E9,  1.E9,  1.E9,  1.E9,
 &END
  1   1   6   1   1   4   5        REB FOR CELLS
  1   5   6   1   1   2   3
  1   4   4   1   1   1   2
```

```
FILE: EBR2I2   DATA     A   ANL VM/CMS LEVEL 102


   2   5  11   1   1   1   1
   2   7  11   1   1   2   2
   2   7  10   1   1   3   7
   2   1   6   1   1   6   7
   3   1  10   1   1   8   8
   4   1  10   1   1   9  11
   5   1  10   1   1  12  14
   6   1  10   1   1  15  18
   7   1  11   1   1  19  24
   8  12  13   1   1  17  24
   1   4   4   1   1   1   1        X-SURS
   7  11  11   1   1  20  24
   8  13  13   1   1  19  21
   1   1   6   1   1   5   5        Z-SURS
   2   1  10   1   1   7   7
   3   1  10   1   1   8   8
   4   1  10   1   1  11  11
   5   1  10   1   1  14  14
   6   1  10   1   1  18  18
FORC
ZFOR   1   1   6   1   1   4   4      HPP BAFFLE  40 HOLES
XFOR   2   6   6   1   1   1   1      LPP BAFFLE  50 HOLES
ZFOR   3   7  11   1   1   1   1      LPP BAFFLE 592 HOLES
XFOR   4  11  11   1   1  20  24      SKIRT RADIAL
XFOR   5   1   5   1   1   4   5      TRANSV. RESIST. LOWER ADPTR
XFOR   6   1   6   1   1  19  24      TOP END S/A
XFOR   6   7  10   1   1  19  20
ZFOR   7   1   6   1   1   7  15      DRIVER
ZFOR   8   7   8   1   1   7  15      REFLECTOR
ZFOR   9   9  10   1   1   7  15      BLANKET
XFOR  10   4   4   1   1   2   2      HP - INLET
XFOR  11   4   4   1   1   1   1      LP - INLET
XFOR  12  13  13   1   1  19  21      OUTLET - RESIST.
END
 &STRUCT
  NSTRUC=32,
  NTSEL=12*4, 12*8, 8*12,
  NTSMAT= 6*2,6*1,12*1,4*1,2*2,2*1,
  OUTR= 6*0.00186, 6*0.002032, 6*0.02640, 6*0.002032,
        2*0.0262,  2*0.002032, 2*0.00626, 2*0.002032,
  RODFR= 60.59,  103.86,  155.80,  207.70,  259.60,  311.60,
          6.66,   11.42,   17.13,   22.81,   28.55,   34.25,
          0.33,   0.565,   0.848,    1.13,    1.41,    1.70,
          3.33,    5.71,    8.56,   11.42,   14.28,   17.13,
          4.48,    5.44,   61.86,   75.18,
         191.2,   243.4,   153.2,   195.1,
  IHTSTR= 32*1,
  HYDRAD= 12*0.00365, 12*0.0192, 4*0.00365, 4*0.00165,
  IXYZ=   32*3,
  NTSADJ= 12*1, 12*1, 8*1,
  MATERL= 2, 1, 2, 1, 2, 1, 2, 1, 2, 1, 2, 1,
          22*2, 2, 3, 2, 3, 2*2,
  NMPAR=  40*1,
  ORPAR= .0005225, .0013375, .0005225, .0013375, .0005225, .0013375,
         .0005225, .0013375, .0005225, .0013375, .0005225, .0013375,
```

```
FILE: EBR2I2   DATA     A   ANL VM/CMS LEVEL 102

         6*0.002032, 6*0.0264, 6*0.002032,
         2*0.0262,  2*0.002032, 0.00076, 0.0055, 0.00076, 0.0055,
         2*0.002032,
 QSPAR= 69673.5, 4062440.0, 69673.5, 4062440.0, 69673.5, 4062440.0,
        69673.5, 4062440.0, 69673.5, 4062440.0, 69673.5, 4062440.0,
        18*69673.5, 4*112757.3, 3154.6, 126421.0, 3154.6, 126421.0,
        2*3154.6,
 NGAPTY=1,
 SGAP=0.0,
 HGAP=10000.0,
 IGAP=8*1,
 &END
  1   1   1   1   1  10  13
  2   2   2   1   1  10  13
  3   3   3   1   1  10  13
  4   4   4   1   1  10  13
  5   5   5   1   1  10  13
  6   6   6   1   1  10  13
  7   1   1   1   1  10  13
  8   2   2   1   1  10  13
  9   3   3   1   1  10  13
 10   4   4   1   1  10  13
 11   5   5   1   1  10  13
 12   6   6   1   1  10  13
 13   1   1   1   1   7   9
 13   1   1   1   1  14  18
 14   2   2   1   1   7   9
 14   2   2   1   1  14  18
 15   3   3   1   1   7   9
 15   3   3   1   1  14  18
 16   4   4   1   1   7   9
 16   4   4   1   1  14  18
 17   5   5   1   1   7   9
 17   5   5   1   1  14  18
 18   6   6   1   1   7   9
 18   6   6   1   1  14  18
 19   1   1   1   1   7   9
 19   1   1   1   1  14  18
 20   2   2   1   1   7   9
 20   2   2   1   1  14  18
 21   3   3   1   1   7   9
 21   3   3   1   1  14  18
 22   4   4   1   1   7   9
 22   4   4   1   1  14  18
 23   5   5   1   1   7   9
 23   5   5   1   1  14  18
 24   6   6   1   1   7   9
 24   6   6   1   1  14  18
 25   7   7   1   1   7  18
 26   8   8   1   1   7  18
 27   7   7   1   1   7  18
 28   8   8   1   1   7  18
 29   9   9   1   1   7  18
 30  10  10   1   1   7  18
 31   9   9   1   1   7  18
```

```
FILE: EBR2I2   DATA     A   ANL VM/CMS LEVEL 102


  32  10  10    1   1   7  18
END
ALX      0.       1   9   1   1   6  18      S/A
ALX      0.       7   9   1   1   3   5
ALX      0.      11  11   1   1  19  19      LOWER SKIRT
ALX    .2540     11  11   1   1  20  24      UPPER SKIRT
ALX      0.       6   6   1   1   2   5      LOWER PLENUM
ALZ      0.       5   6   1   1   1   1
AL     .3627      1   6   1   1   7   9      CORE S/A
AL     .3398      1   6   1   1  10  14
AL     .3309      1   6   1   1  15  15
AL     .3922      1   6   1   1  16  17
AL     .9090      1   6   1   1  18  18
AL     .9090      7   8   1   1   7   7      REFL S/A
AL     .1177      7   8   1   1   8  17
AL     .9090      7   8   1   1  18  18
AL     .9090      9  10   1   1   7   7      BLANKET S/A
AL     .1093      9  10   1   1   8  16
AL     .9090      9  10   1   1  17  18
ALZ    .3627      1   6   1   1   6   8      CORE S/A
ALZ    .3398      1   6   1   1   9  13
ALZ    .3309      1   6   1   1  14  14
ALZ    .3922      1   6   1   1  15  16
ALZ    .9090      1   6   1   1  17  17
ALZ    .9090      7   8   1   1   6   6      REFL S/A
ALZ    .1177      7   8   1   1   7  16
ALZ    .9090      7   8   1   1  17  17
ALZ    .9090      9  10   1   1   6   6      BLANKET S/A
ALZ    .1093      9  10   1   1   7  15
ALZ    .9090      9  10   1   1  16  17
ALX     .04675   13  13   1   1  19  21      OUTLET
AL      .04371   14  14   1   1  19  21
ALZ       .0     14  14   1   1  19  20
AL     .07375     4   4   1   1   1   1      INLET LOWER TUBE
AL      .3774     4   4   1   1   2   2      INLET UPPER TUBE
ALX   .06563      4   4   1   1   1   1      INLET LOWER TUBE
ALX   .33580      4   4   1   1   2   2      INLET UPPER TUBE
ALZ  1.000        1   6   1   1   4   4      HPP  VERT. BAFFLE  40 HOLES
ALX    .8593      6   6   1   1   1   1      LPP  VERT. BAFFLE  50 HOLES
ALZ   .2069       7  10   1   1   1   1      LPP HORIZ. BAFFLE 592 HOLES
AL     .9050      1   3   1   1  19  24      TOP END FIXTURE S/A,
AL     .6261      4   4   1   1  19  24      RETAIN. PINS
AL     .9050      5   6   1   1  19  24
AL     .9050      7  10   1   1  19  20
ALZ     .9050     1   3   1   1  19  23
ALZ     .6261     4   4   1   1  19  23
ALZ     .9050     5   6   1   1  19  23
ALZ     .9050     7  10   1   1  19  20
AL    .0829       7  10   1   1   3   3      LPP LOWER GRID, REFL & BLANK
AL    .0829       7  10   1   1   6   6      LPP UPPER GRID, REFL & BLANK
ALZ   .0829       7  10   1   1   2   5      LPP
ALZ     .3191     1   6   1   1   4   5      HPP CORE S/A
END
=============  END OF DATA ====================
  EBR2I2.DATA   MAR 19/82   (LOW POWER,  THERM.STR.)
  E B R - II  NATURAL CONVECTION TEST #10, PHASE 2
  ---- ONE-SIXTEENTH MODEL ---- IMPLICIT METHOD
```

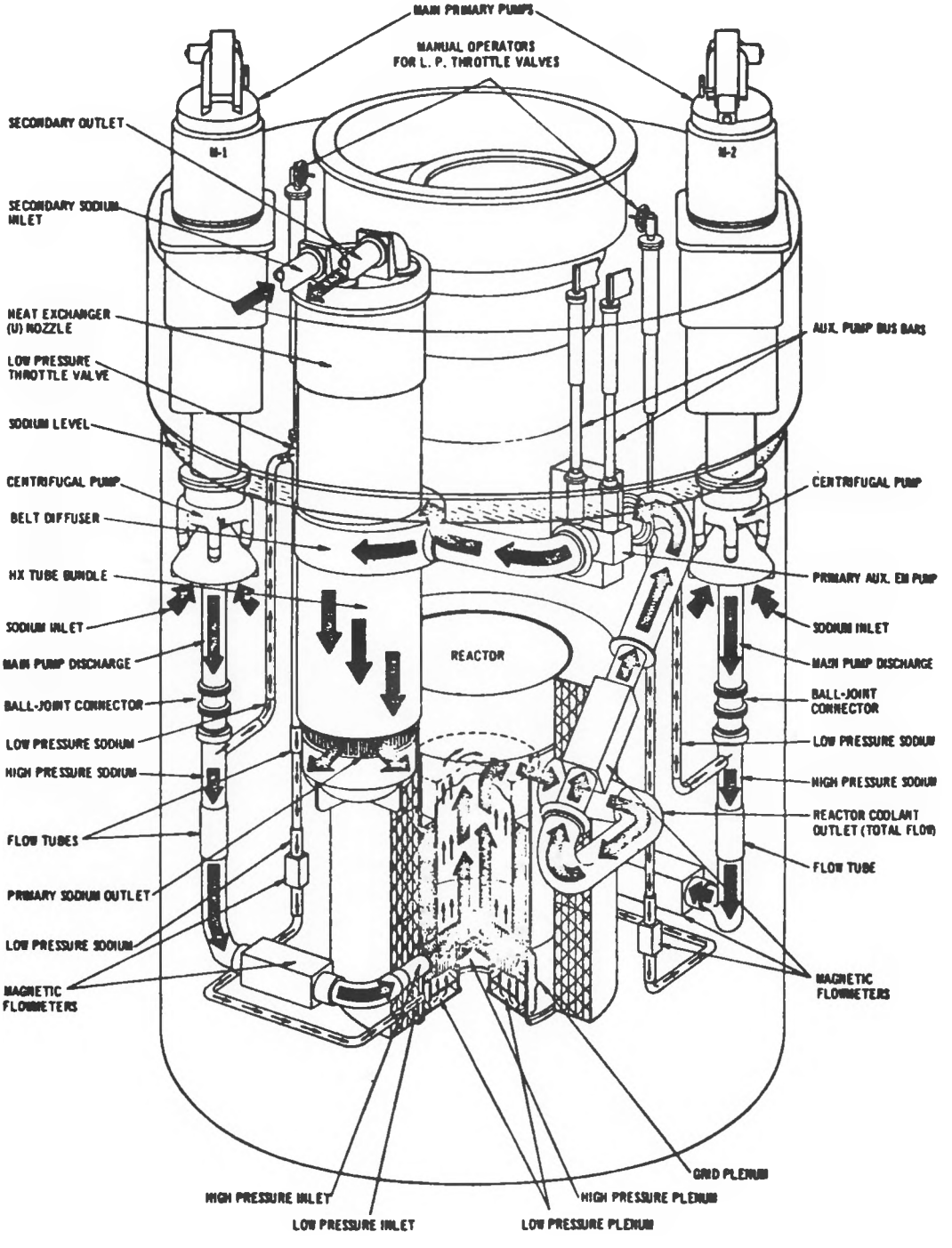

Fig. 1. EBR-II Primary Cooling System

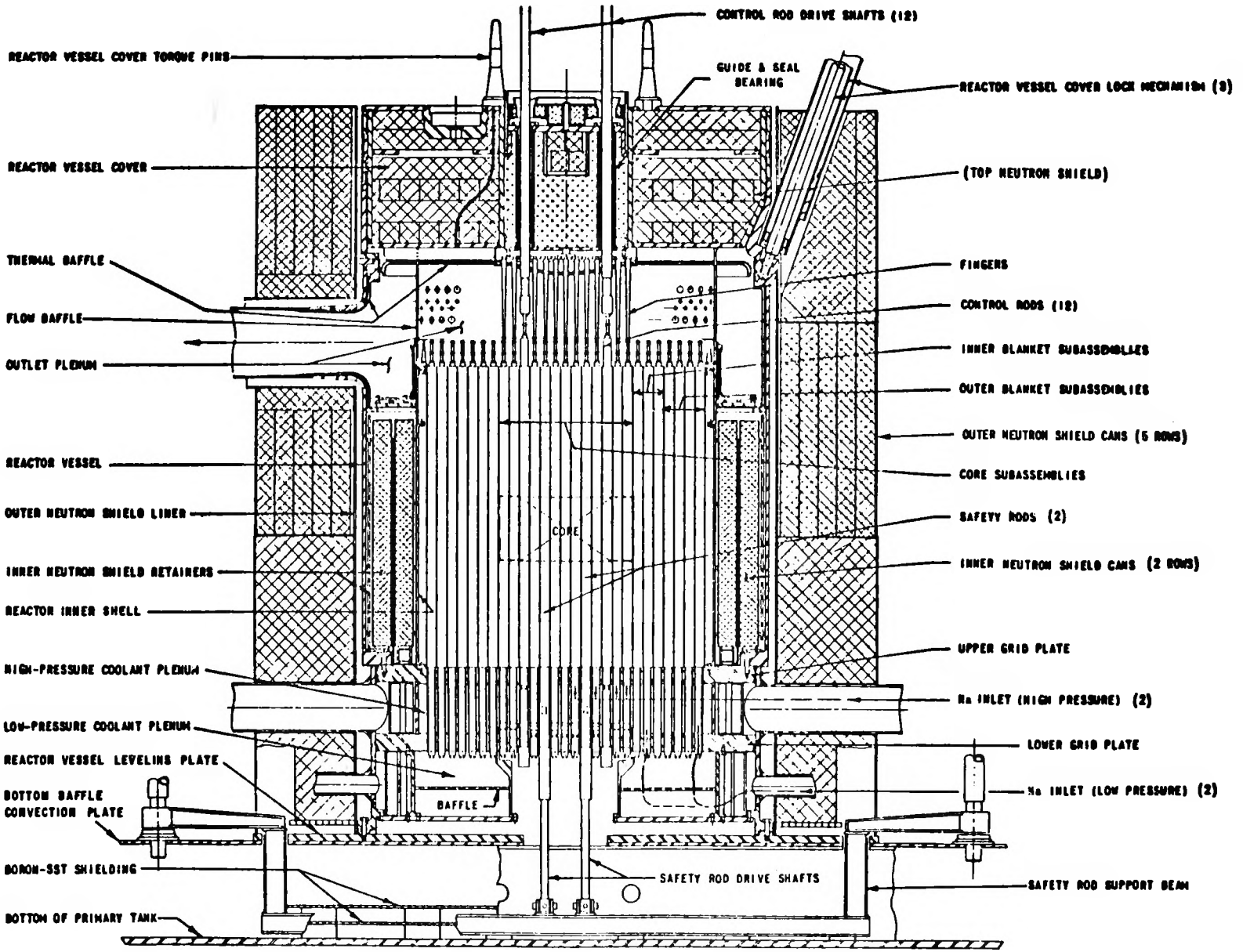

Fig. 2. Reactor Vessel and Neutron Shield Assembly

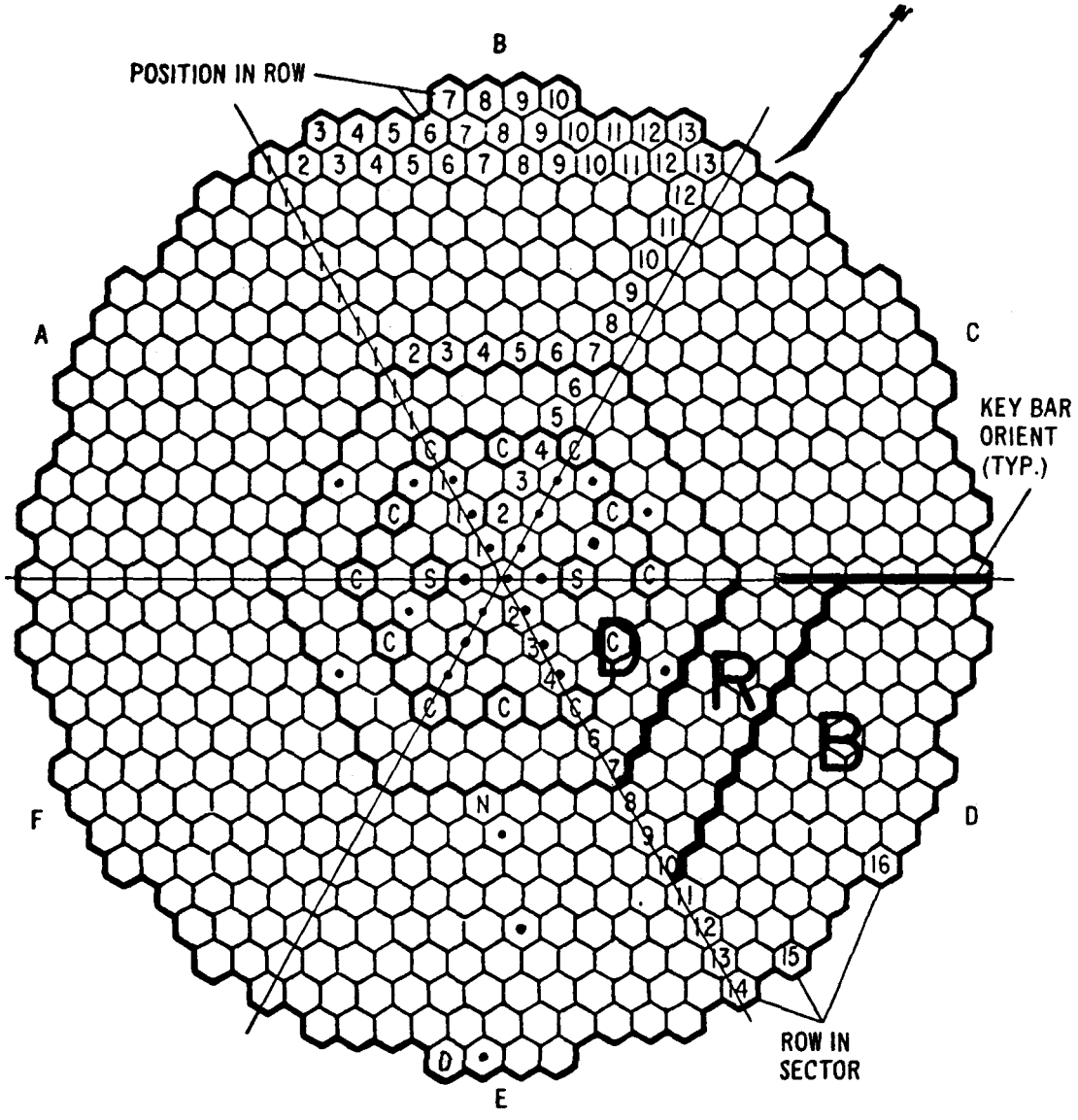

LEGEND

1. SECTORS	A to F	
2. CONTROL RODS (12)	C	D = Driver
3. SAFETY RODS (2)	S	R = Reflector
4. THERMOCOUPLES (26)	•	B = Blanket
5. FIXED DUMMY	D	
6. NEUTRON SOURCE	N	
7. GRID POSITIONS		
CORE	61	
INNER BLANKET	66	
OUTER BLANKET	510	
TOTAL	637	

Fig. 3. Subassembly Arrangement in the Reactor

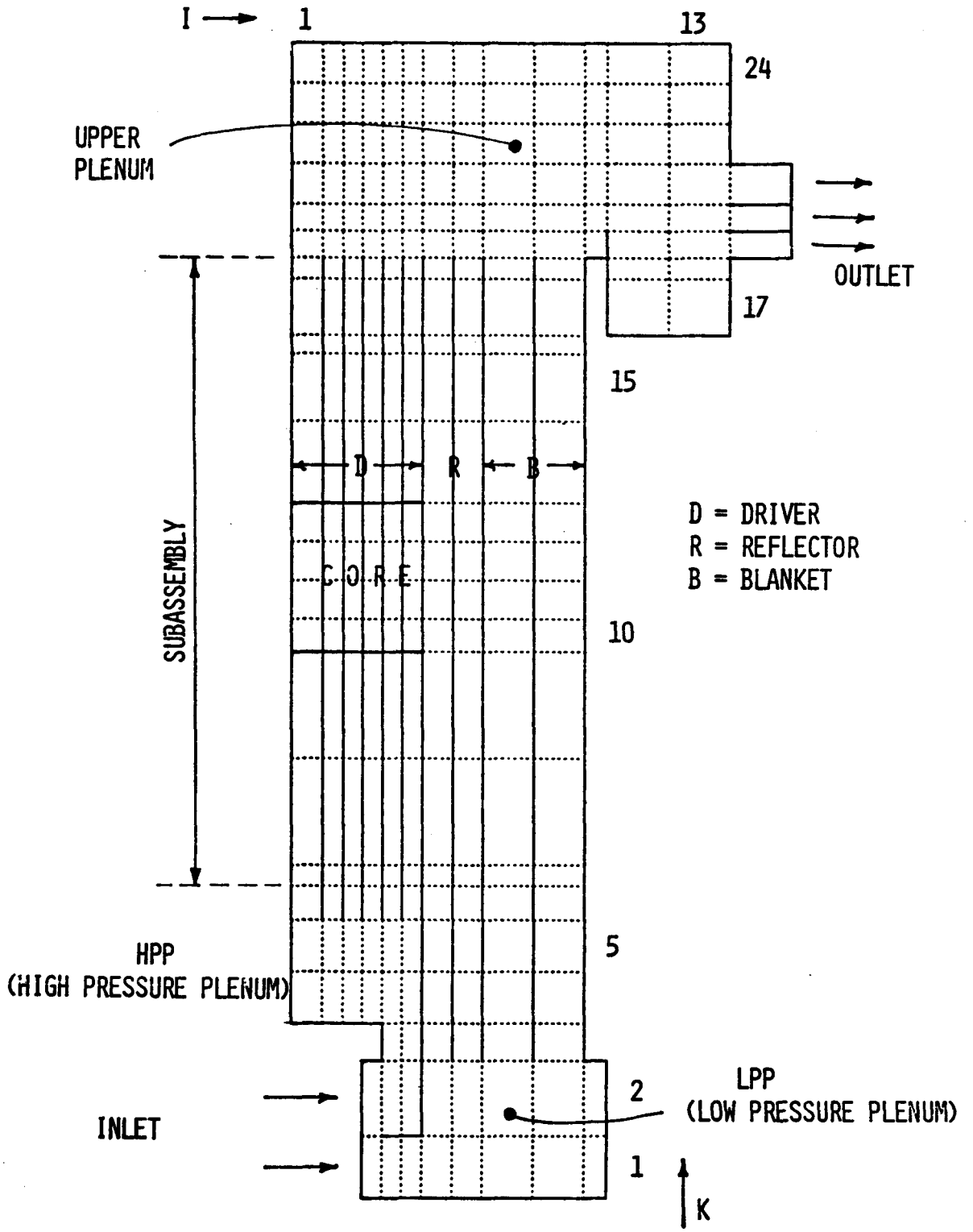

Fig. 4. Grid System

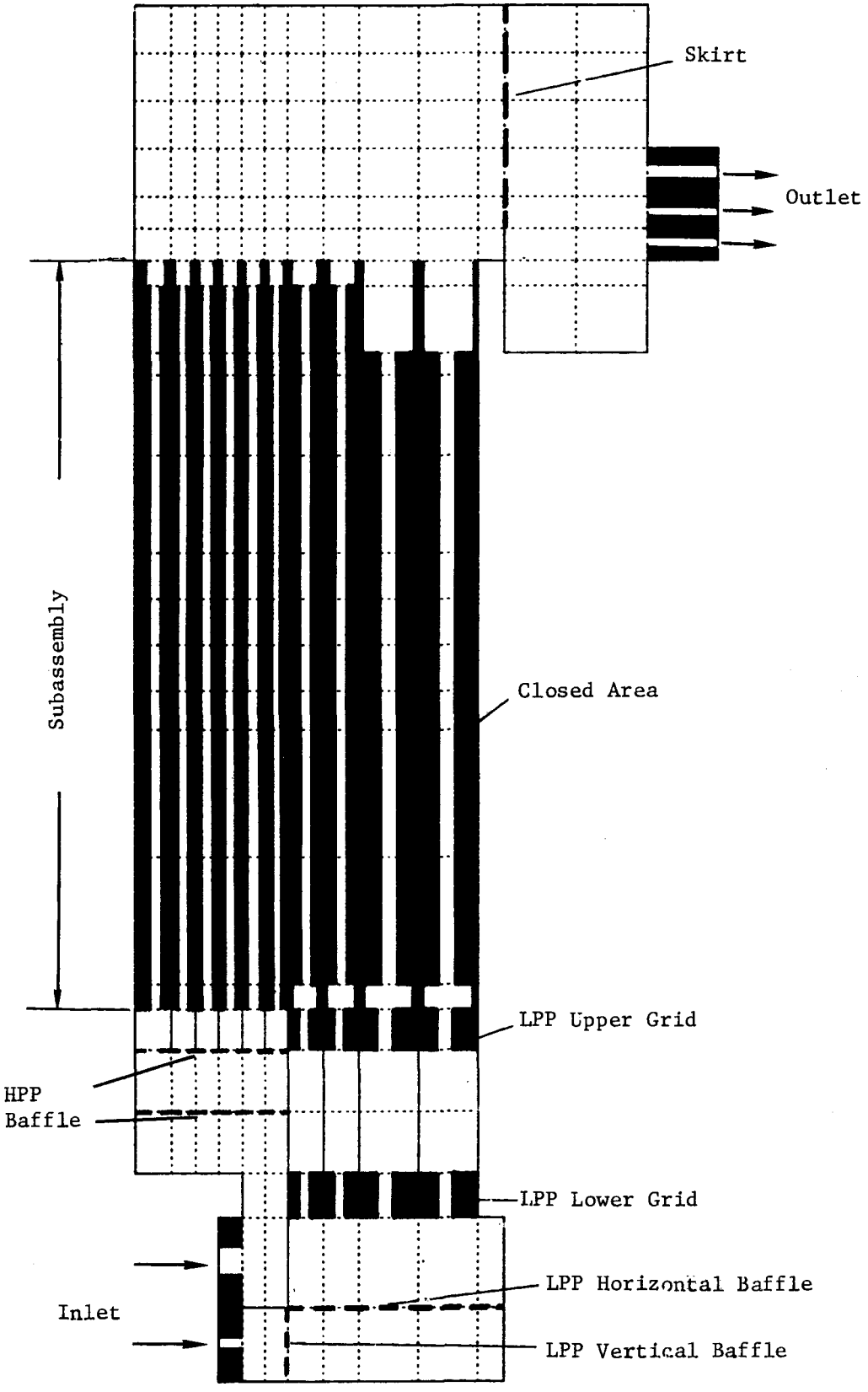

Fig. 5. Basic Porosities and Permeabilities

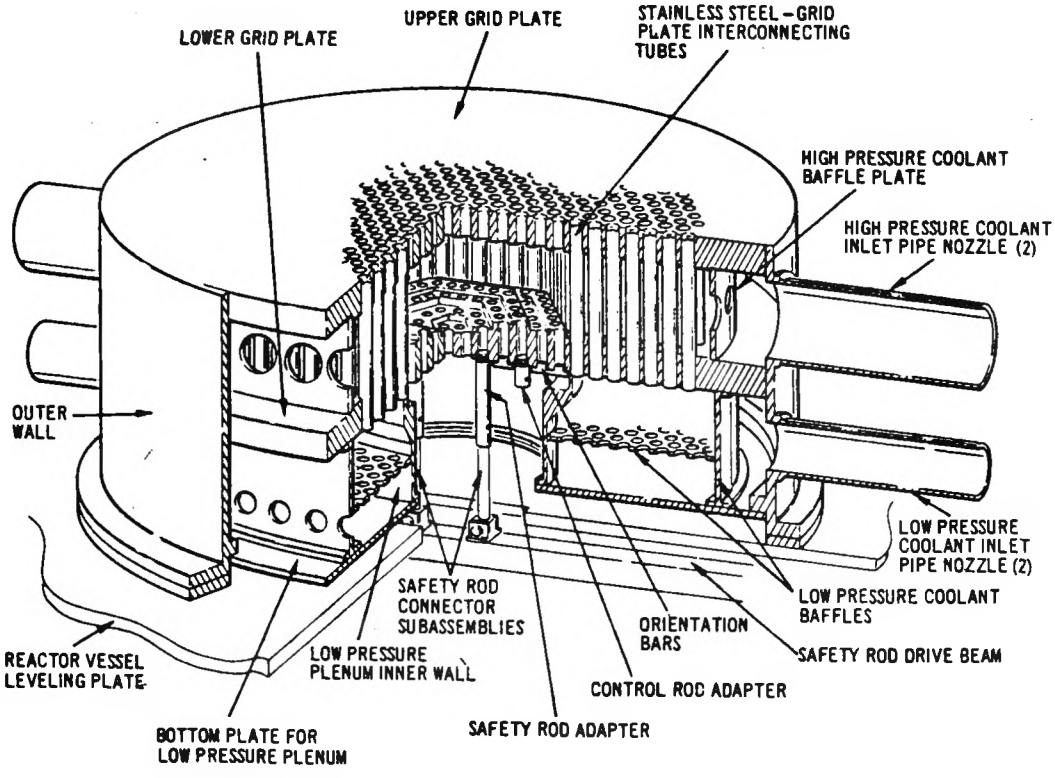

Fig. 6. Reactor Vessel Grid Plenum Assembly

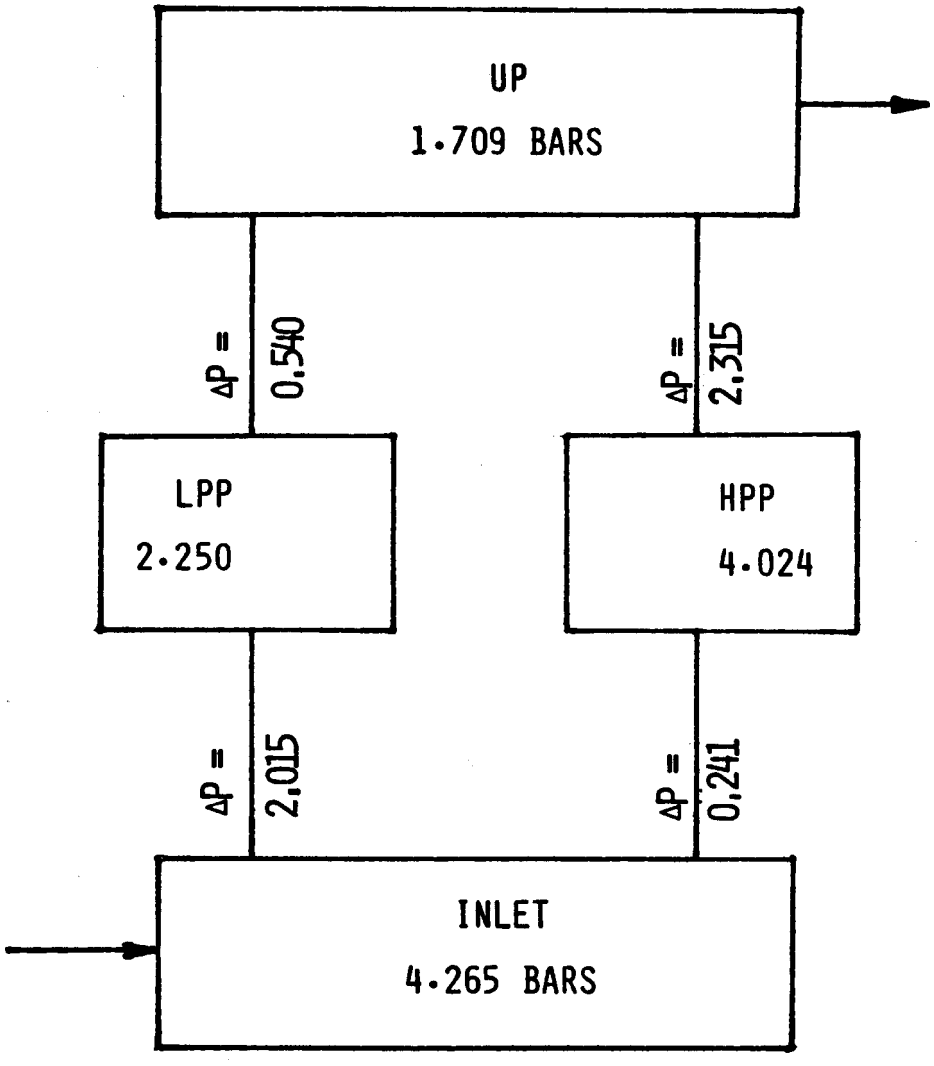

Fig. 7. Pressure Drop Scheme of the EBR-II Transient Test No. 10 (Initial Values)

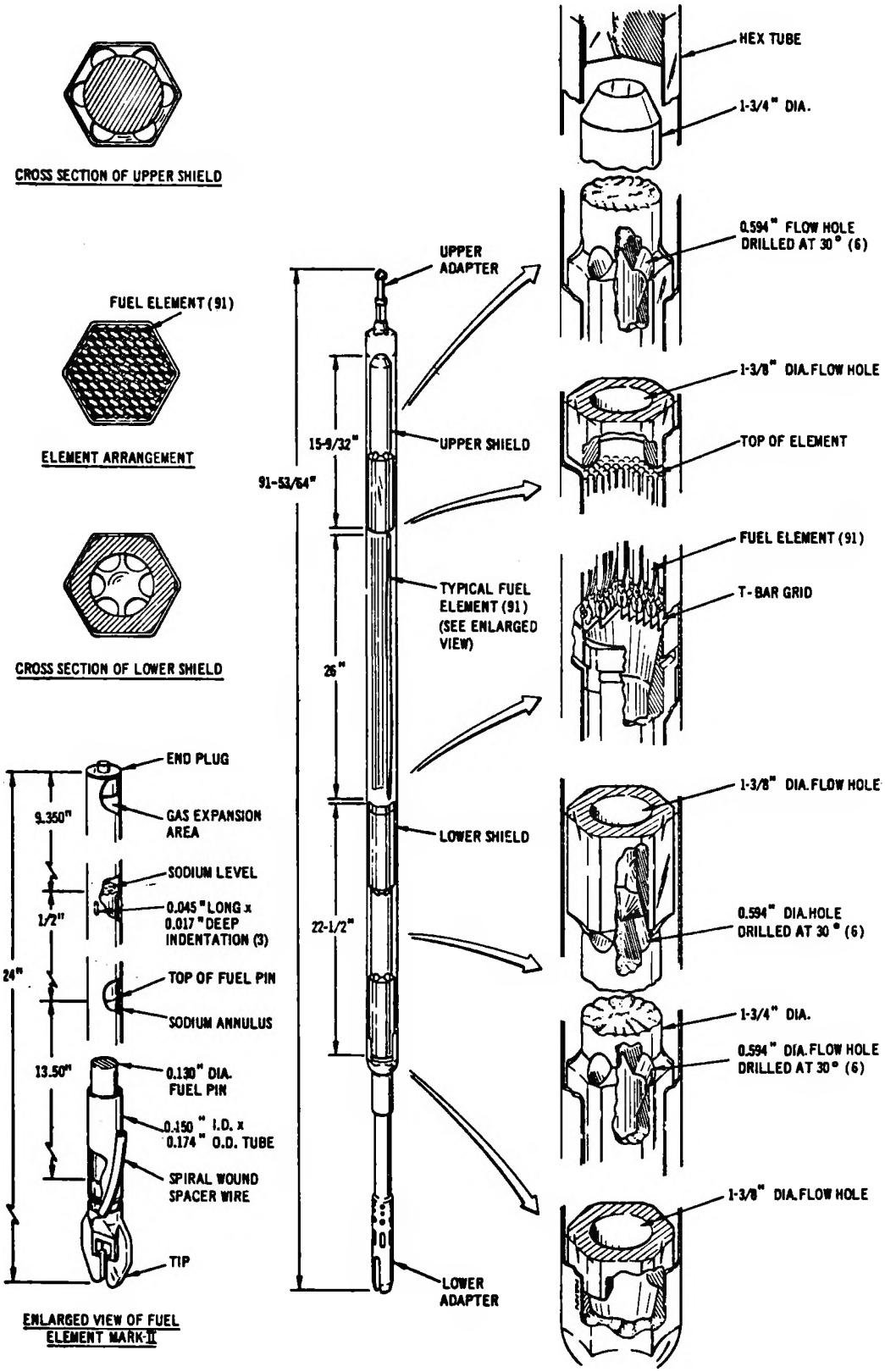

Fig. 8. Mark II Driver Fuel Subassembly

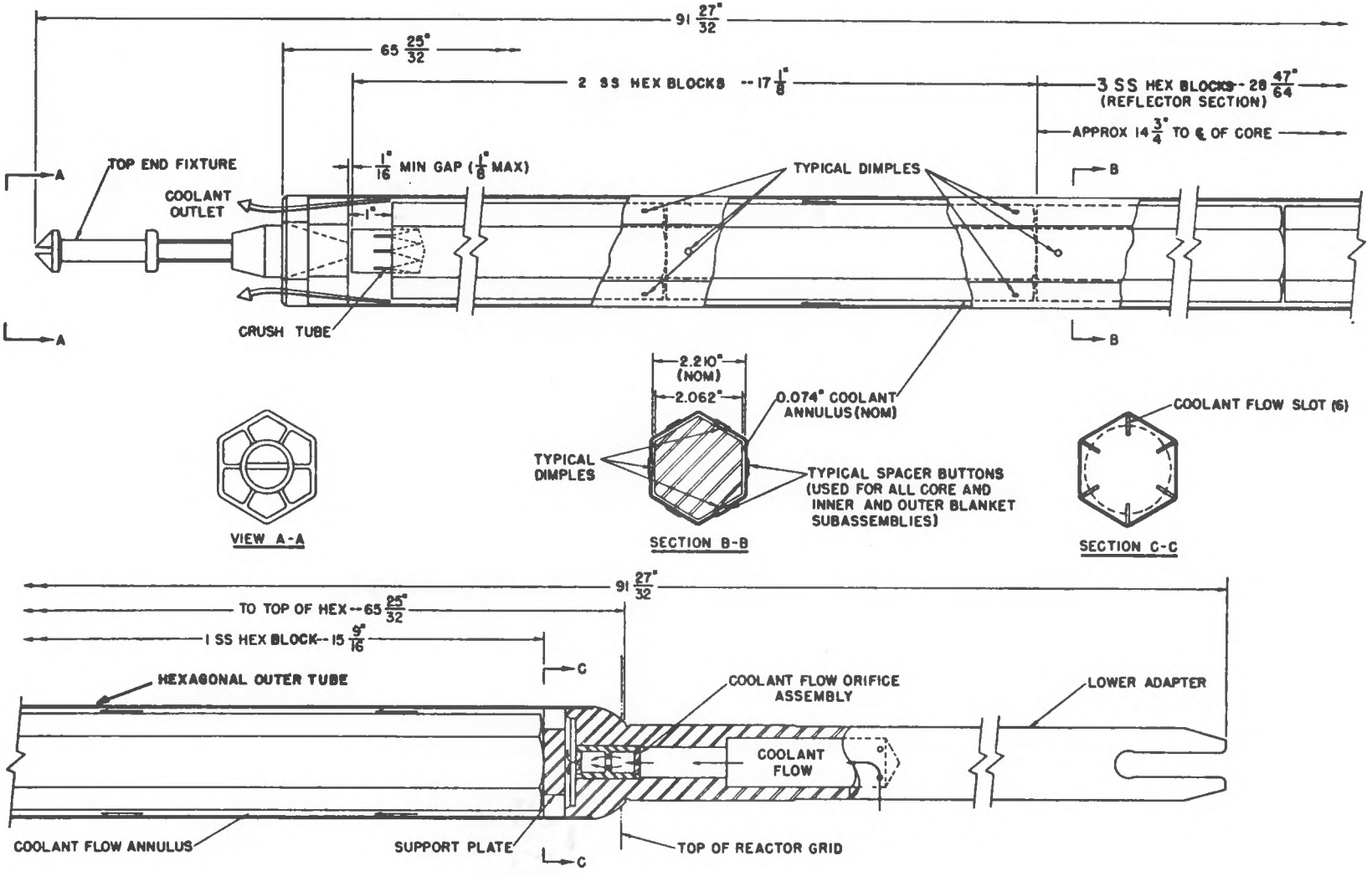

Fig. 9. Stainless Steel Reflector Subassembly

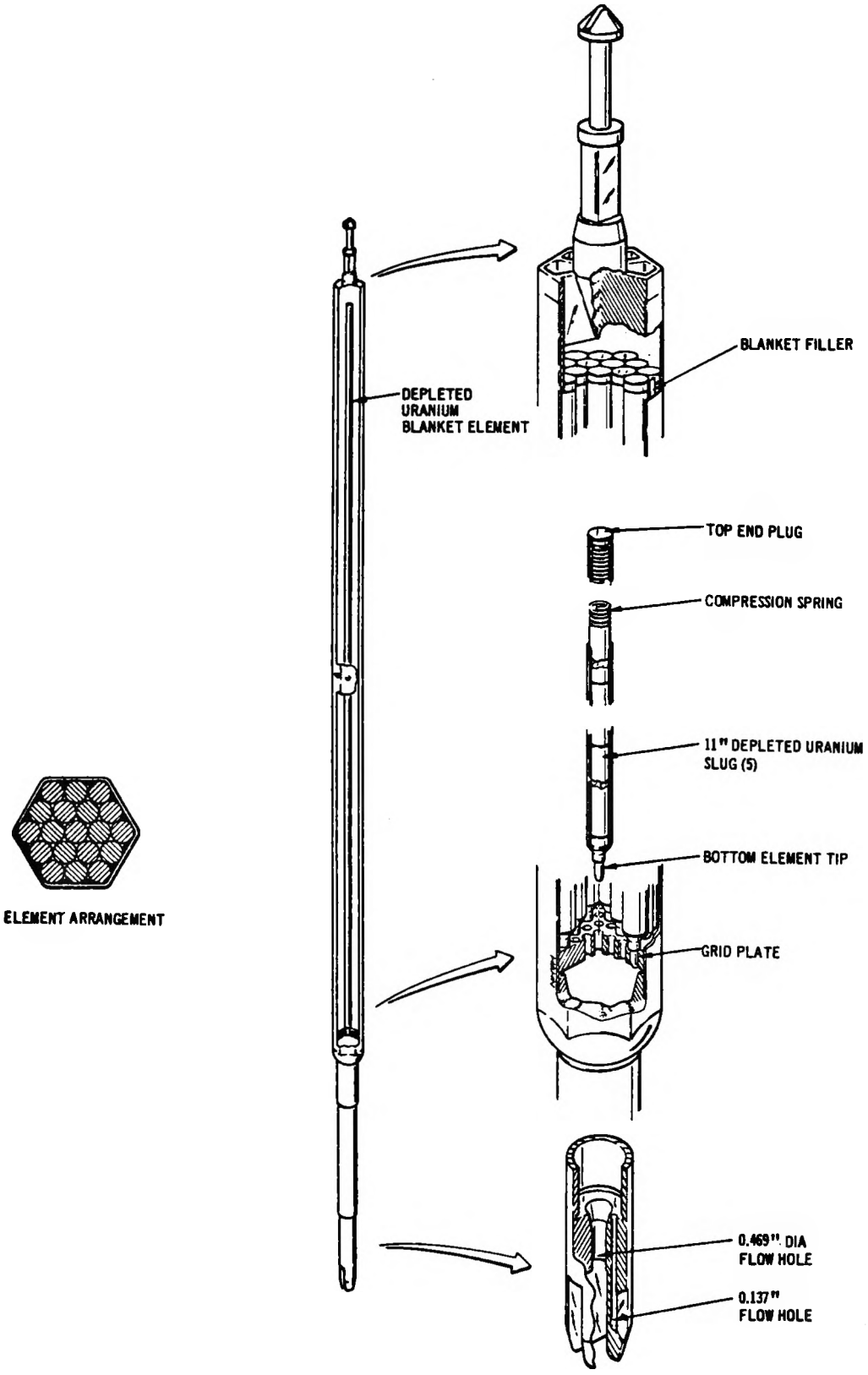

Fig. 10. Outer Blanket Subassembly

		C_0	C_1
DRIVER FUEL	ρ	15506.	0.
	C_p	188.41	0.
	K	23.36	0.
BLANKET FUEL	ρ	17940.7	0.
	C_p	188.41	0.
	K	31.15	0.
STAINLESS STEEL SS 304	ρ	8041.3	-0.4634
	C_p	504.4	0.113
	K	14.176	0.0137

DENSITY	ρ	KG/M^3
HEAT CAPACITY	C_p	Ws/(KG·K)
HEAT CONDUCTION	K	W/(M·K)

$$F = C_0 + C_1 \times T(°C)$$

Fig. 11. Properties of Thermal Structure

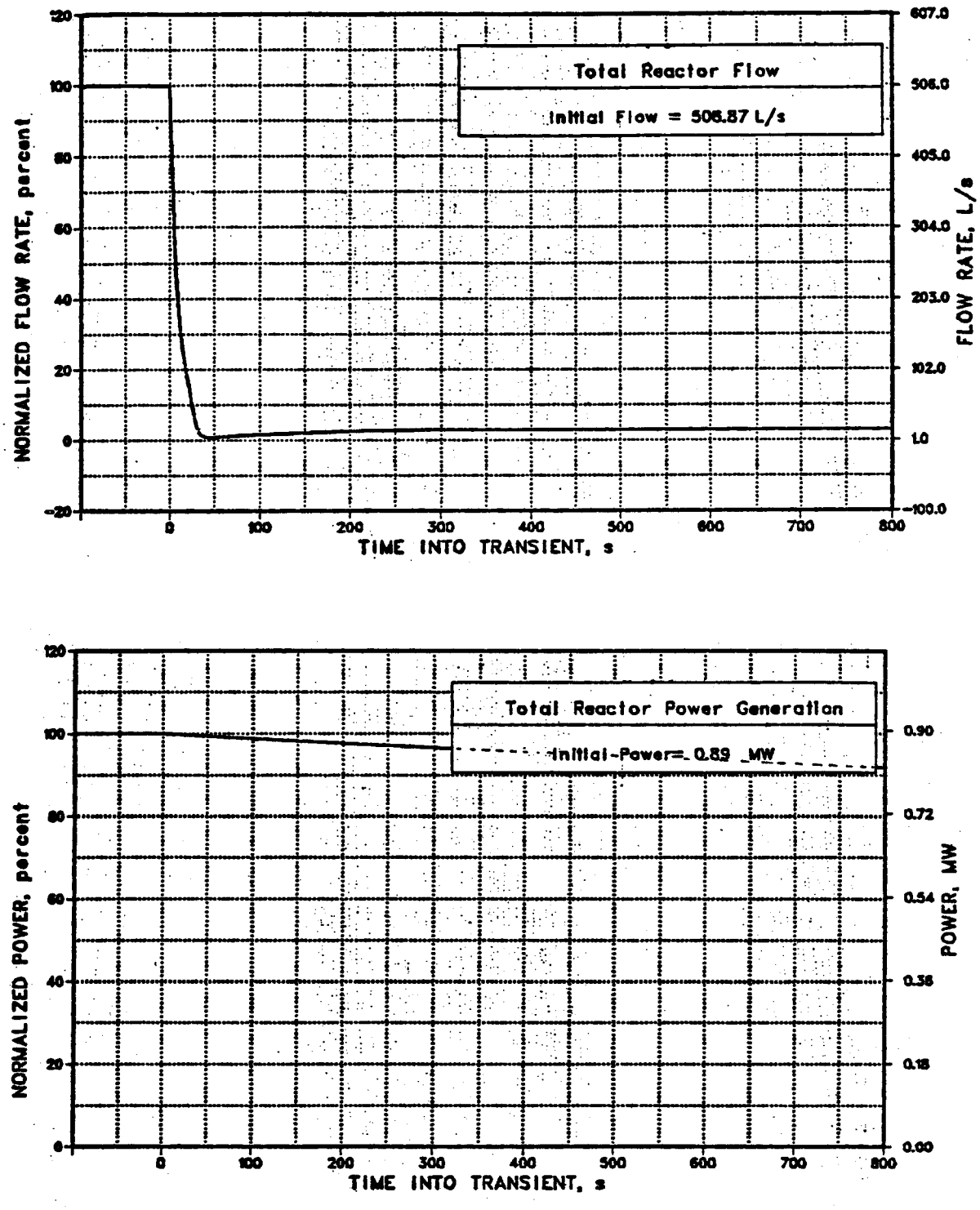

Fig. 12. Transient Functions for Total Reactor Flow and Total Reactor Power Generation

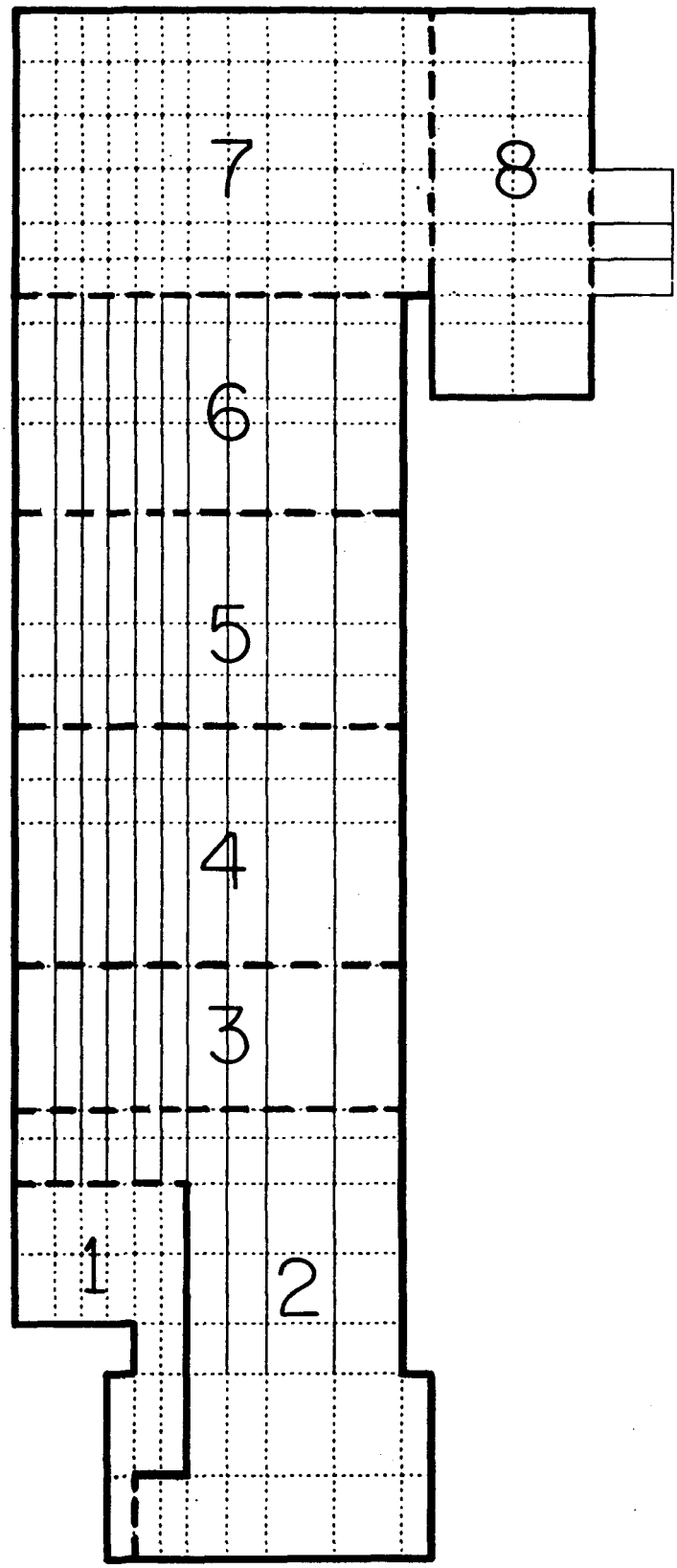

Fig. 13. Rebalancing Regions used for the Simulation

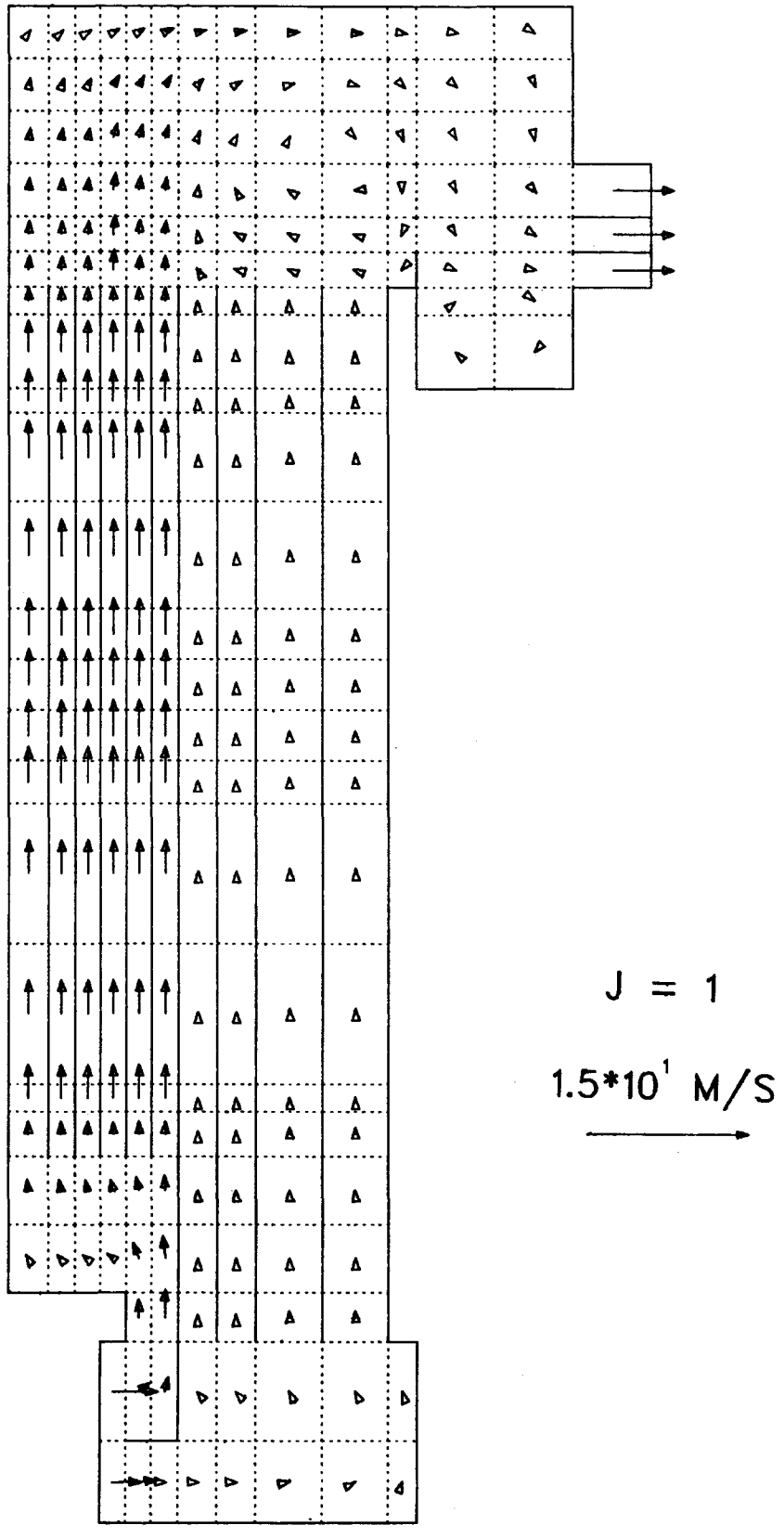

Fig. 14. Steady Velocity Distribution in the Azimuthal Plane J = 1

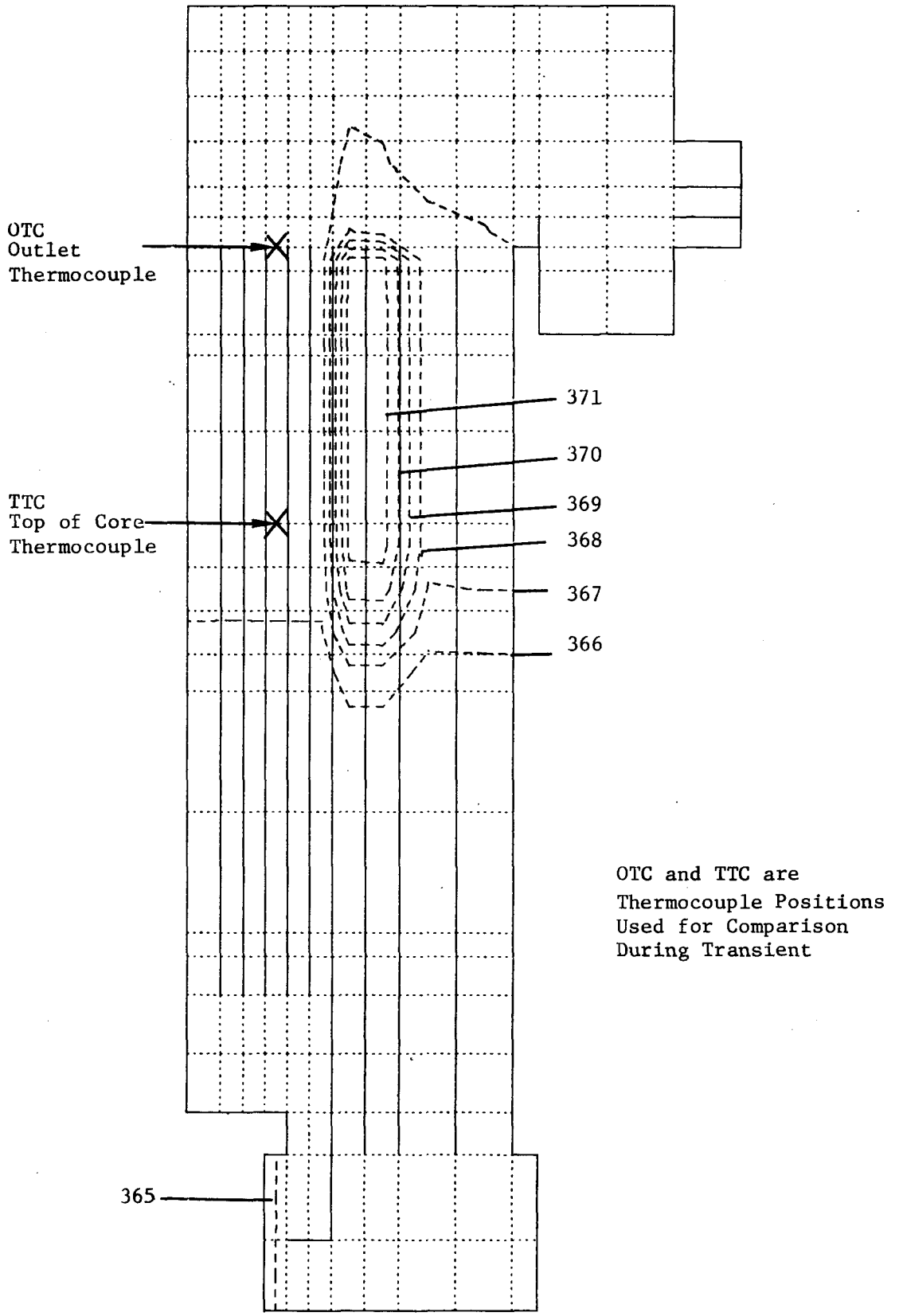

Fig. 15. Steady Isotherm Plot Showing Temperatures in the Azimuthal Plane J = 1

C = Control rod

D = Driver fuel

K--- = SS dummy

P = 1/2 driver fuel, 1/2 SS

R = SS reflector

S = Safety rod

X--- = Experimental subassembly

YY07 = INCOT experiment

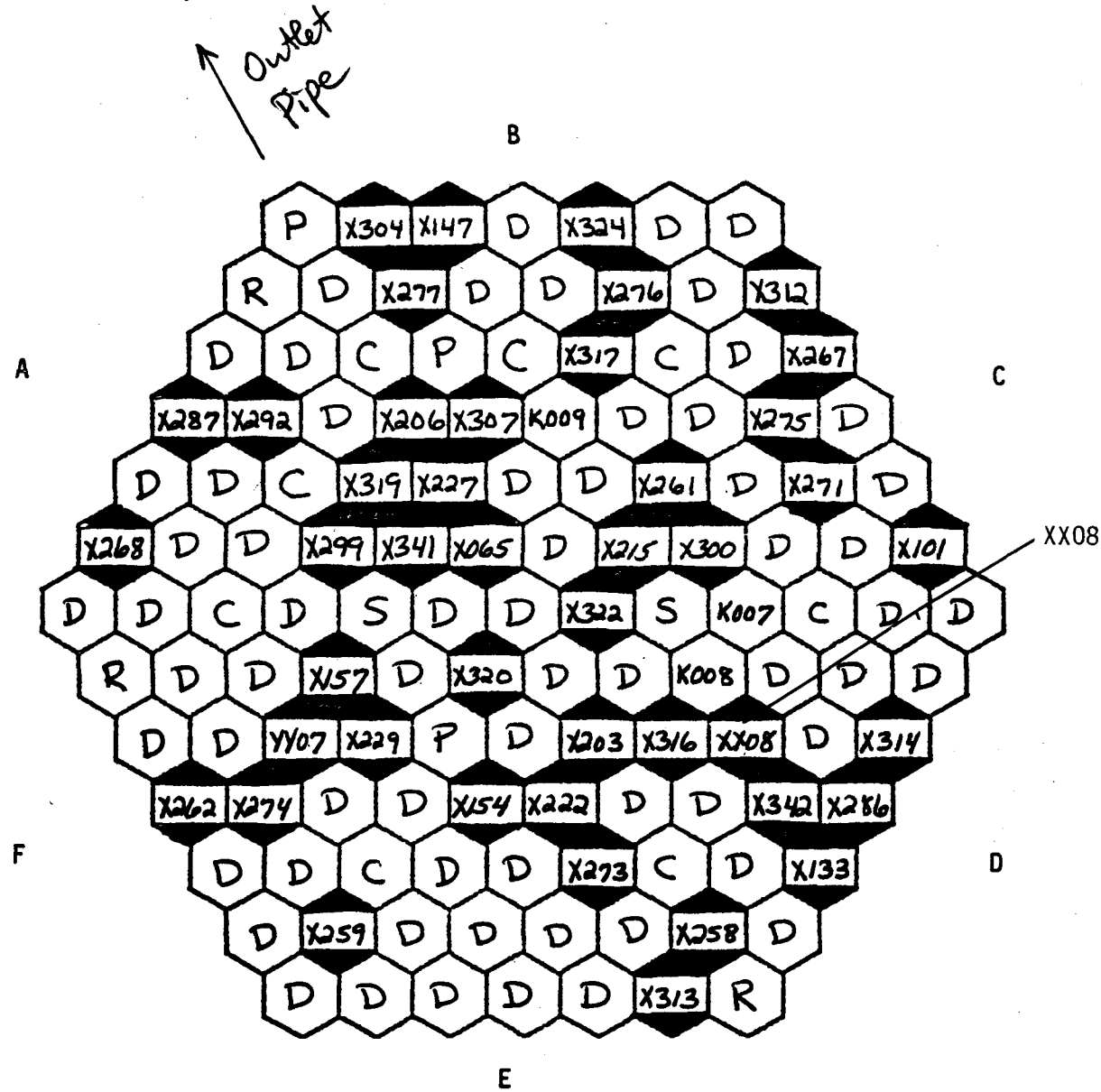

Fig. 16. Loading Configuration for Run 93B

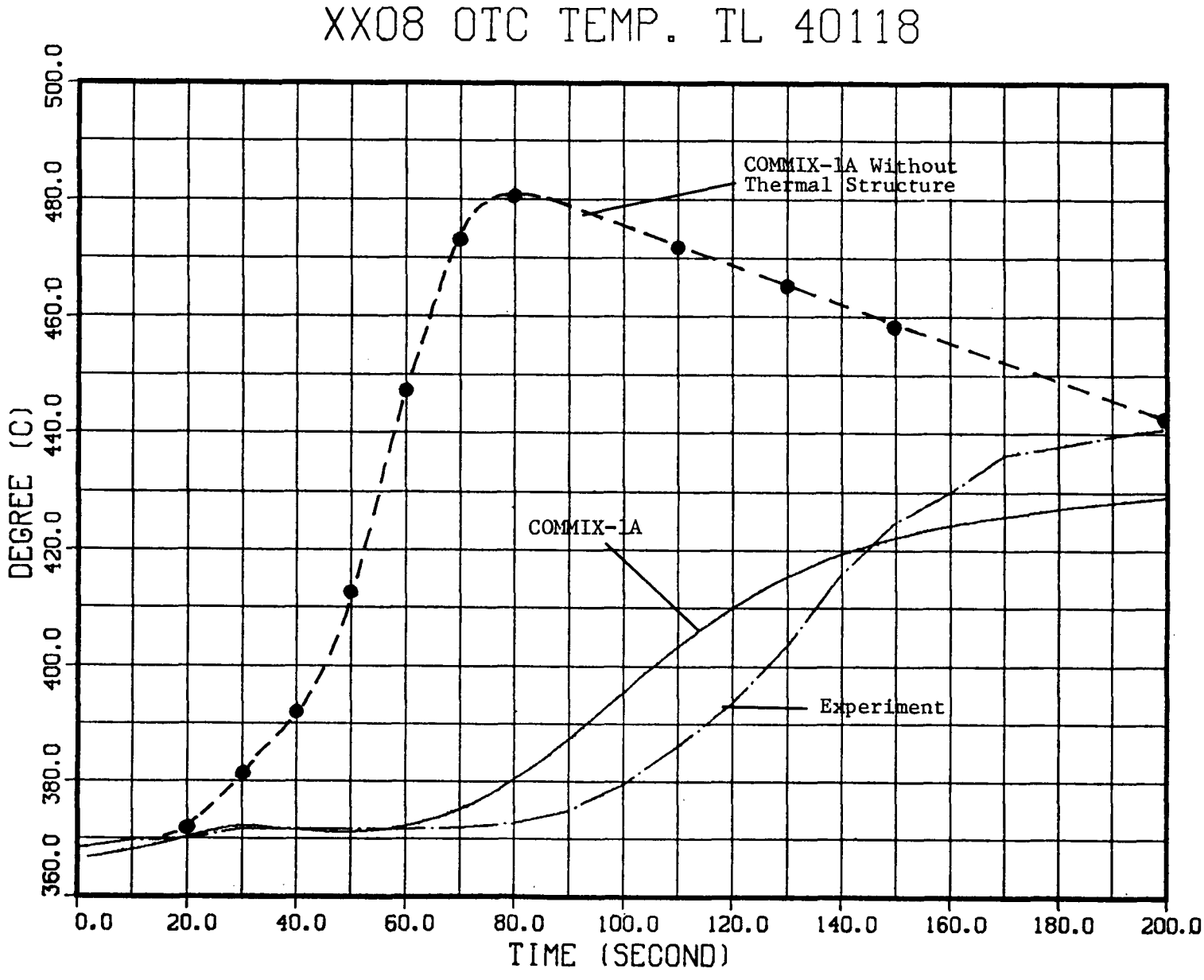

Fig. 17. Outlet Temperatures for Driver Subassembly XX08

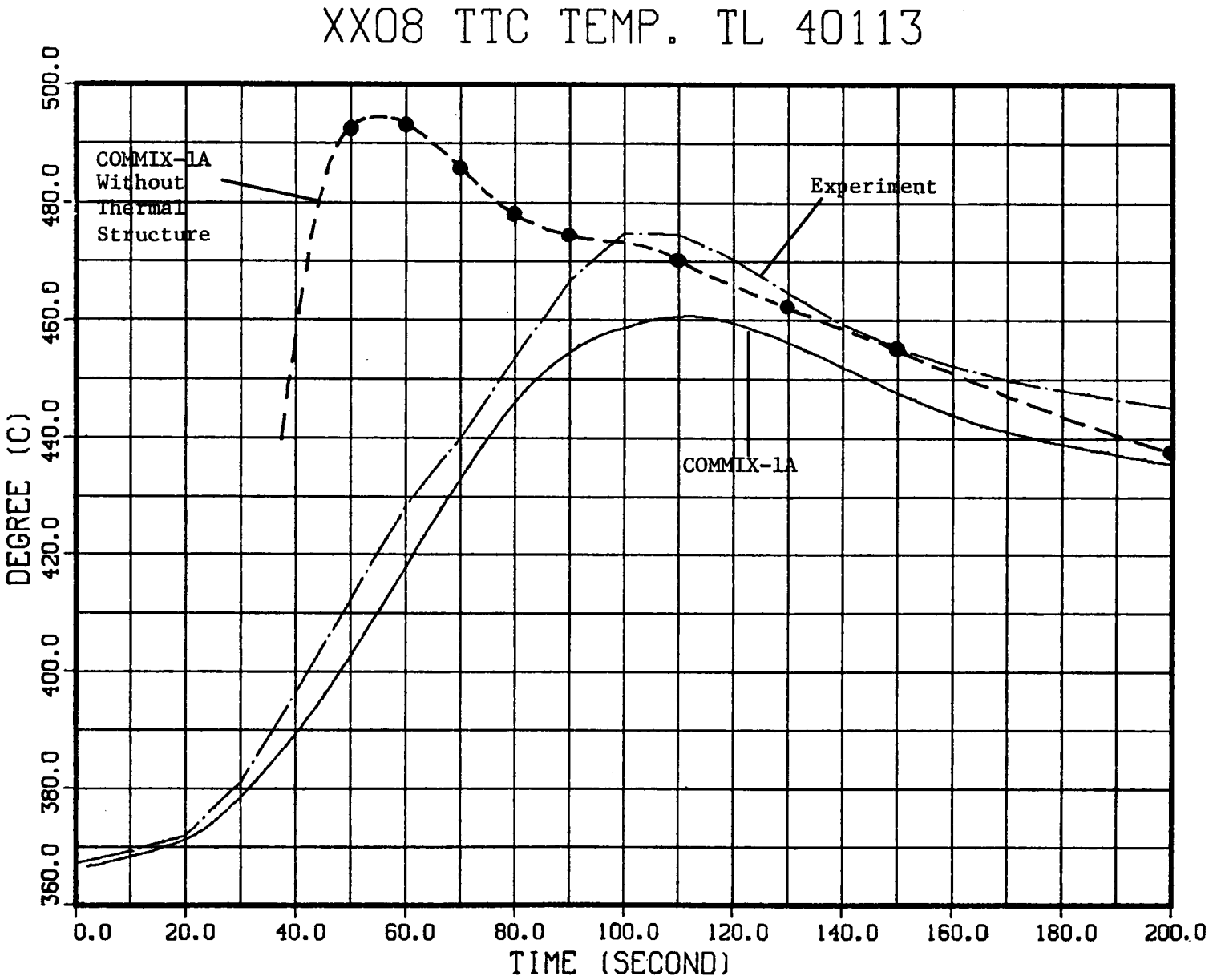

Fig. 18. Top-of-Core Temperatures for Driver Subassembly XX08

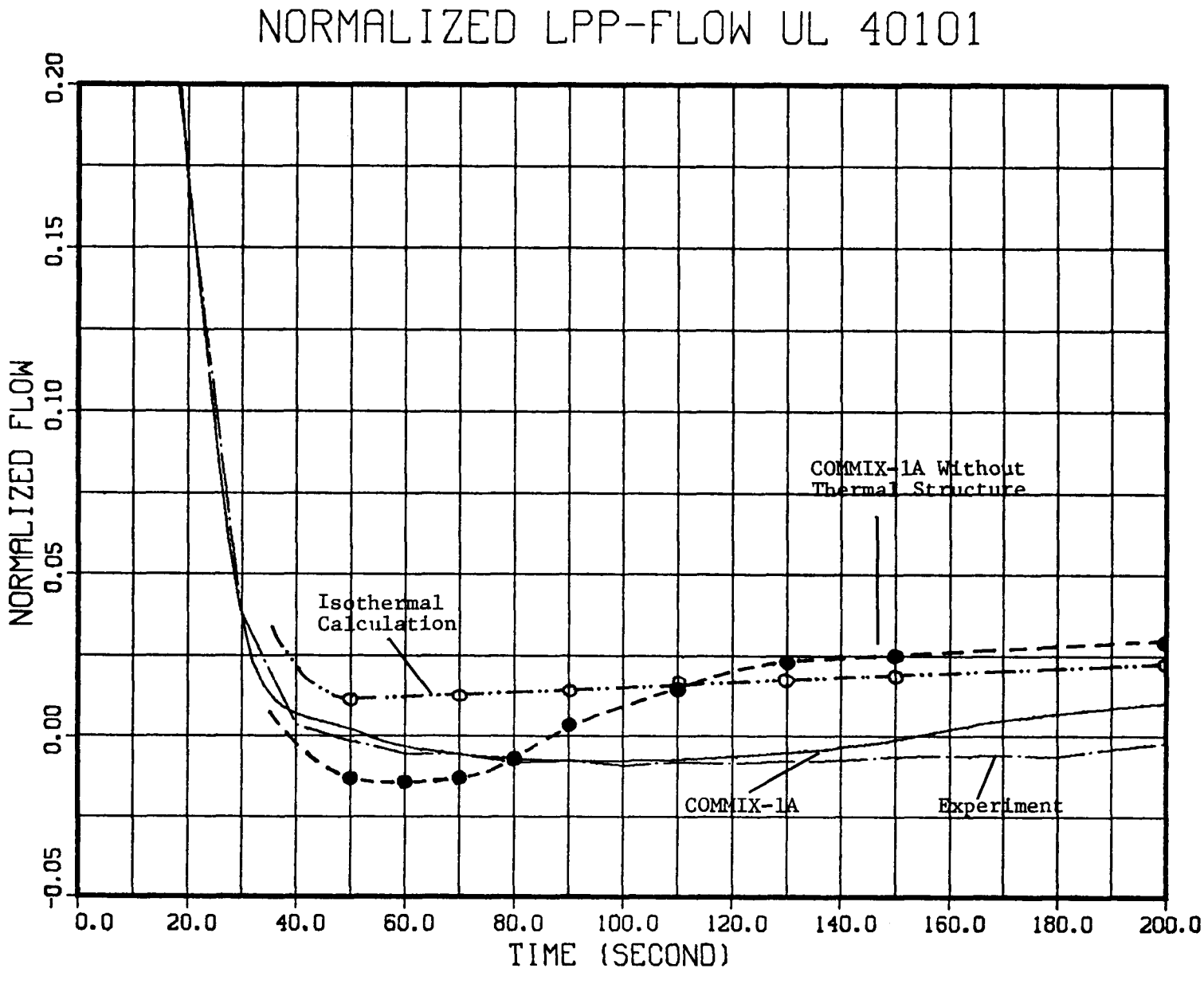

Fig. 19. Low-Pressure Plenum Mass Flow

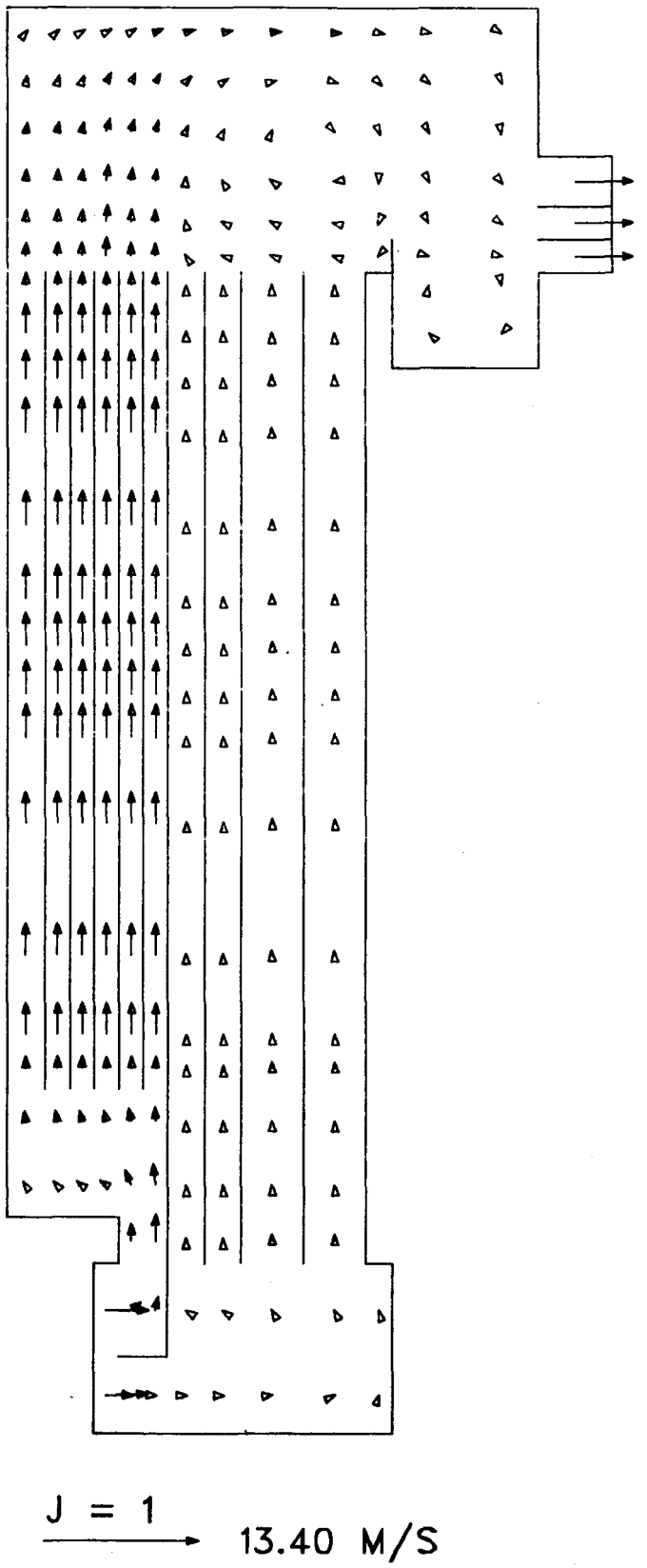

Fig. 20. Velocity Distribution at Time = 2 s

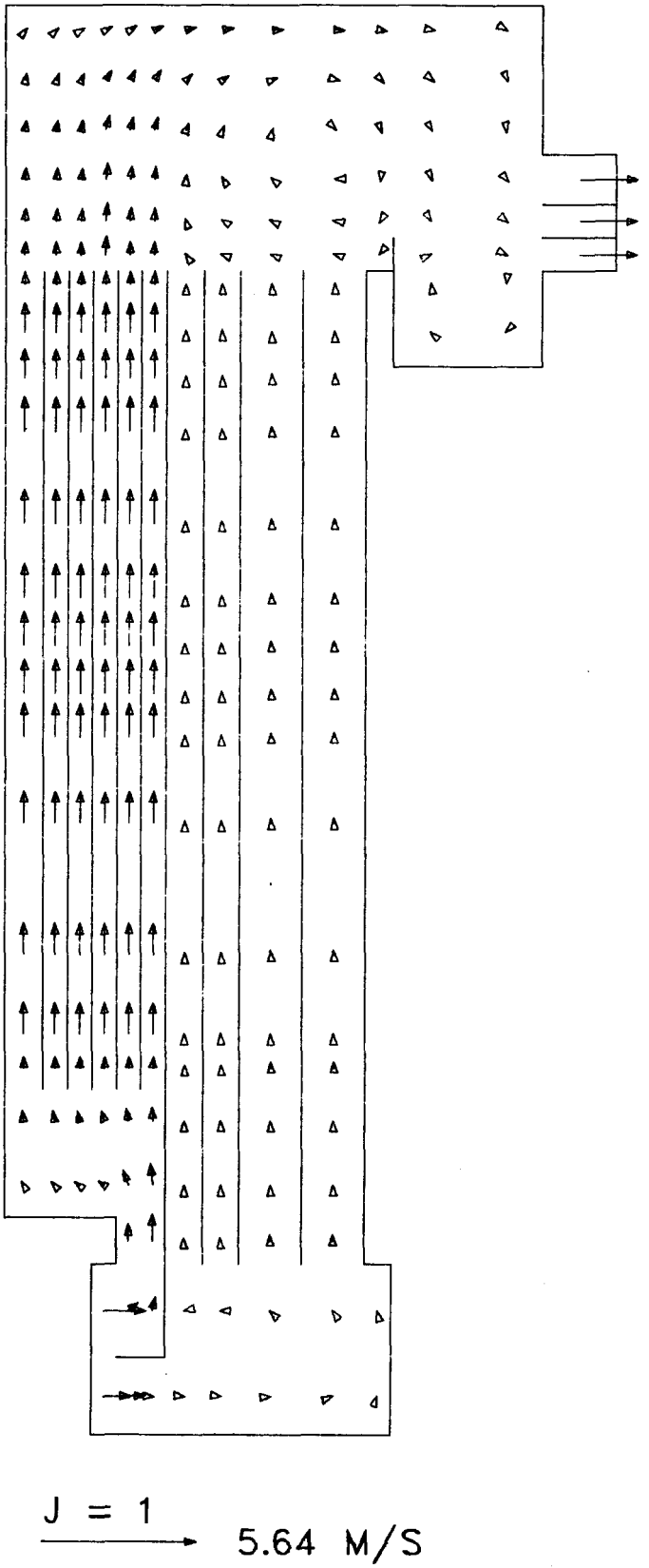

Fig. 21. Velocity Distribution at Time = 10 s

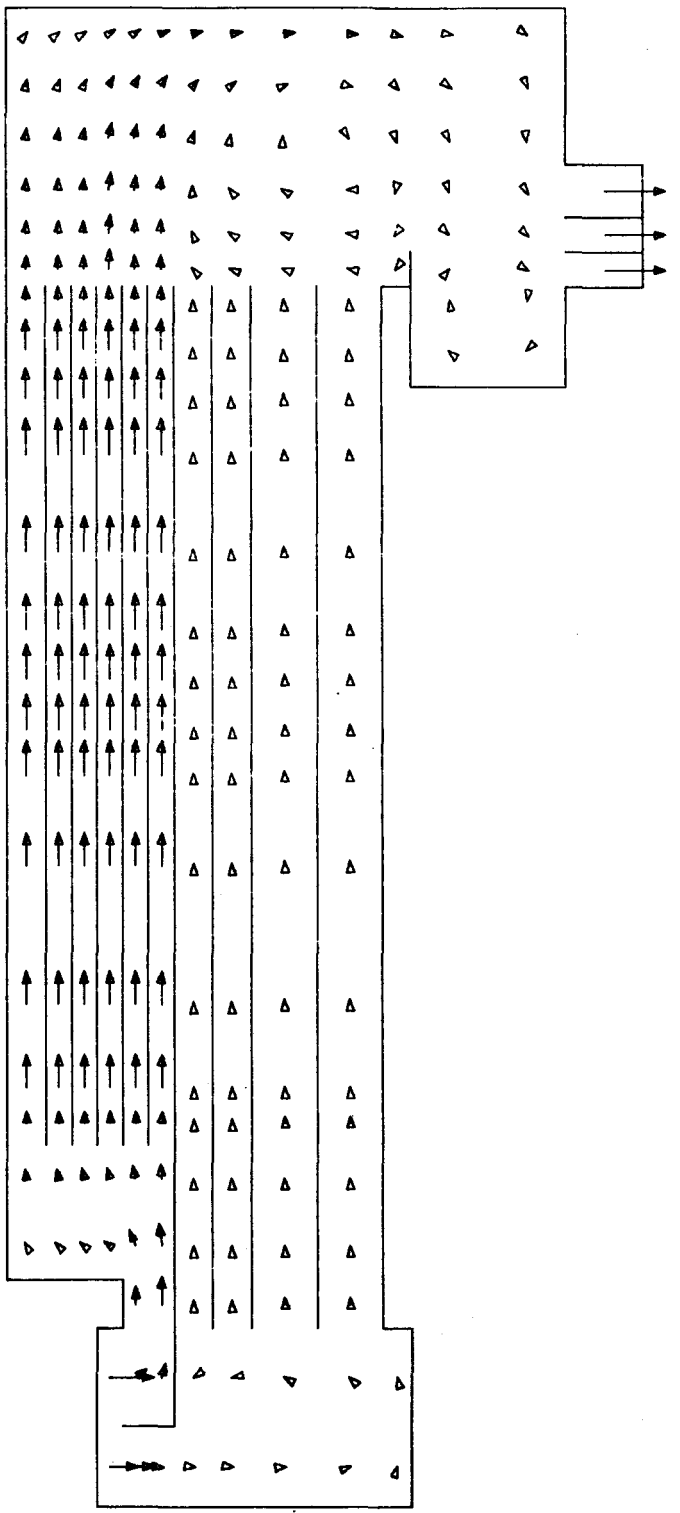

Fig. 22. Velocity Distribution at Time = 20 s

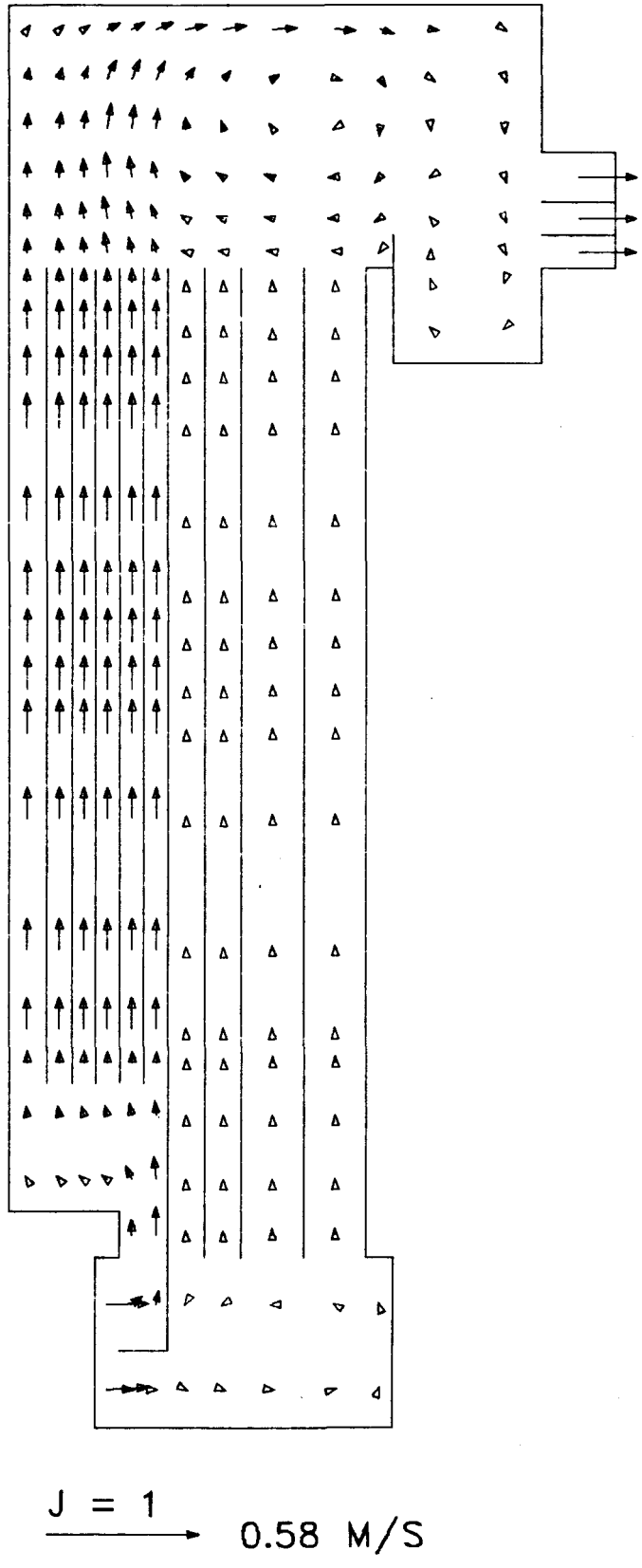

Fig. 23. Velocity Distribution at Time = 30 s

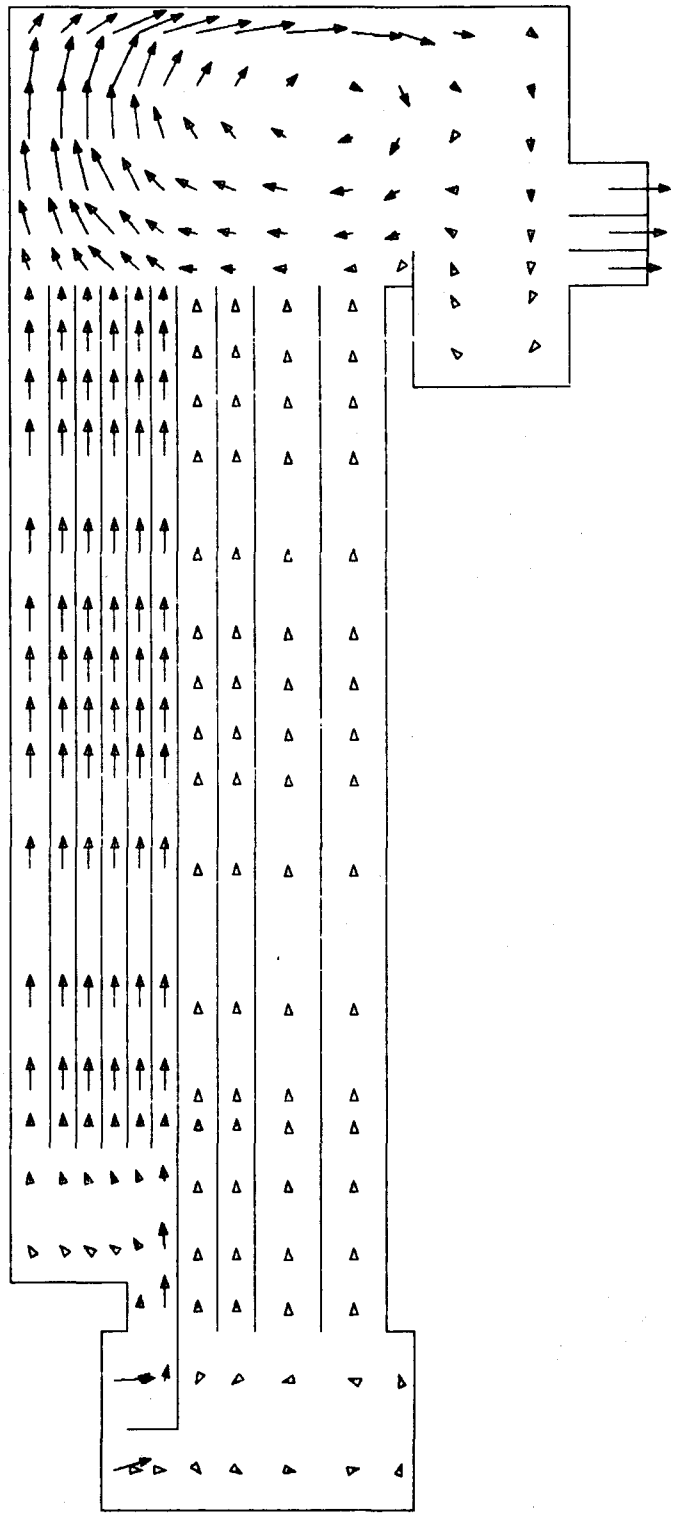

Fig. 24. Velocity Distribution at Time = 40 s

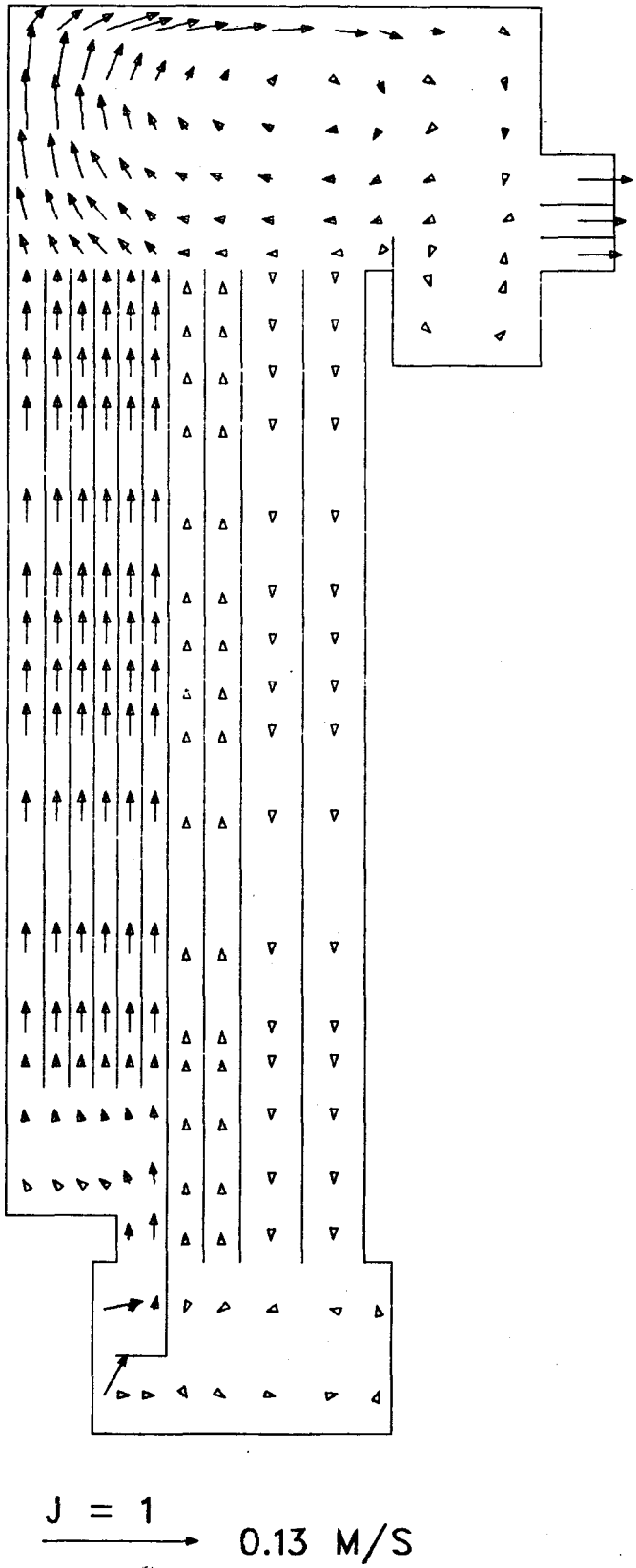

Fig. 25. Velocity Distribution at Time = 50 s

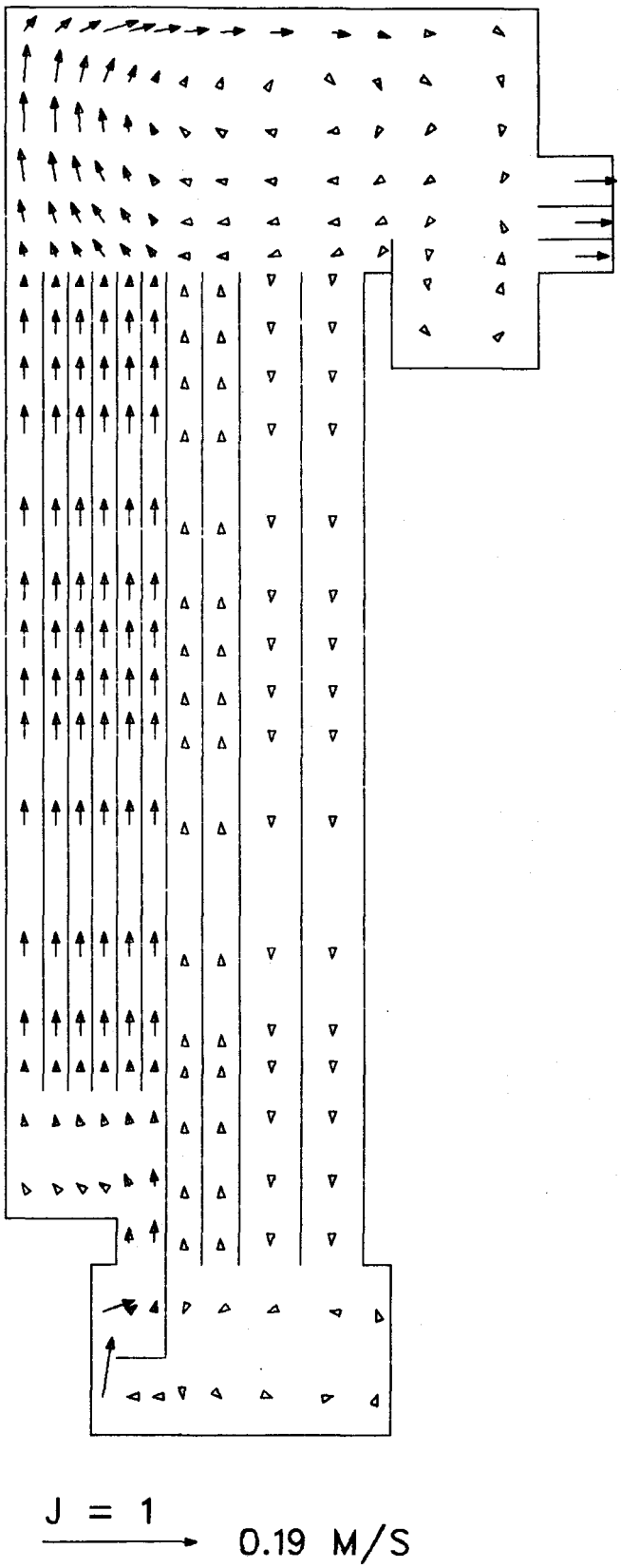

Fig. 26. Velocity Distribution at Time = 60 s

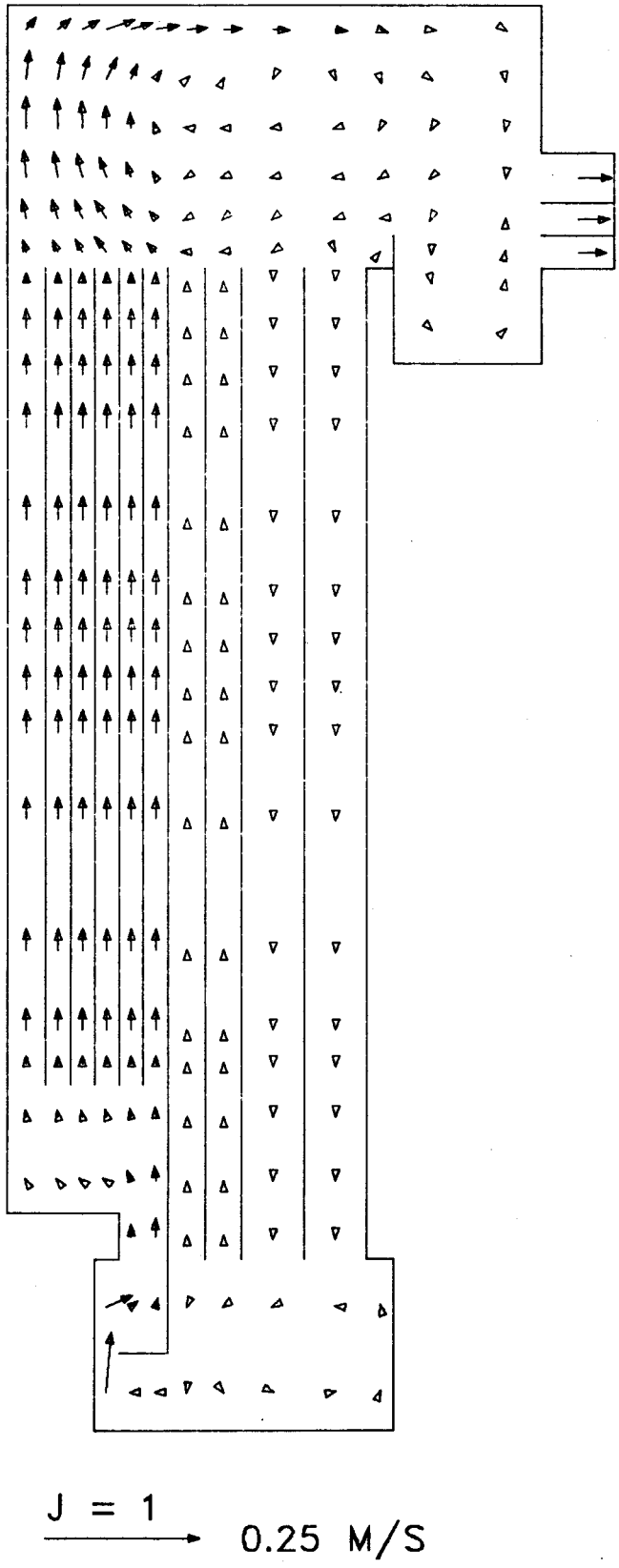

Fig. 27. Velocity Distribution at Time = 70 s

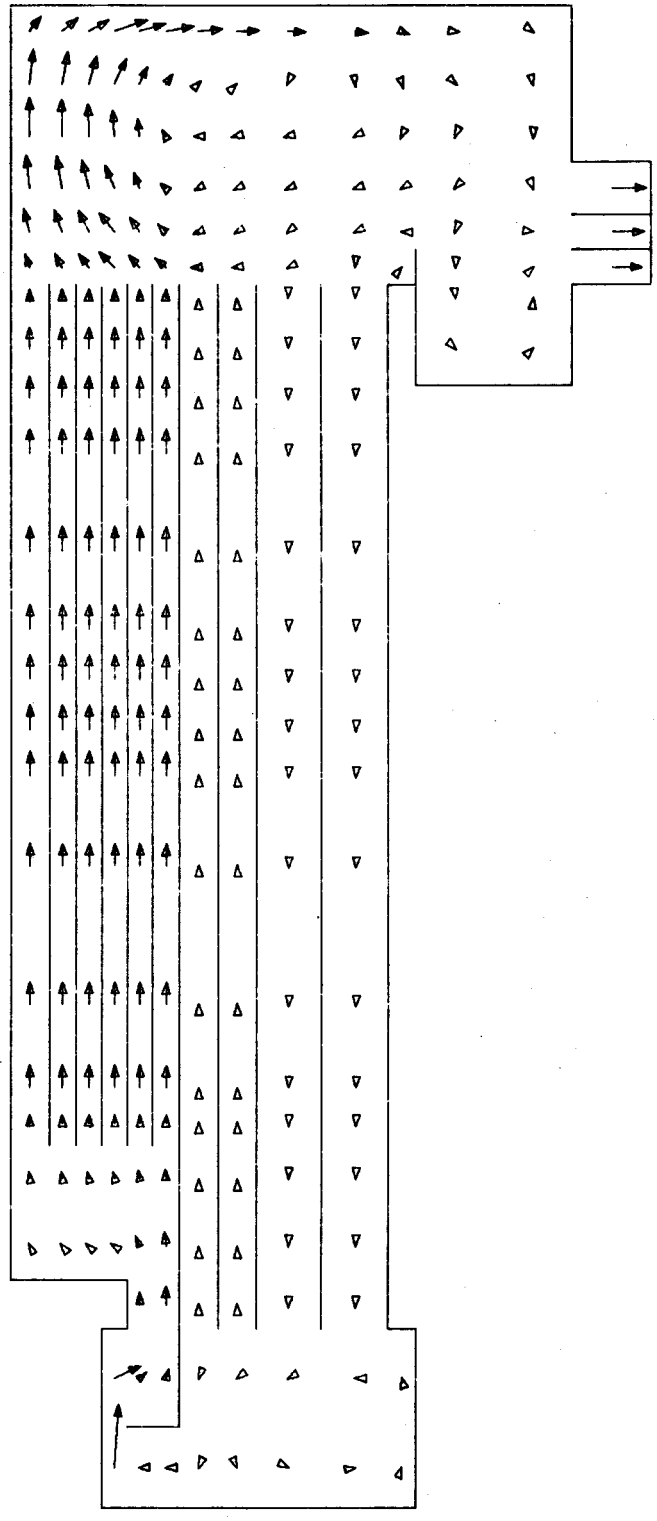

Fig. 28. Velocity Distribution at Time = 80 s

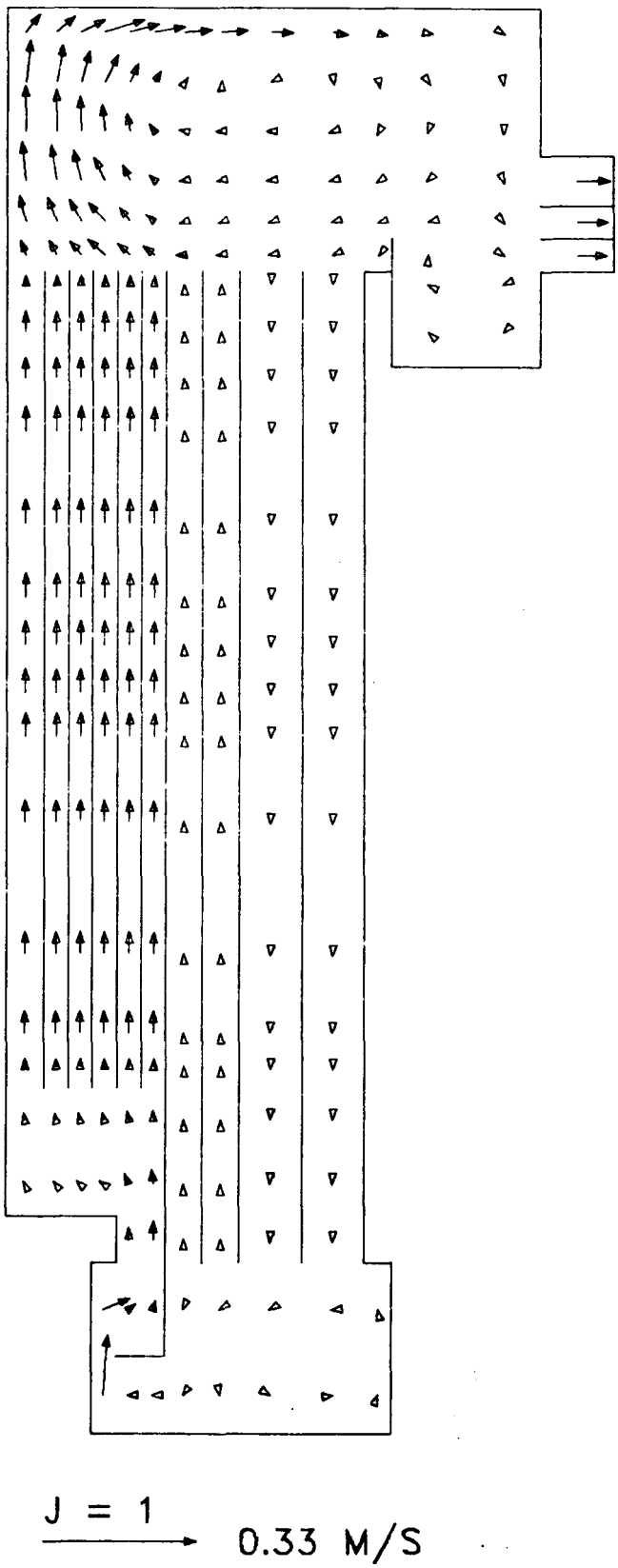

Fig. 29. Velocity Distribution at Time = 90 s

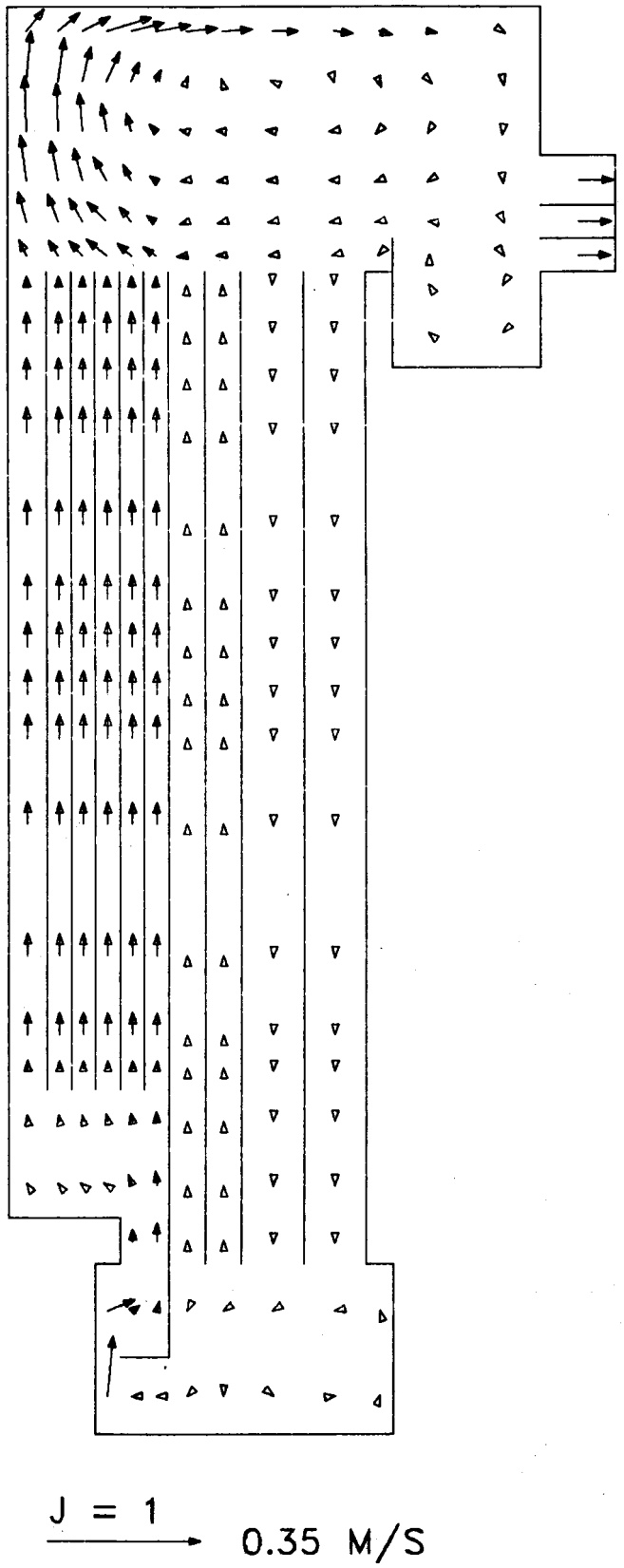

Fig. 30. Velocity Distribution at Time = 100 s

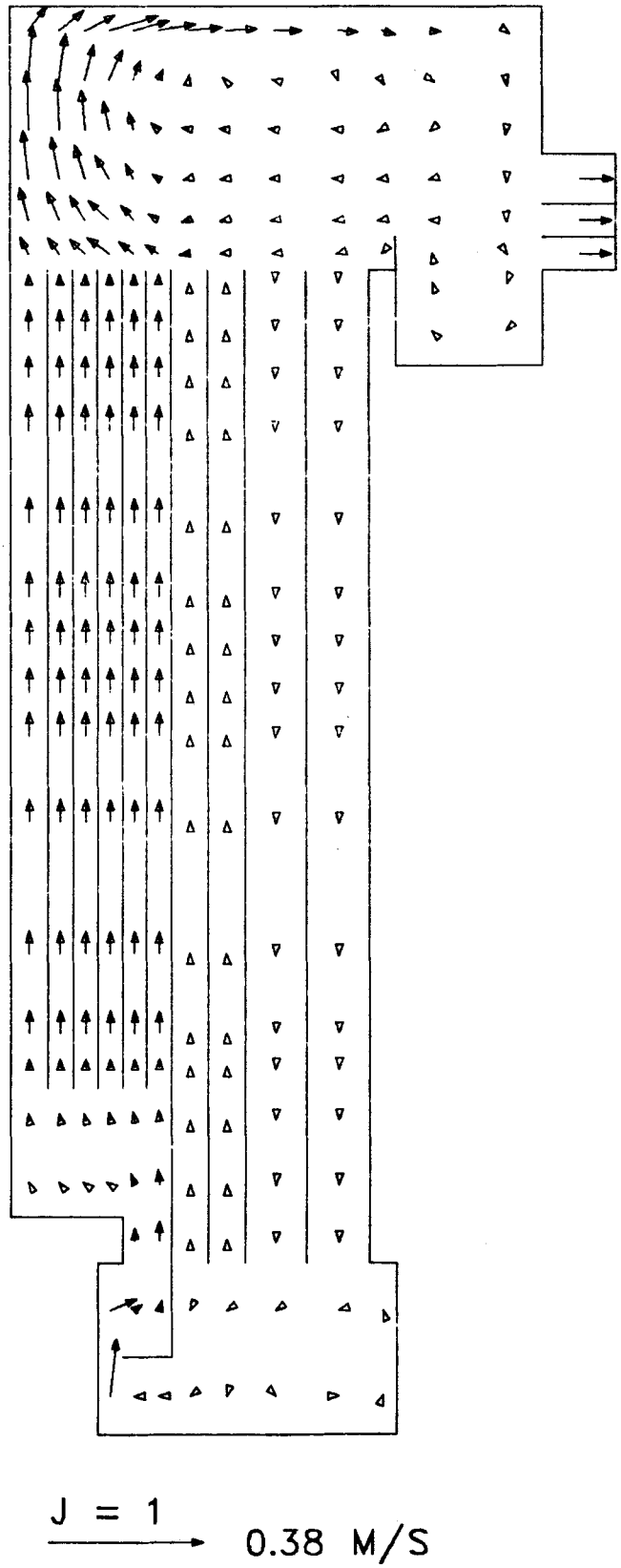

Fig. 31. Velocity Distribution at Time = 110 s

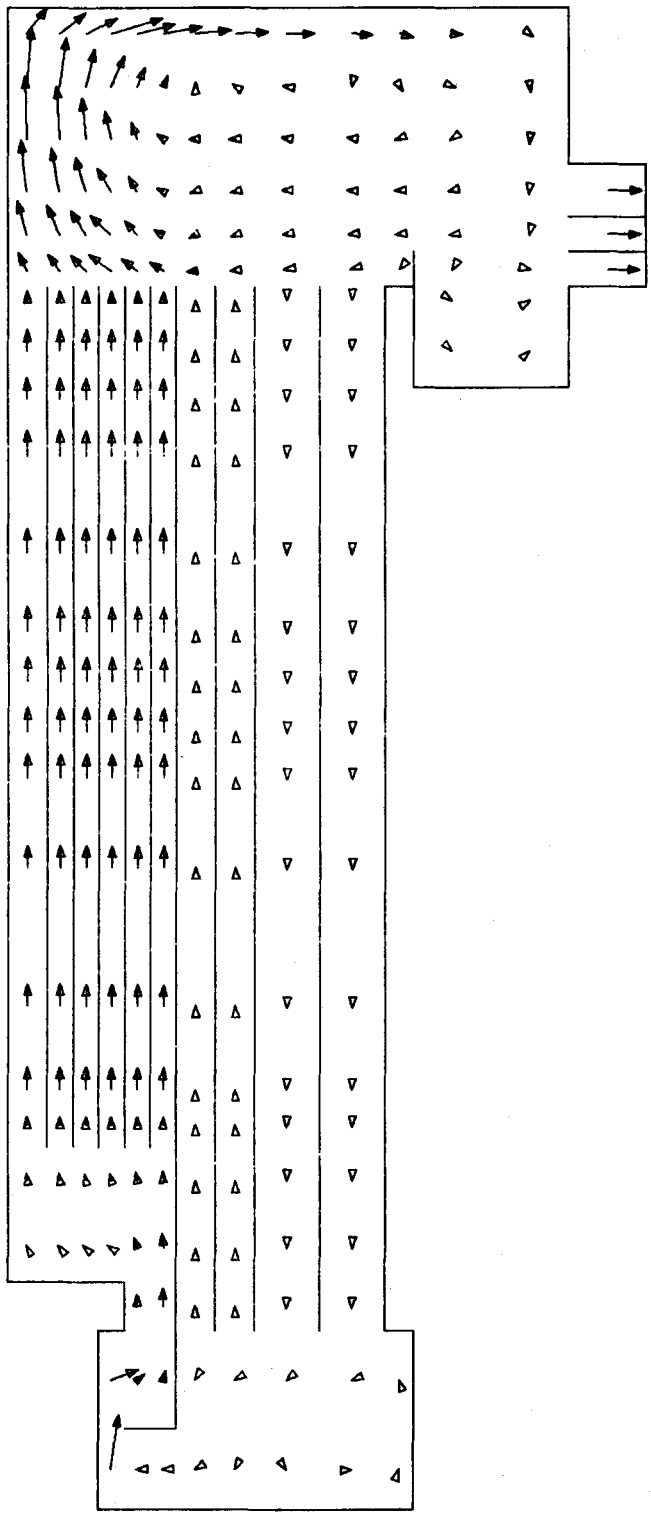

Fig. 32. Velocity Distribution at Time = 120 s

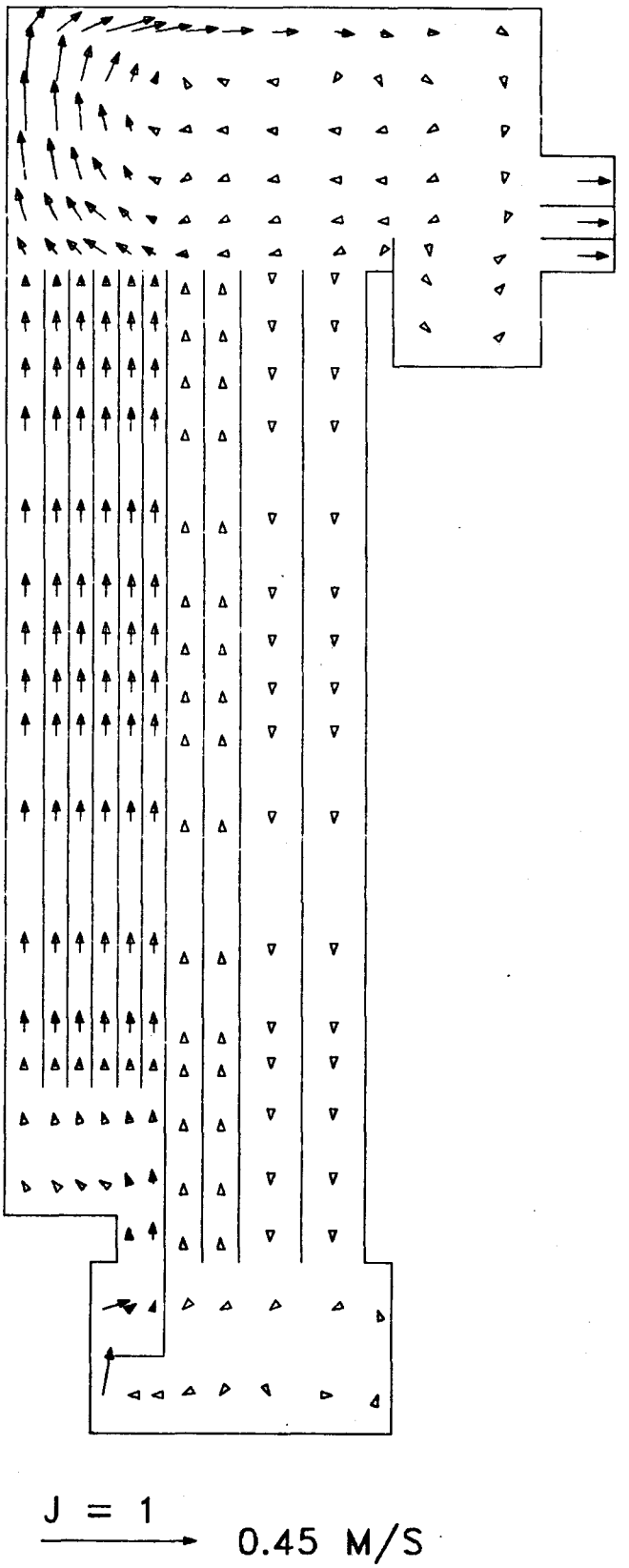

Fig. 33. Velocity Distribution at Time = 130 s

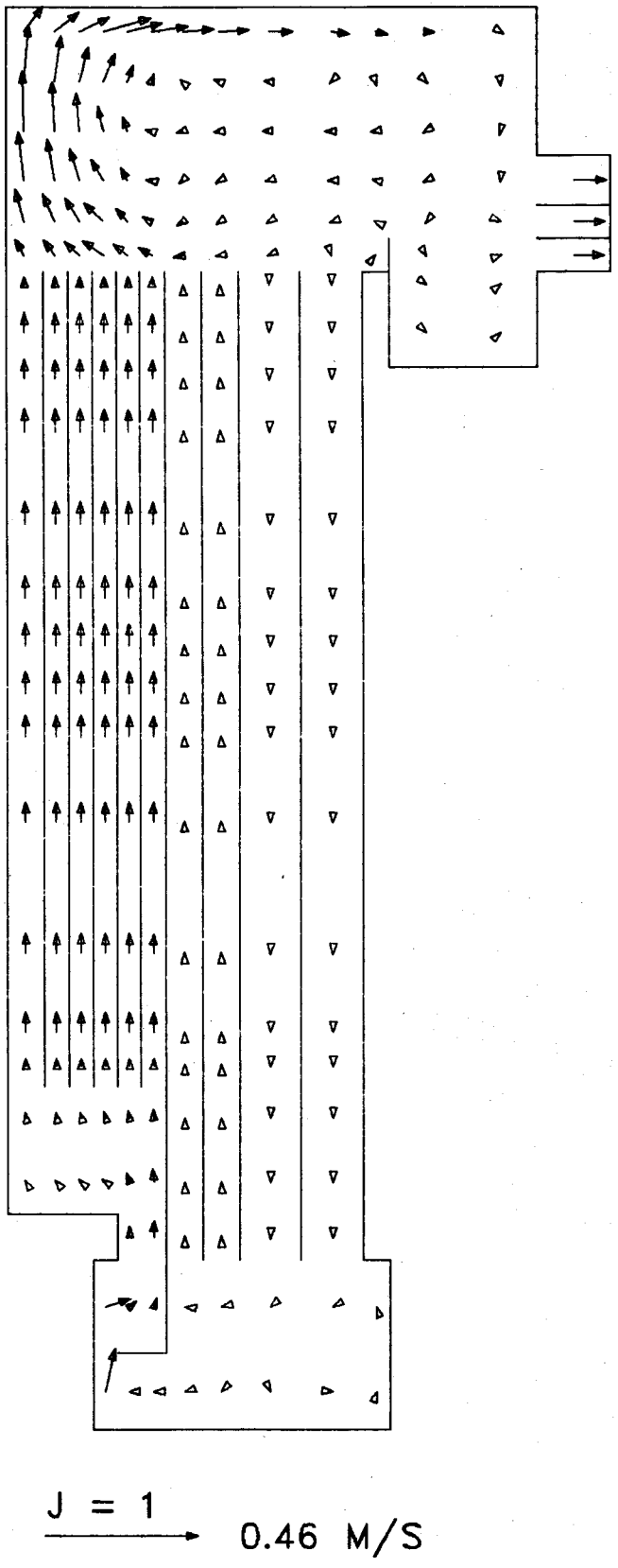

Fig. 34. Velocity Distribution at Time = 140 s

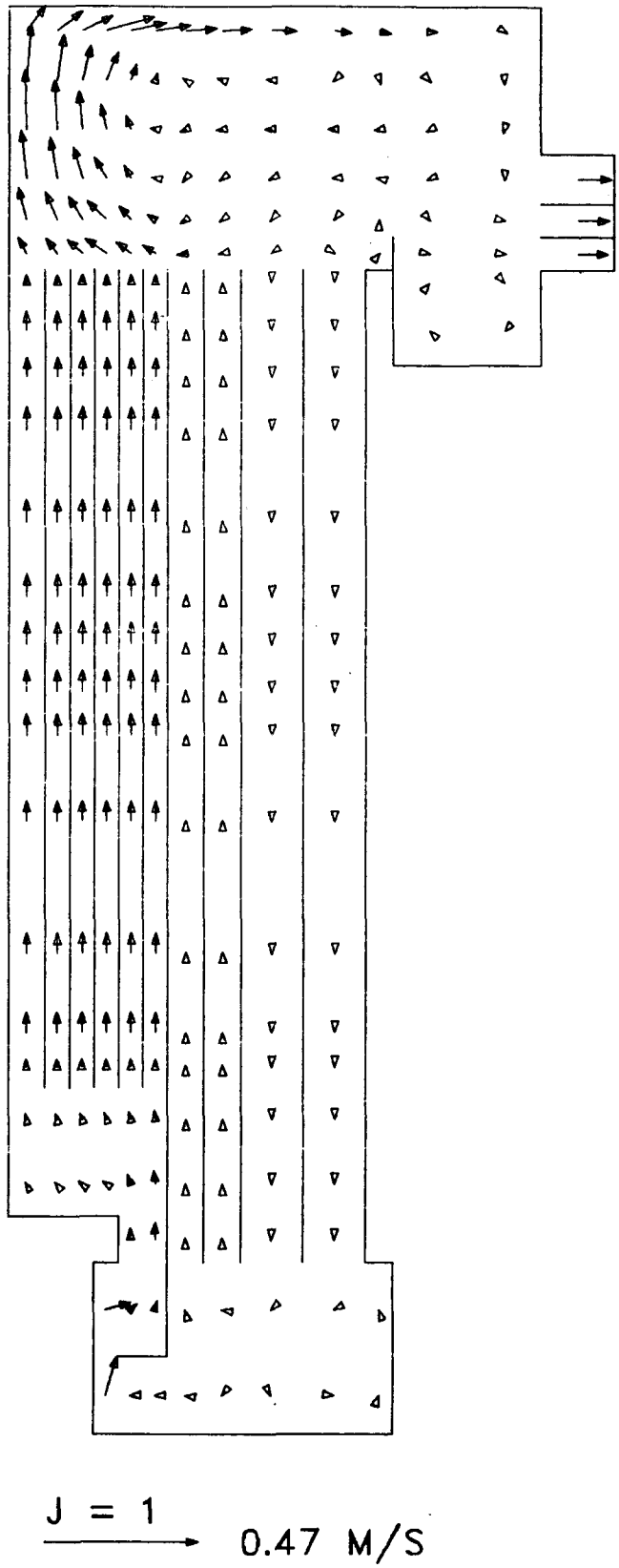

Fig. 35. Velocity Distribution at Time 150 s

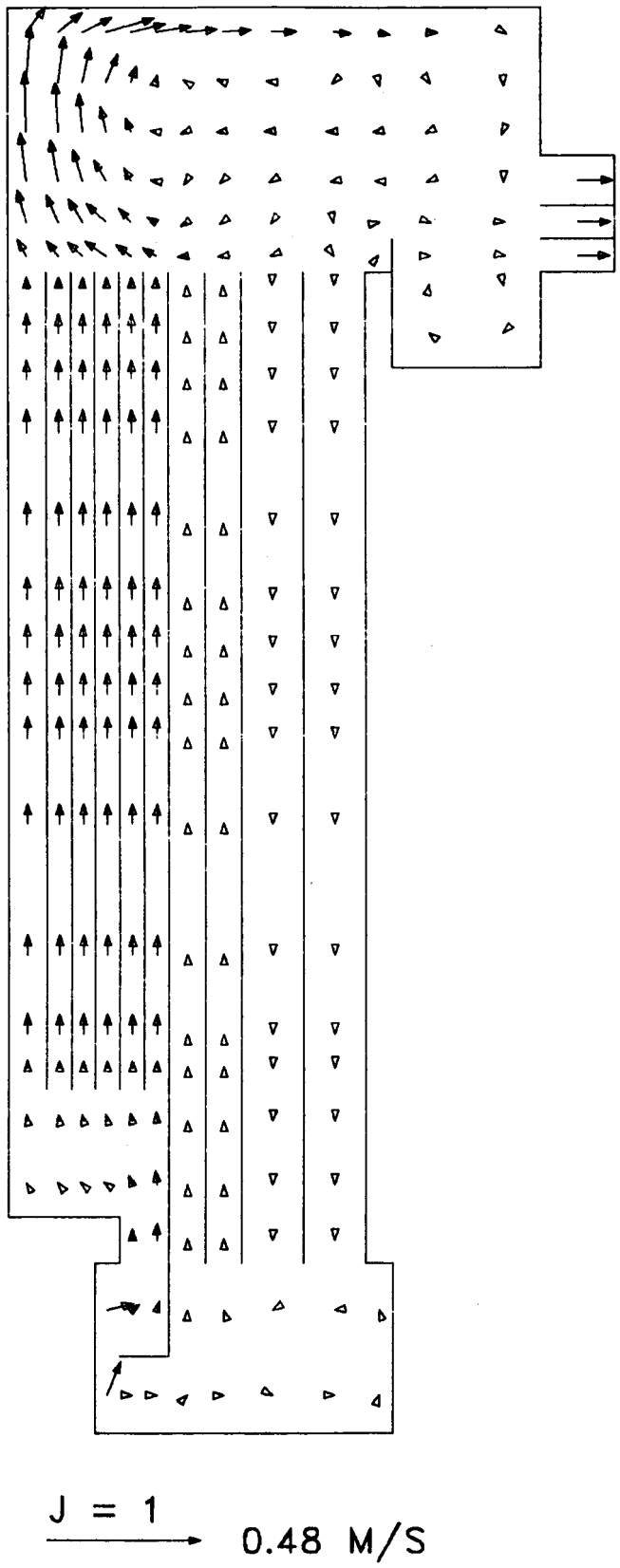

Fig. 36. Velocity Distribution at Time = 160 s

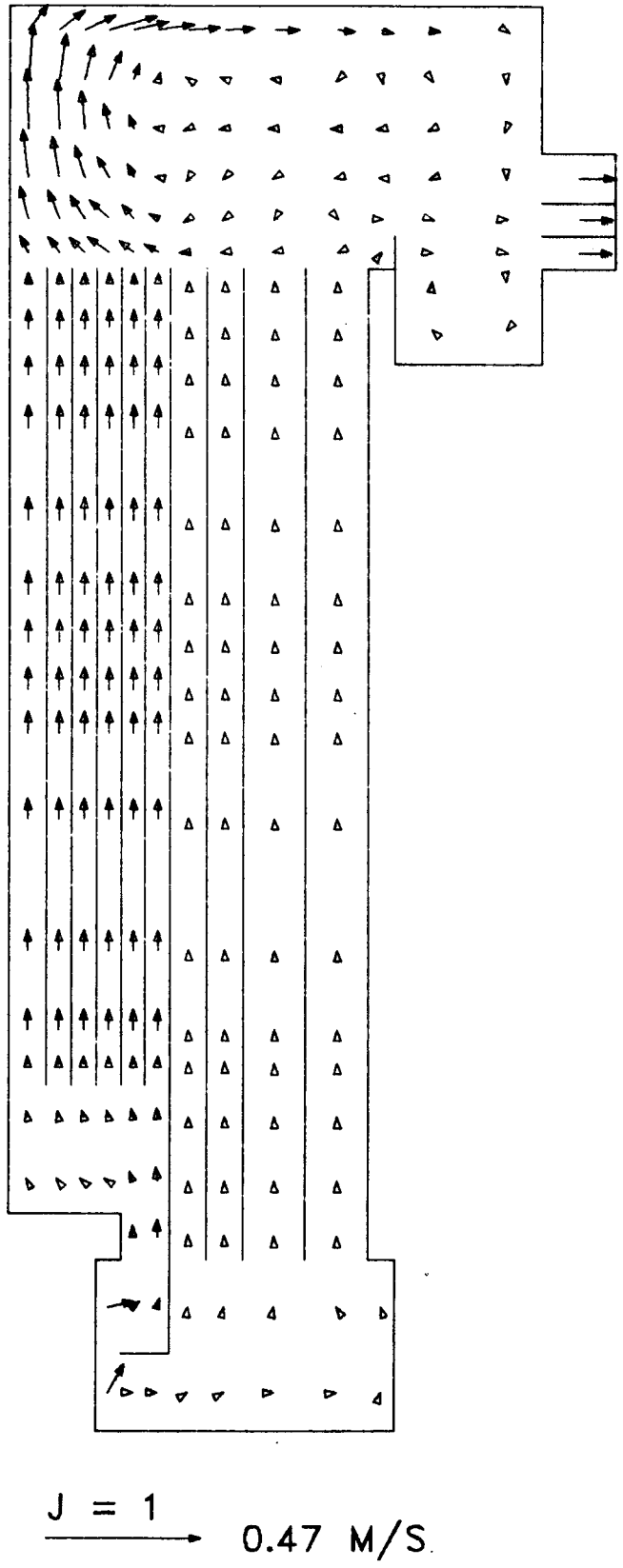

Fig. 37. Velocity Distribution at Time = 170 s

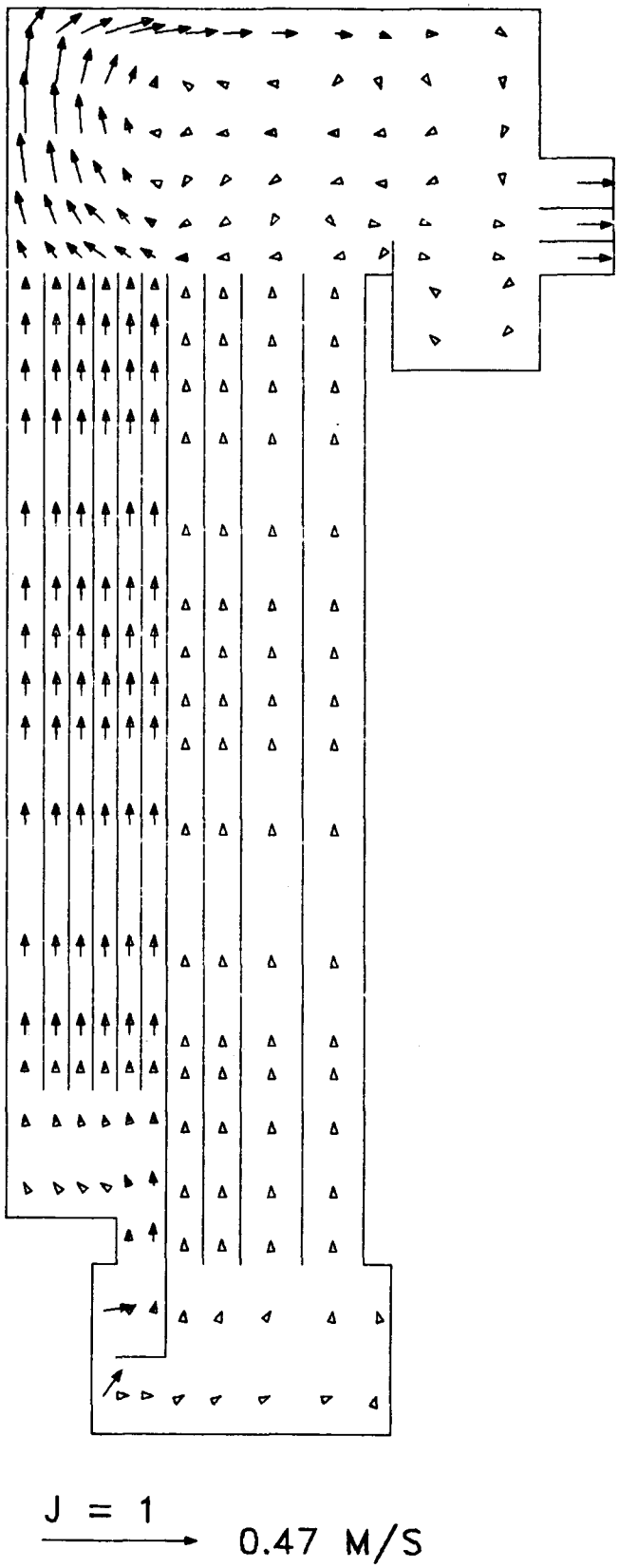

Fig. 38. Velocity Distribution at Time = 180 s

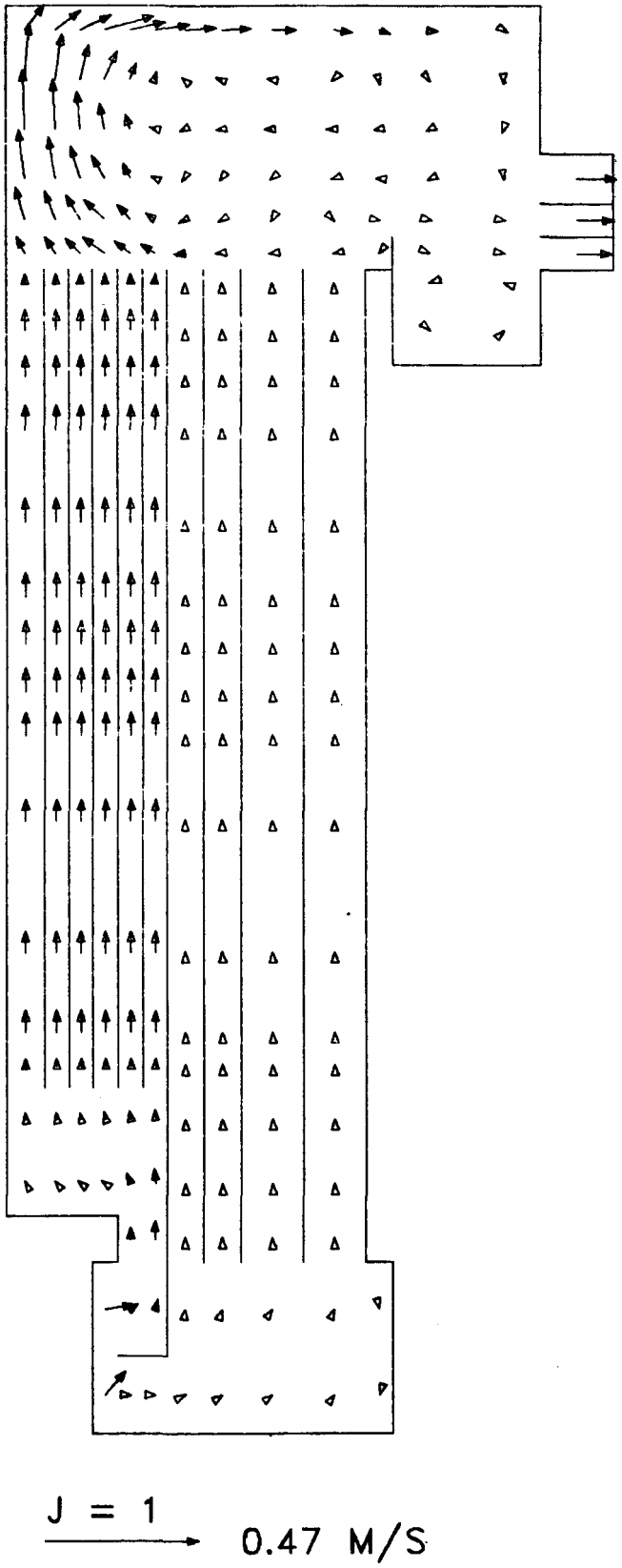

Fig. 39. Velocity Distribution at Time = 190 s

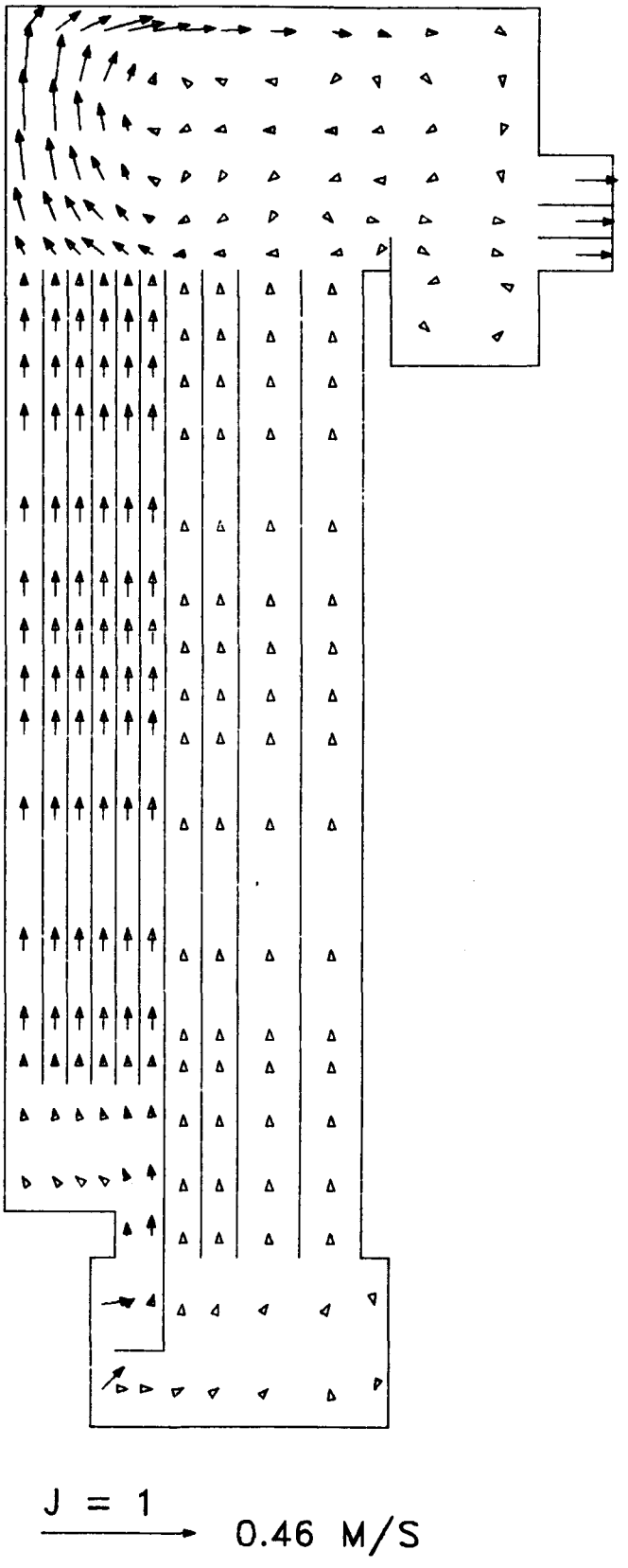

Fig. 40. Velocity Distribution at Time = 200 s

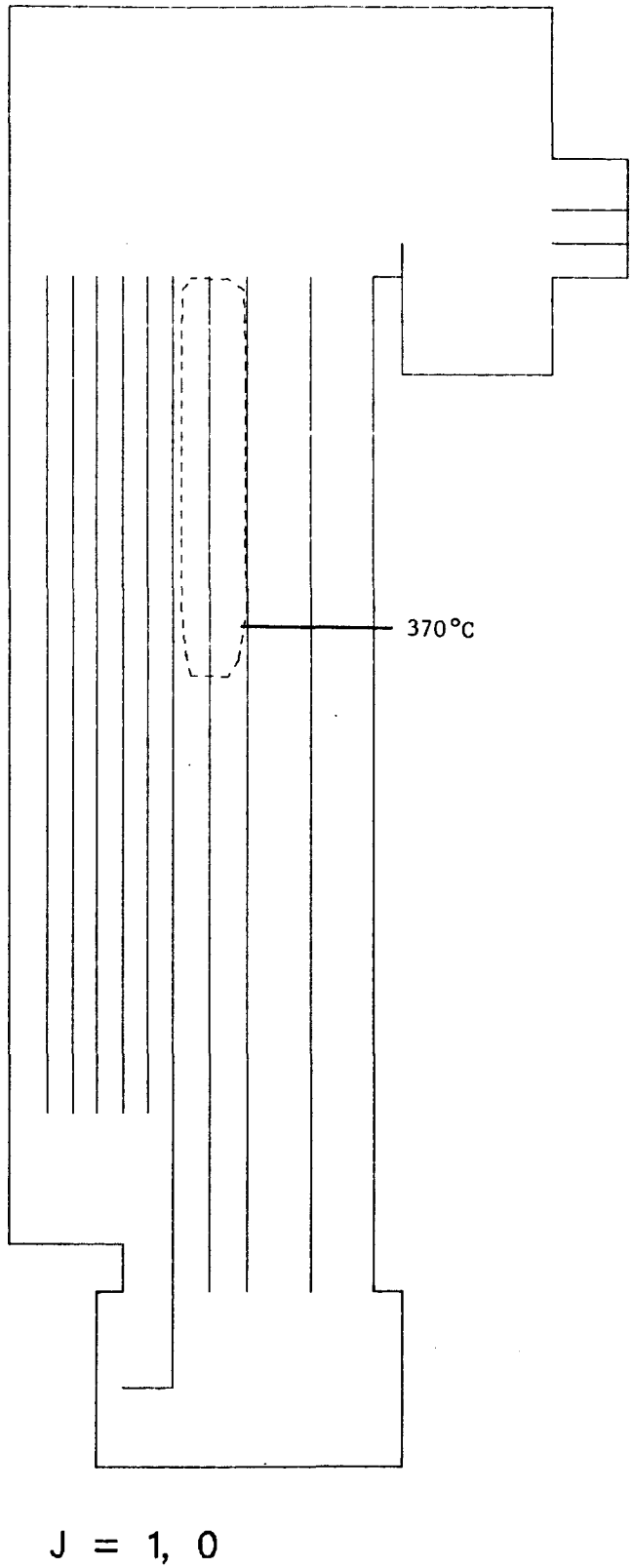

Fig. 41. Temperature Distribution at Time = 2 s

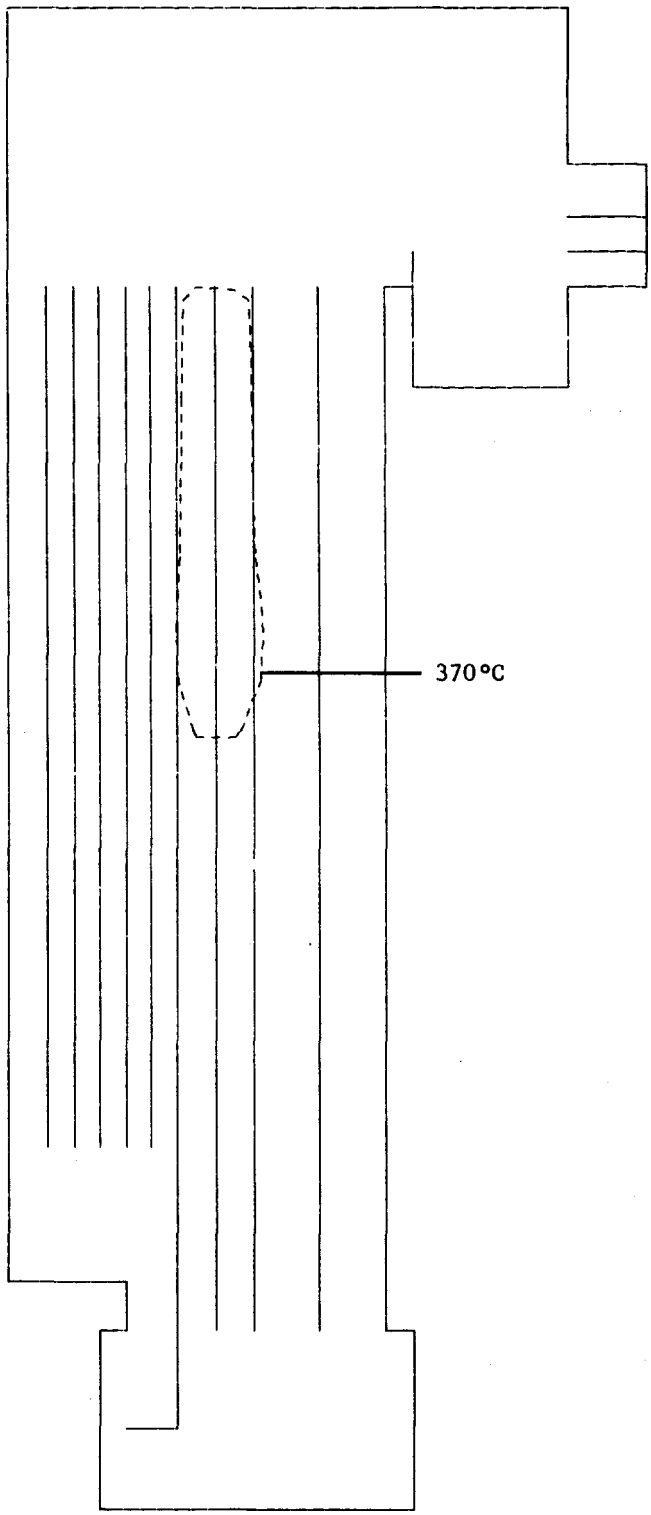

Fig. 42. Temperature Distribution at Time = 10 s

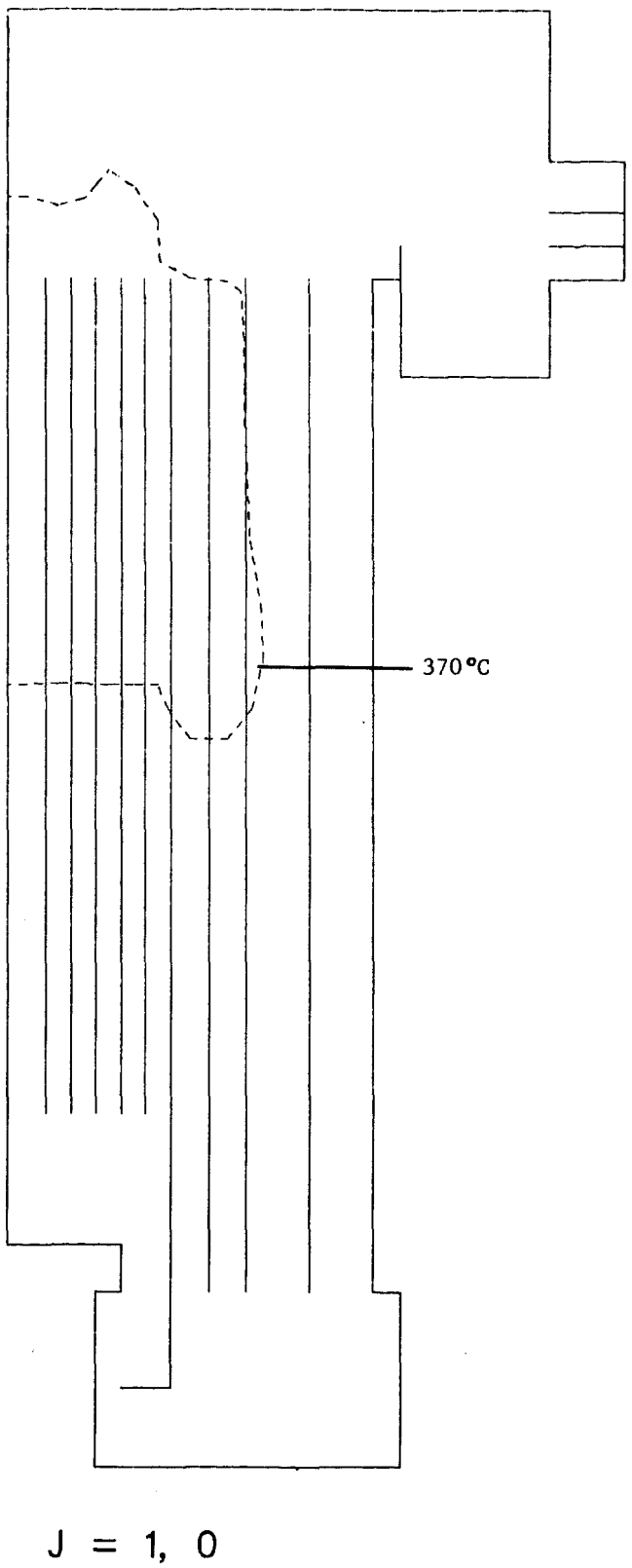

Fig. 43. Temperature Distribution at Time = 20 s

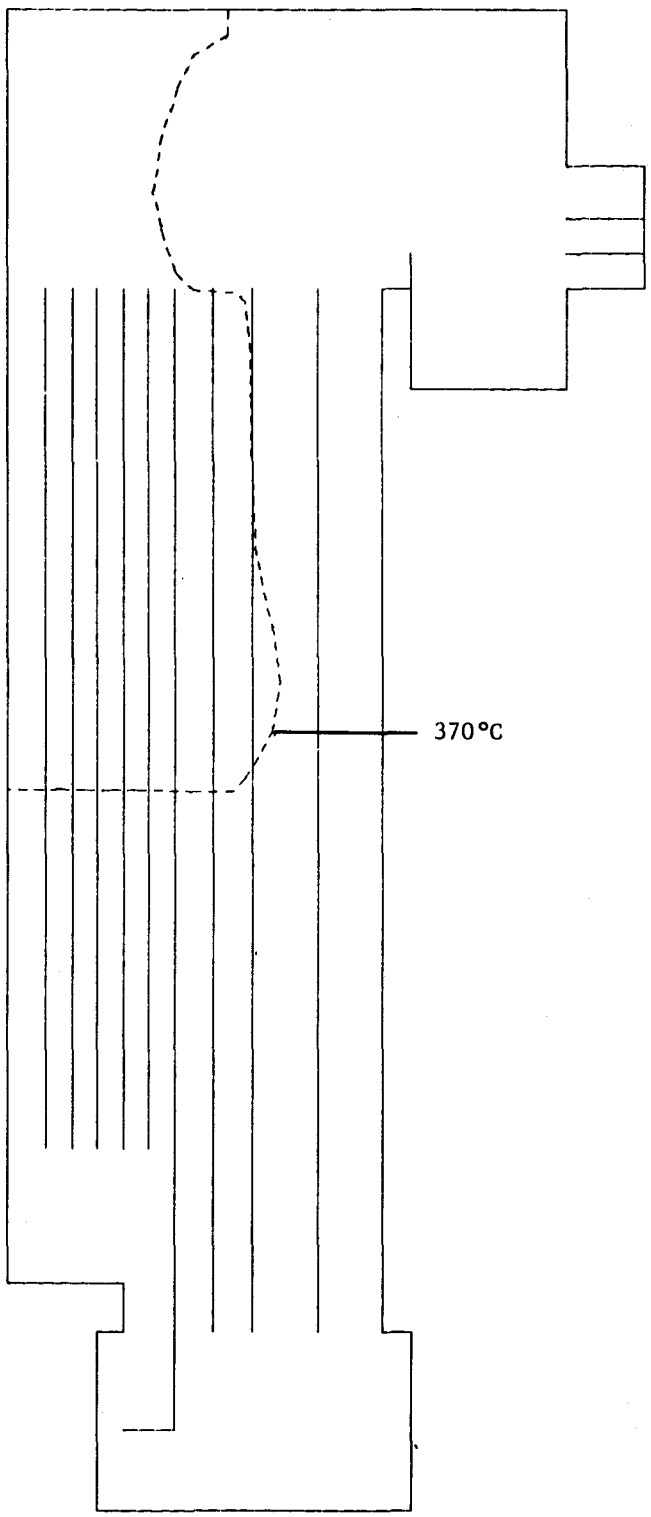

Fig. 44. Temperature Distribution at Time = 30 s

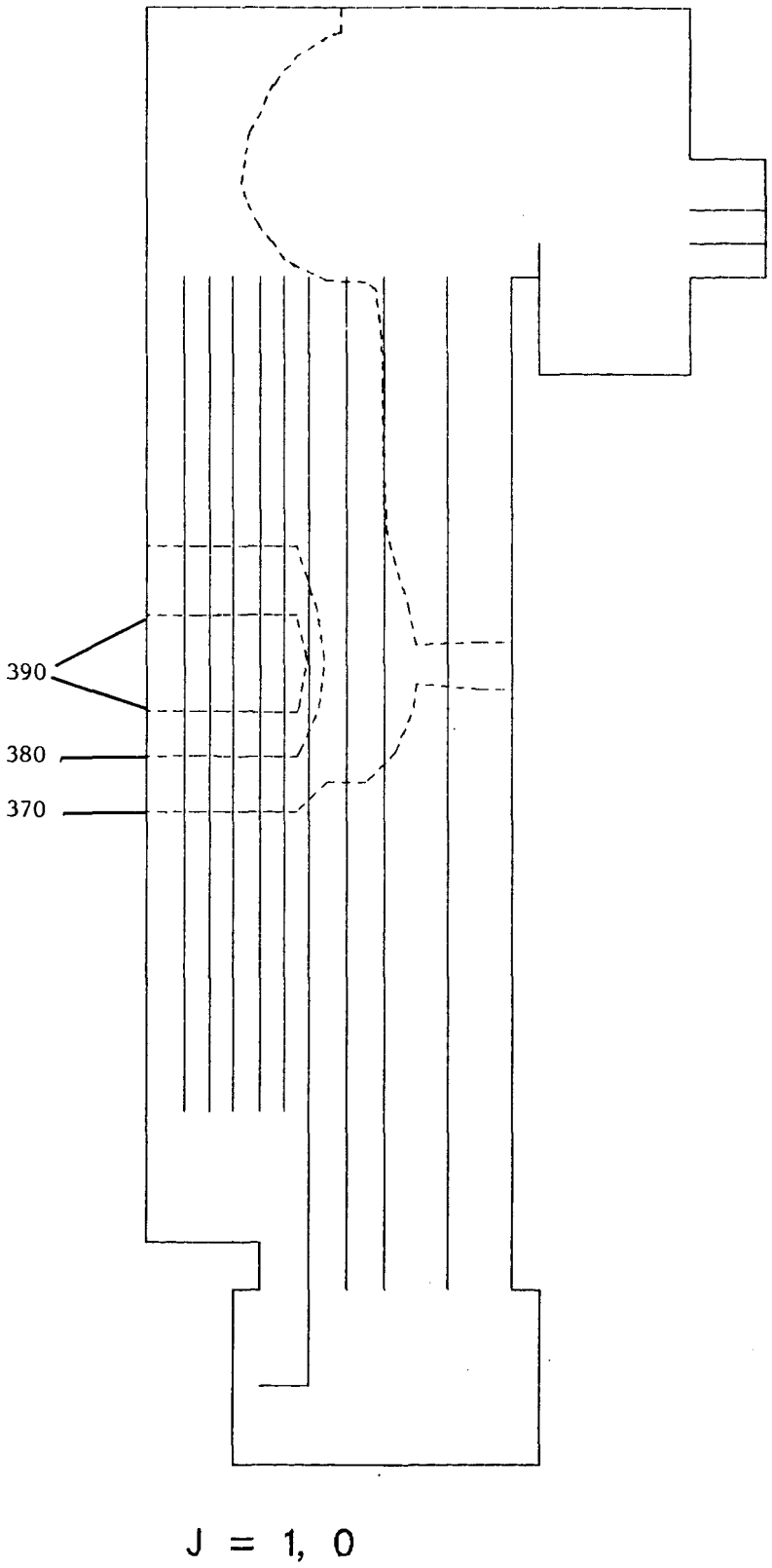

Fig. 45. Temperature Distribution at Time = 40 s

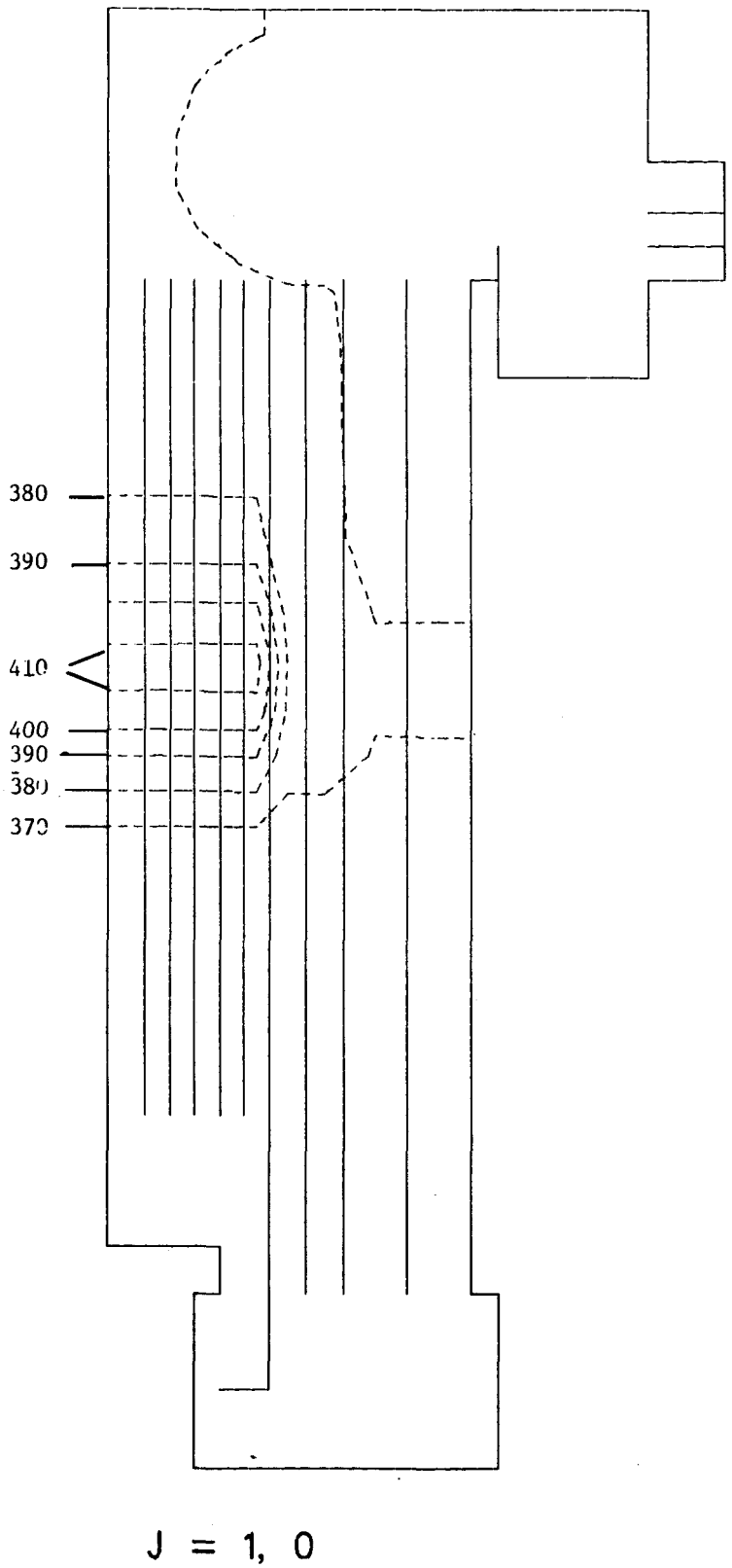

Fig. 46. Temperature Distribution at Time = 50 s

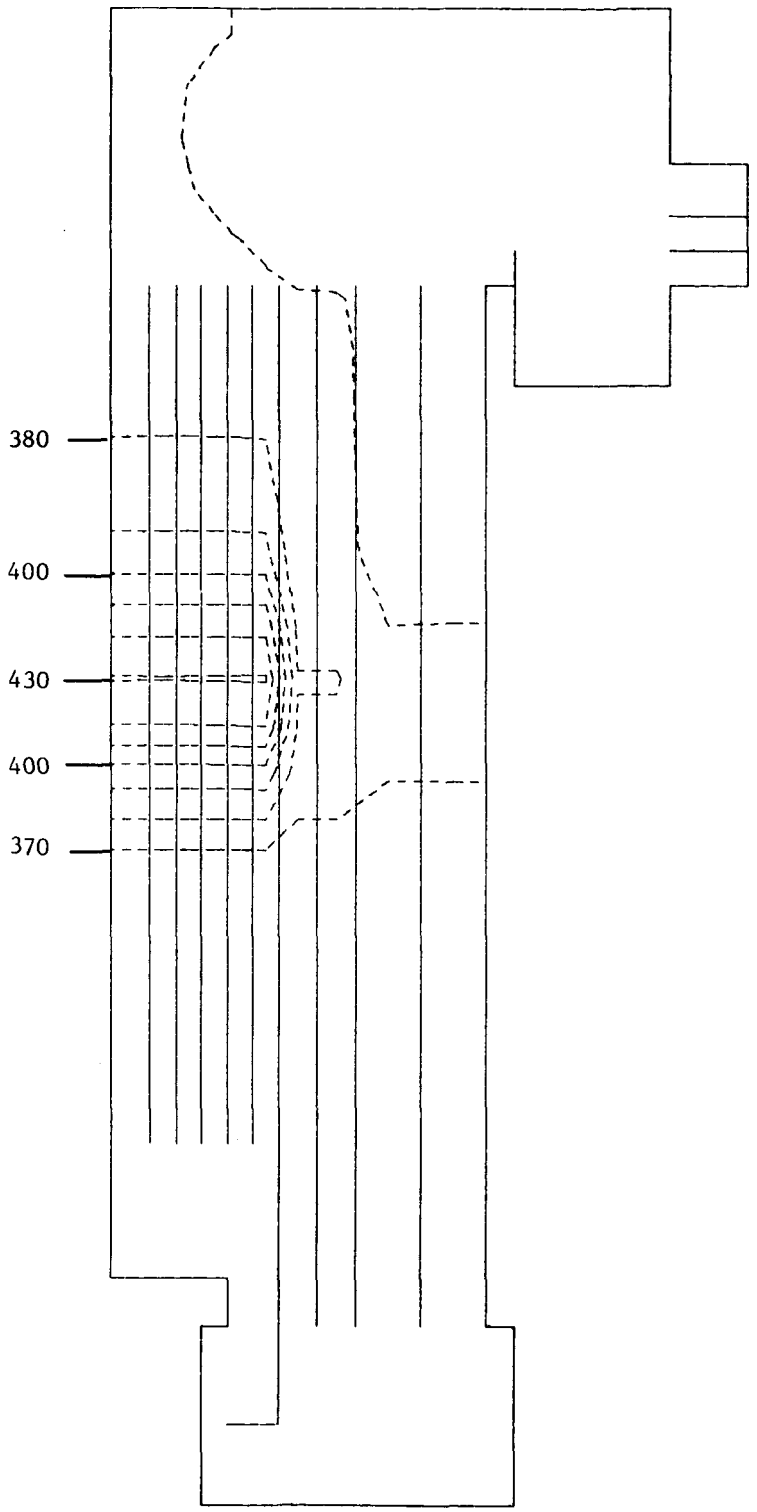

Fig. 47. Temperature Distribution at Time = 60 s

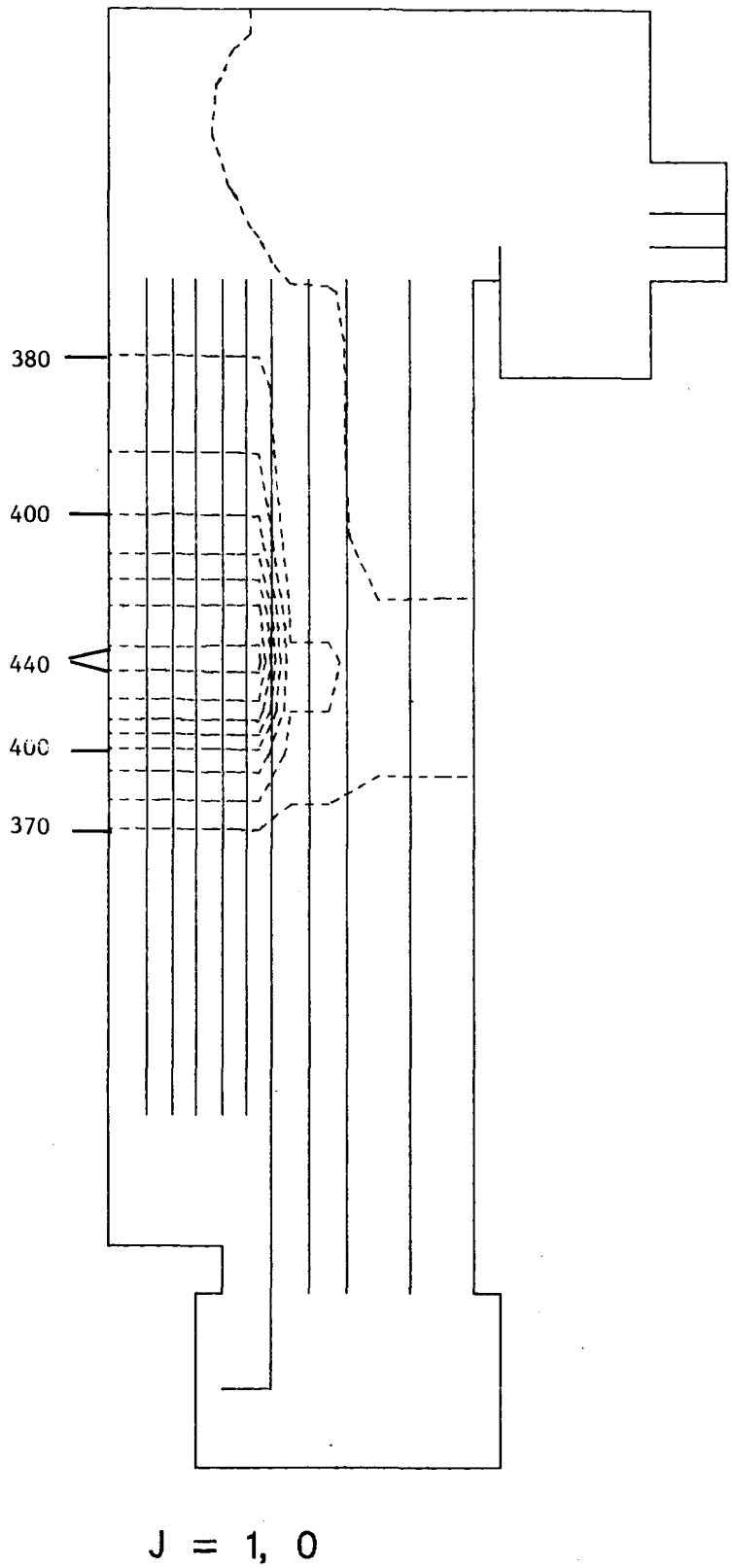

Fig. 48. Temperature Distribution at Time = 70 s

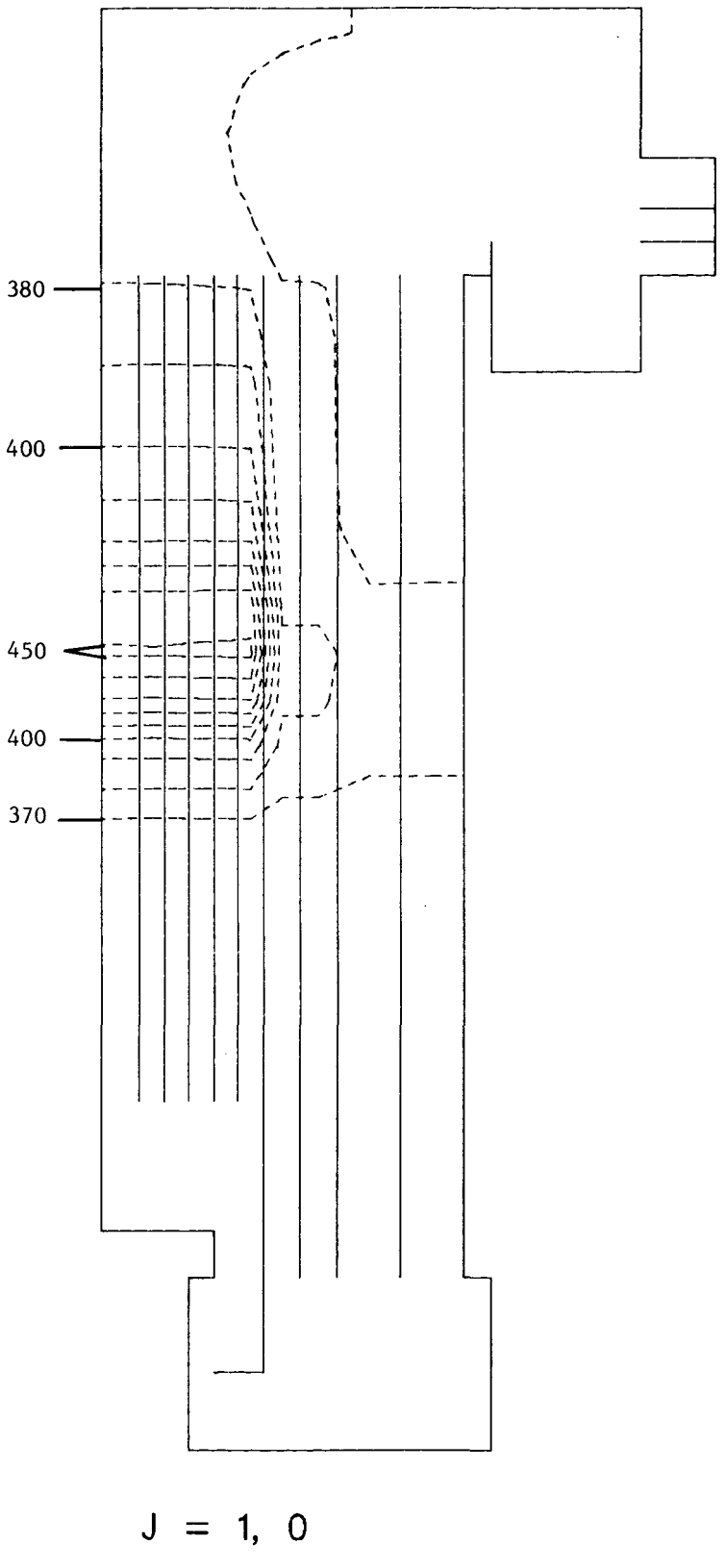

Fig. 49. Temperature Distribution at Time = 80 s

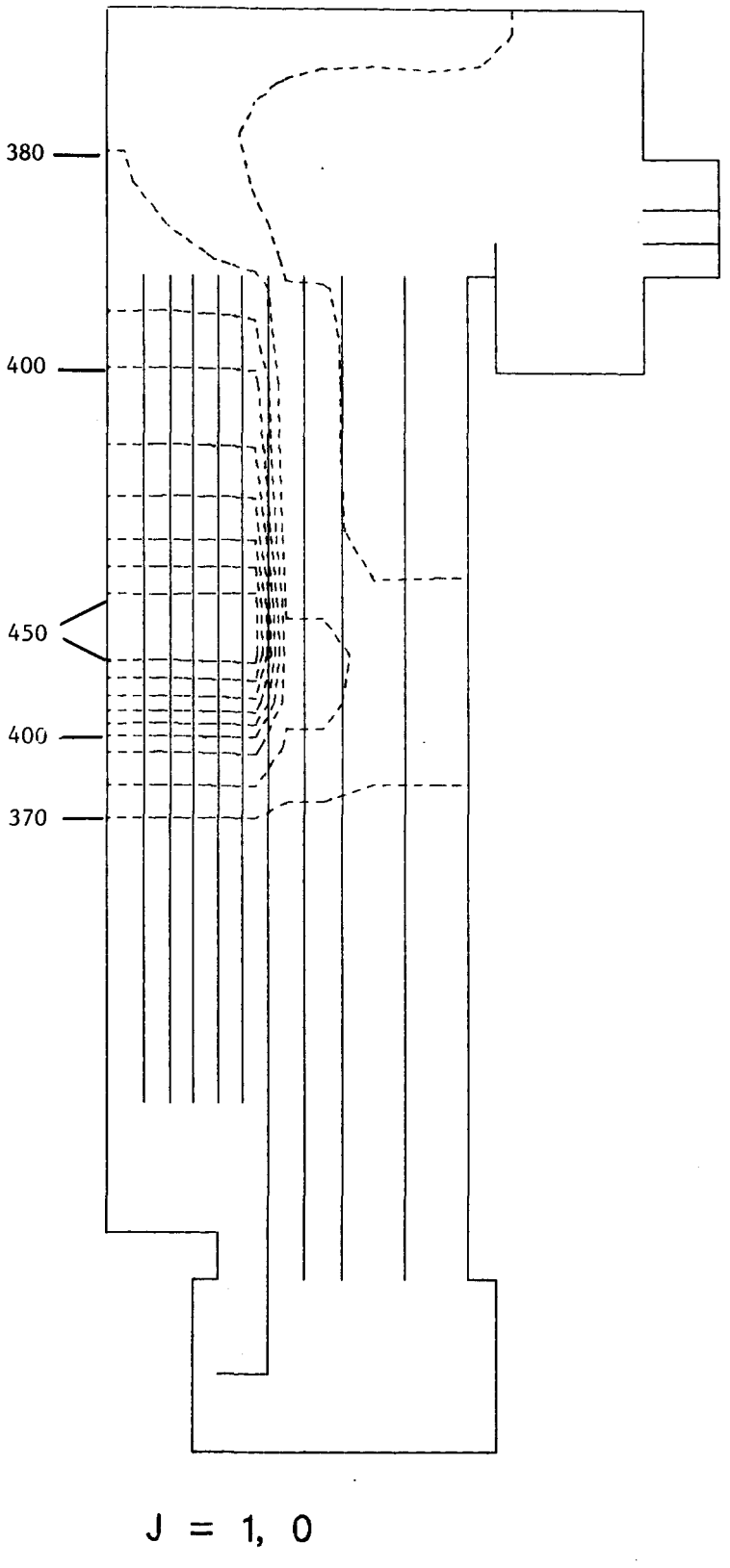

Fig. 50. Temperature Distribution at Time = 90 s

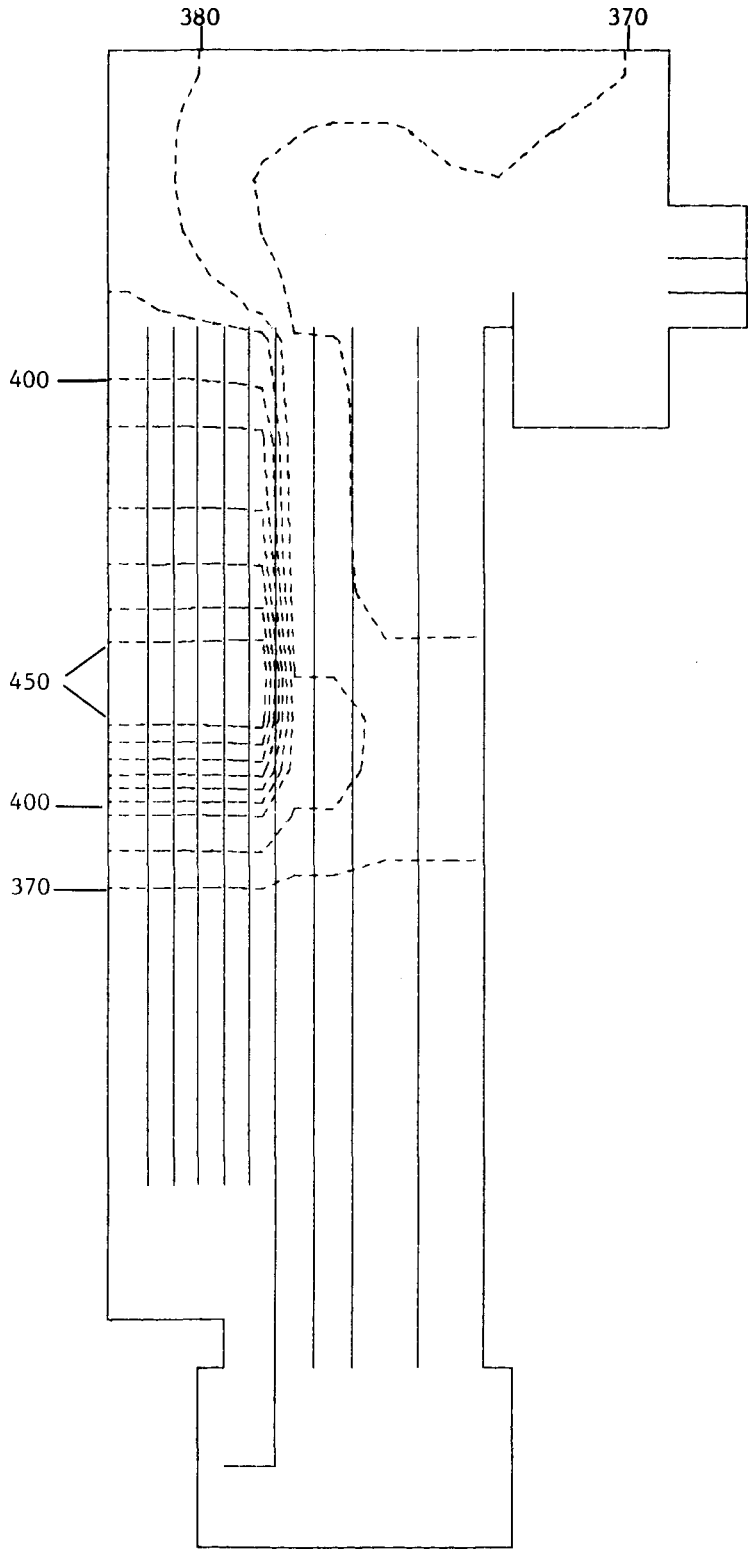

Fig. 51. Temperature Distribution at Time = 100 s

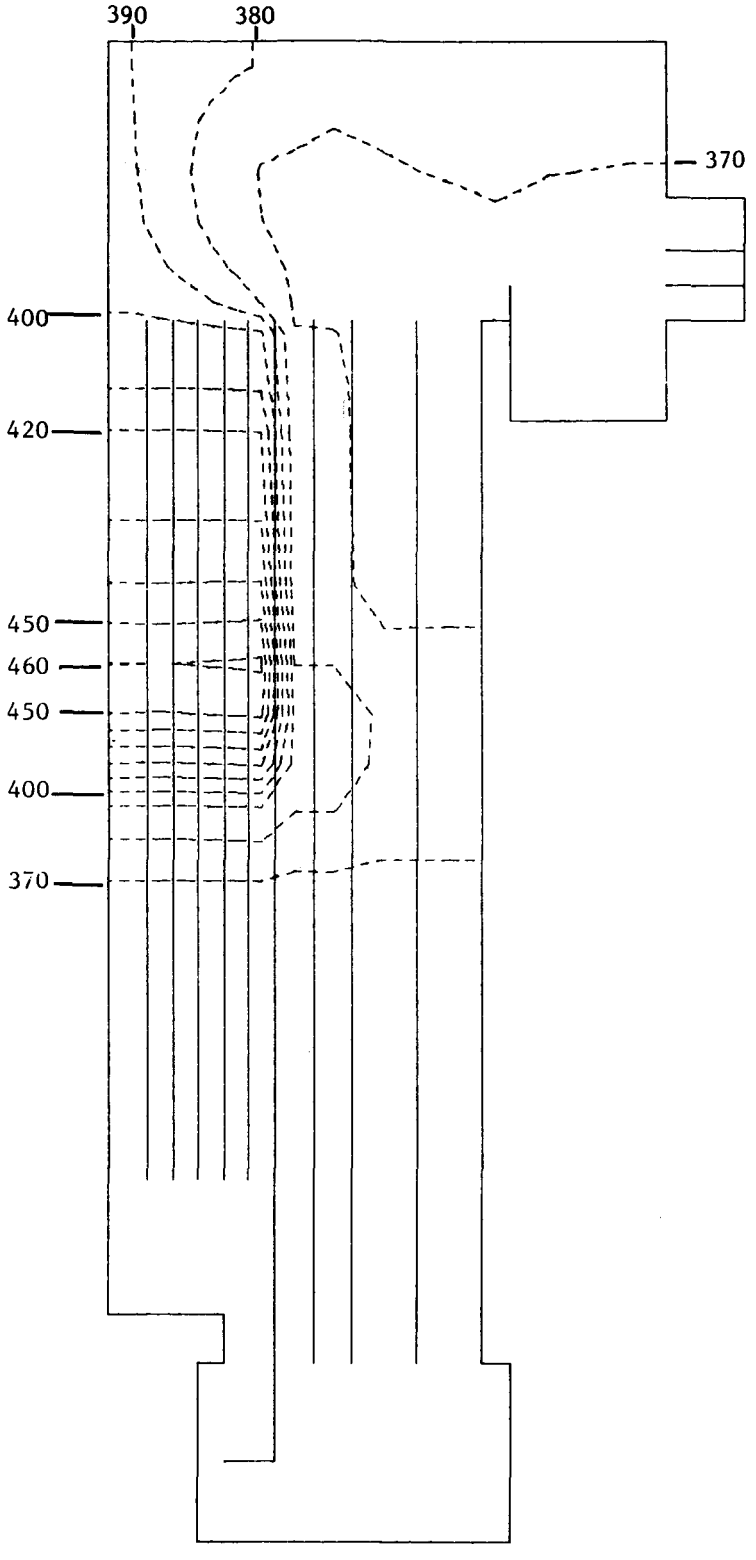

Fig. 52. Temperature Distribution at Time = 110 s

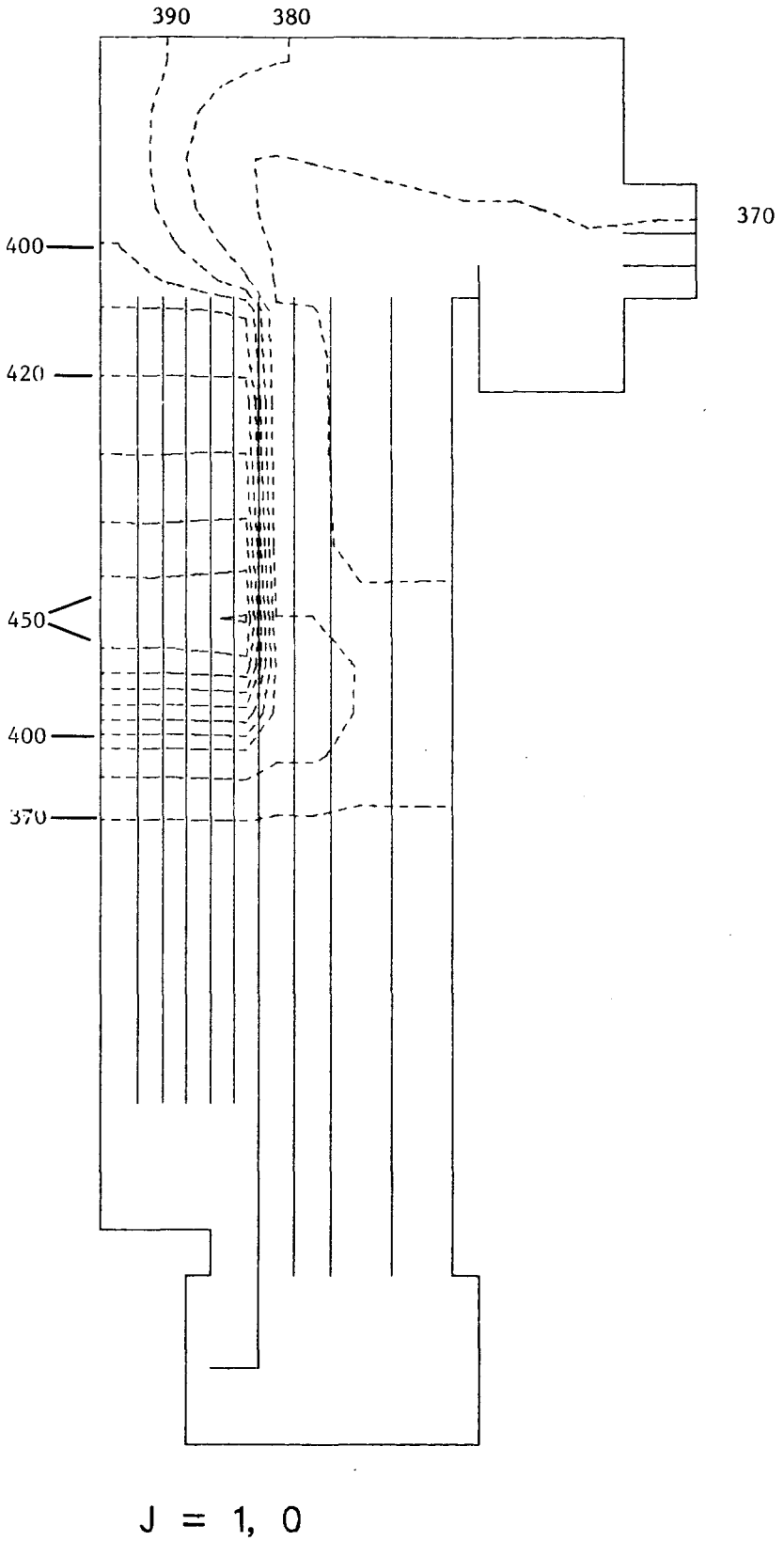

Fig. 53. Temperature Distribution at Time = 120 s

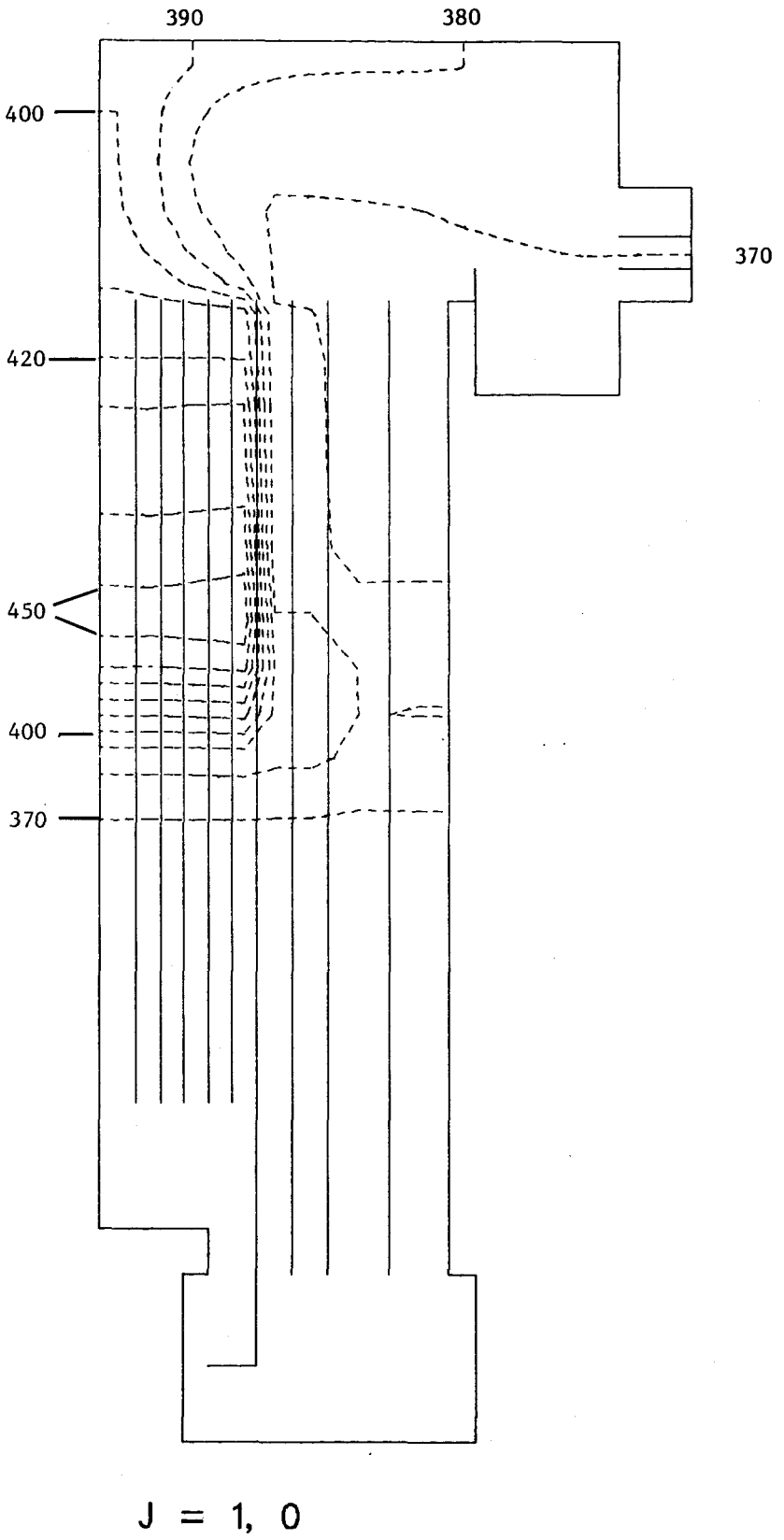

Fig. 54. Temperature Distribution at Time = 130 s

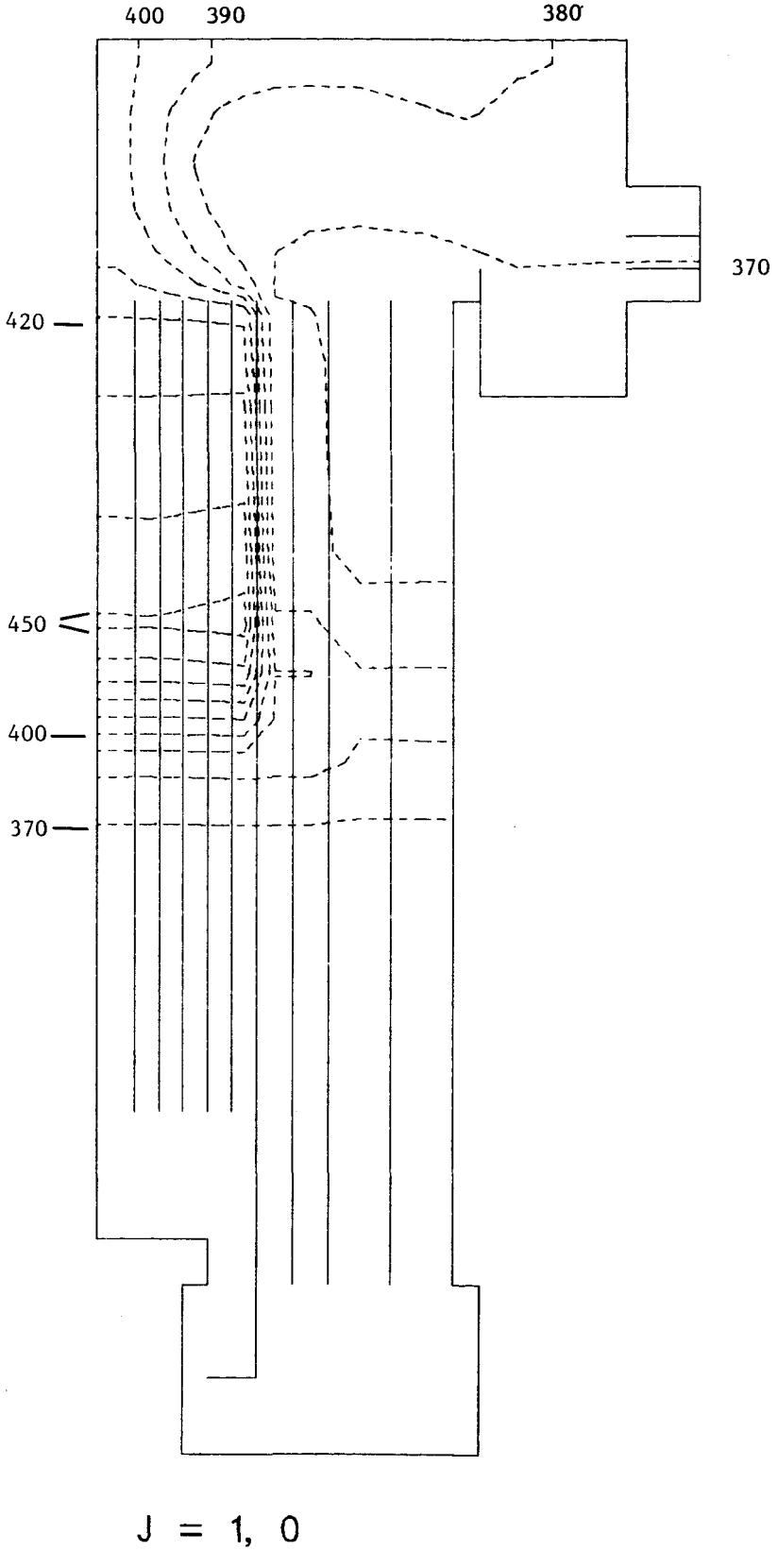

Fig. 55. Temperature Distribution at Time = 140 s

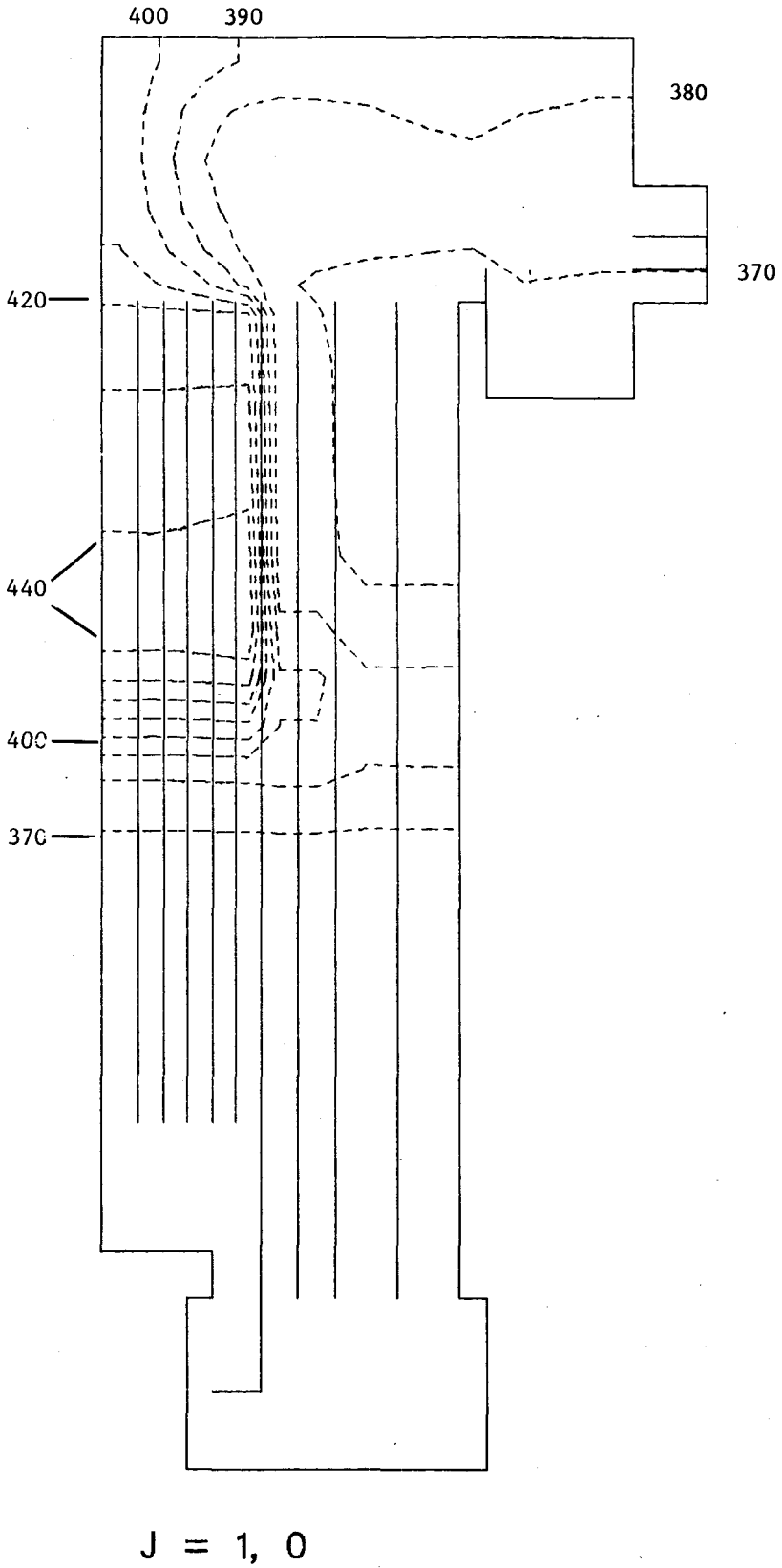

Fig. 56. Temperature Distribution at Time = 150 s

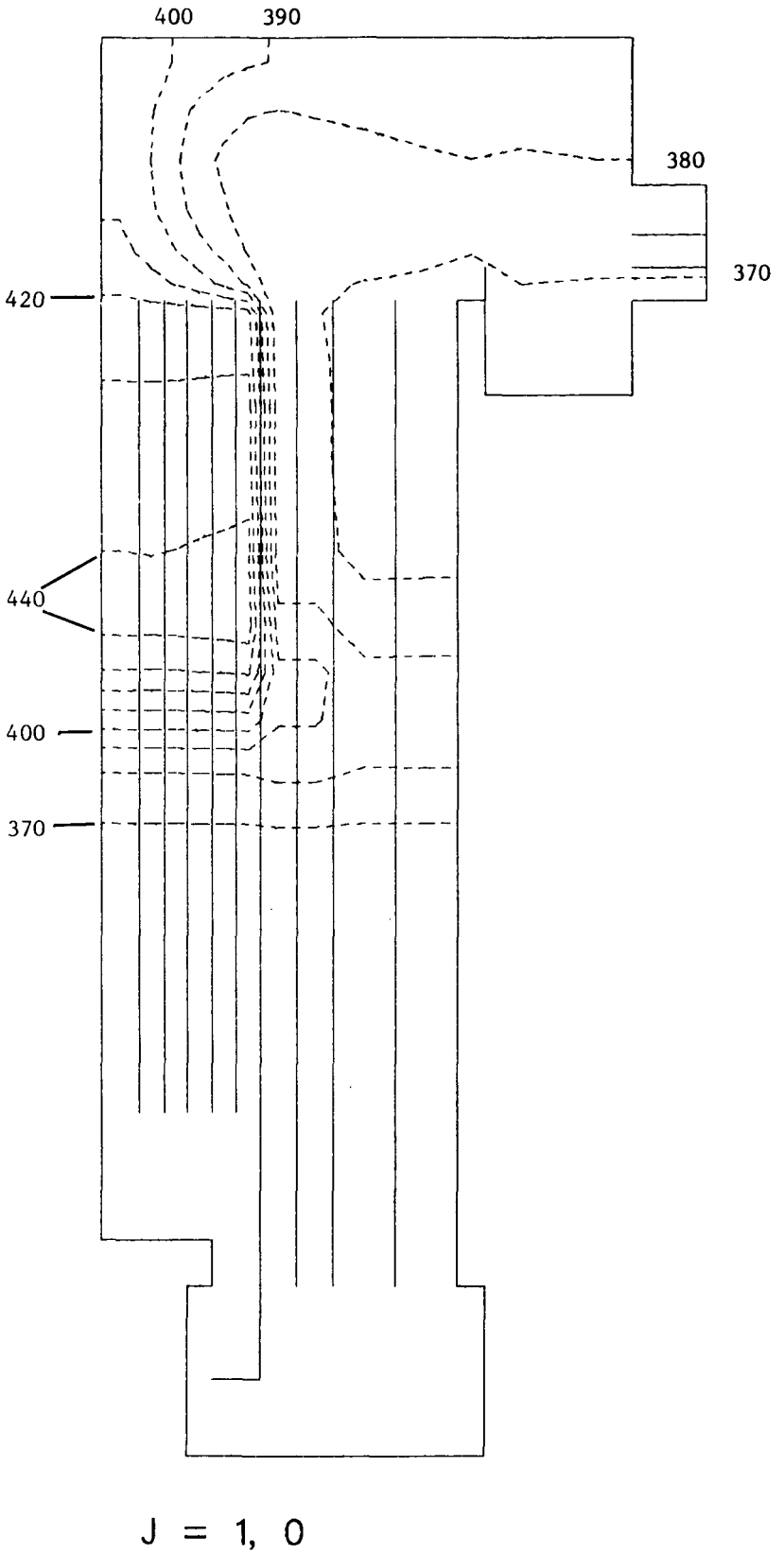

Fig. 57. Temperature Distribution at Time = 160 s

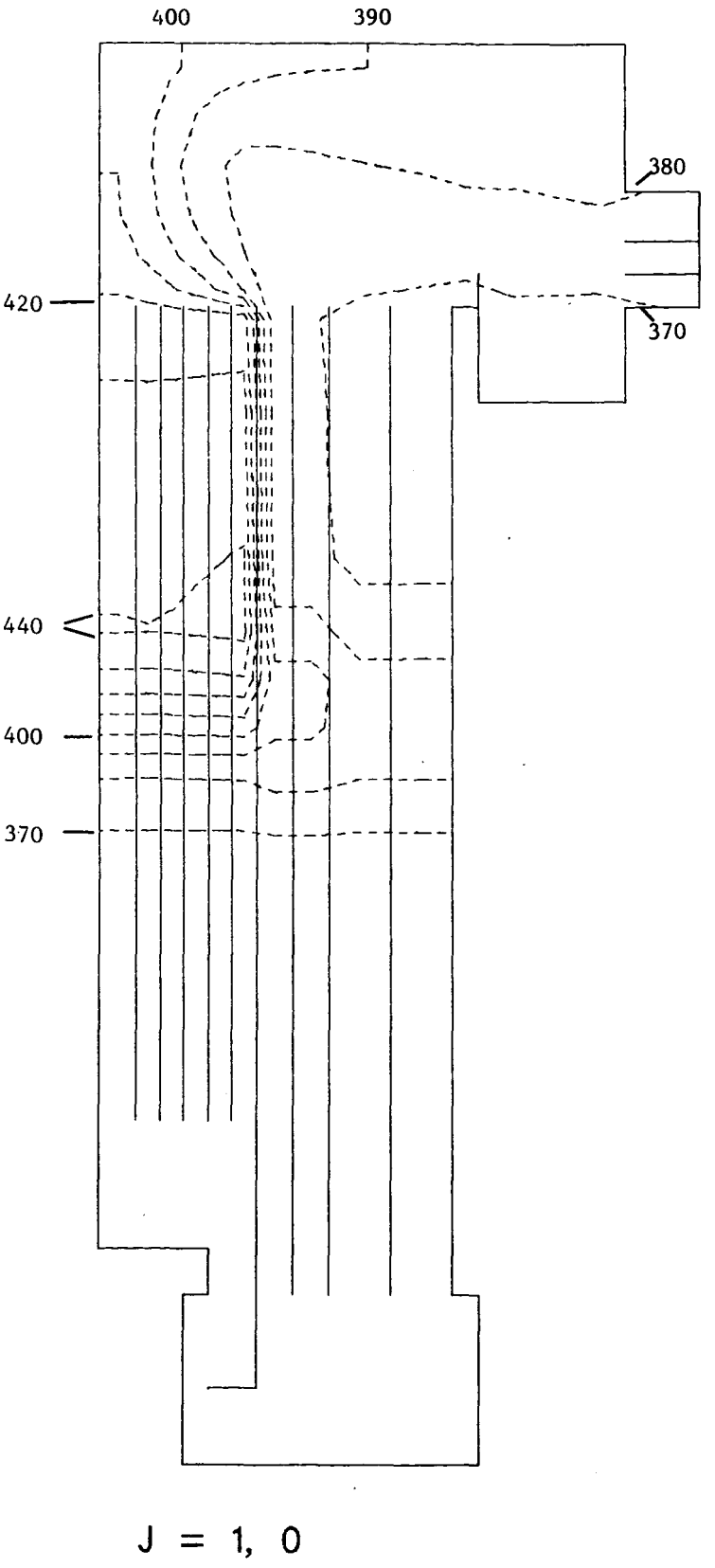

Fig. 58. Temperature Distribution at Time = 170 s

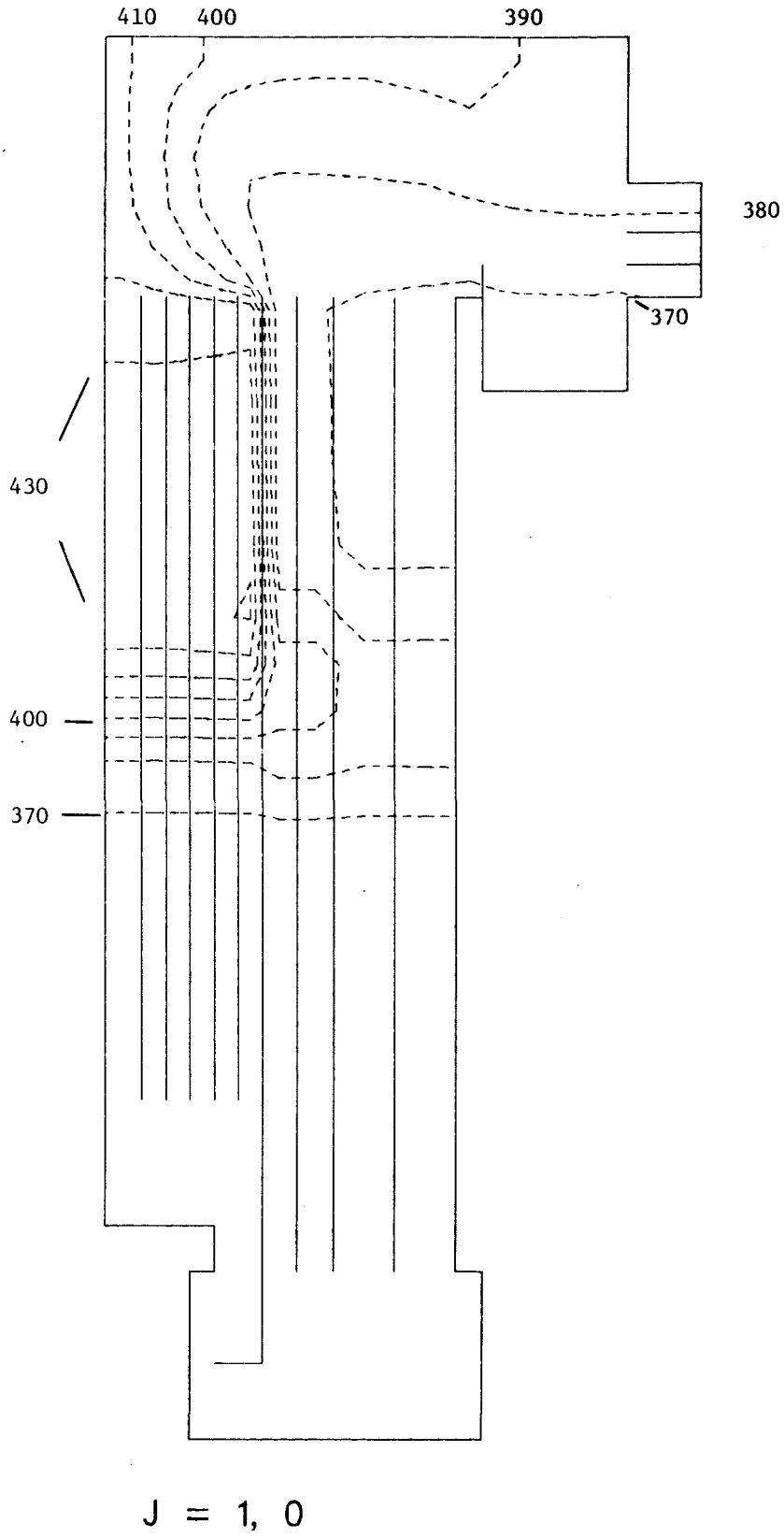

Fig. 59. Temperature Distribution at Time = 180 s

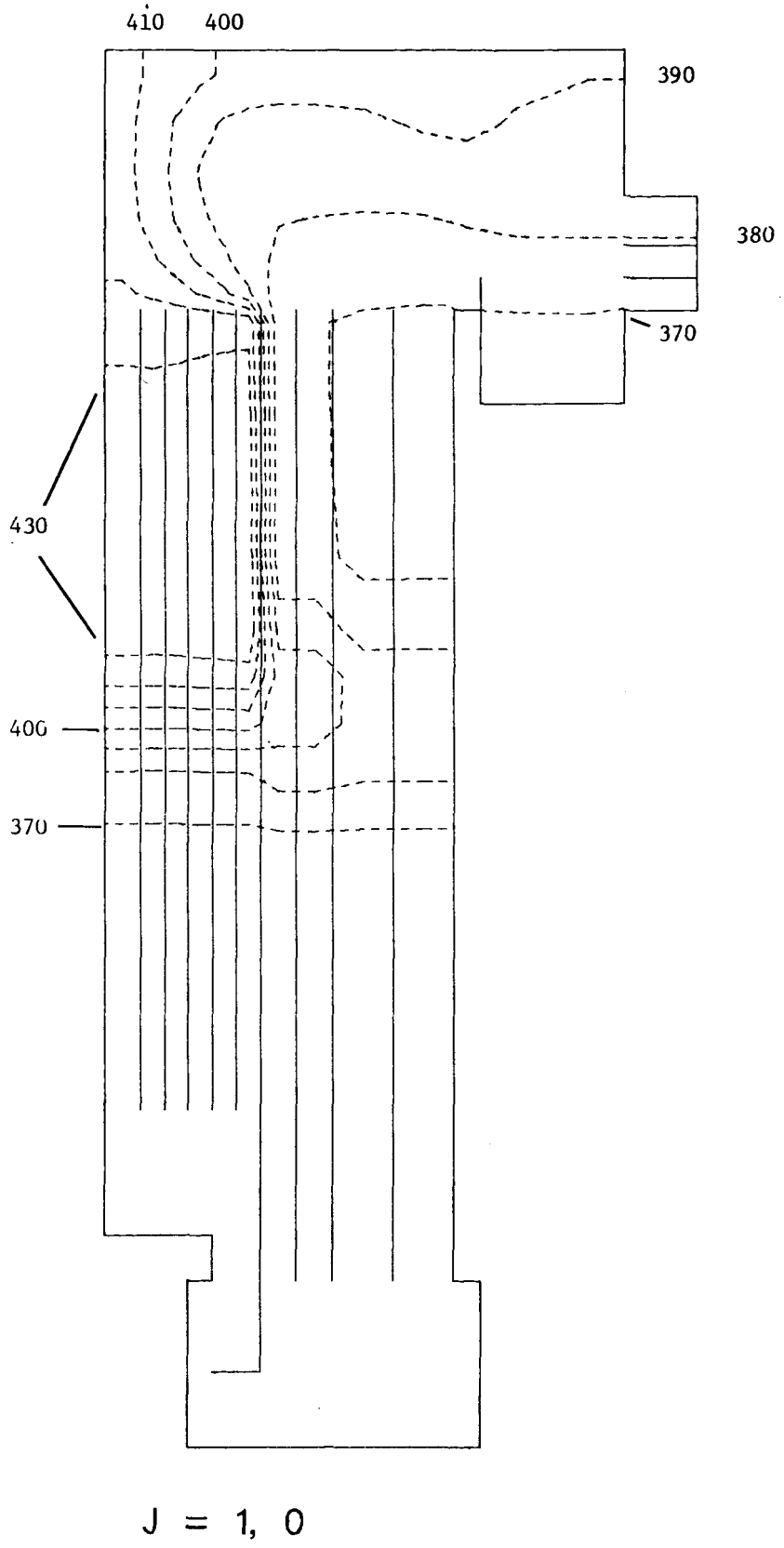

Fig. 60. Temperature Distribution at Time = 190 s

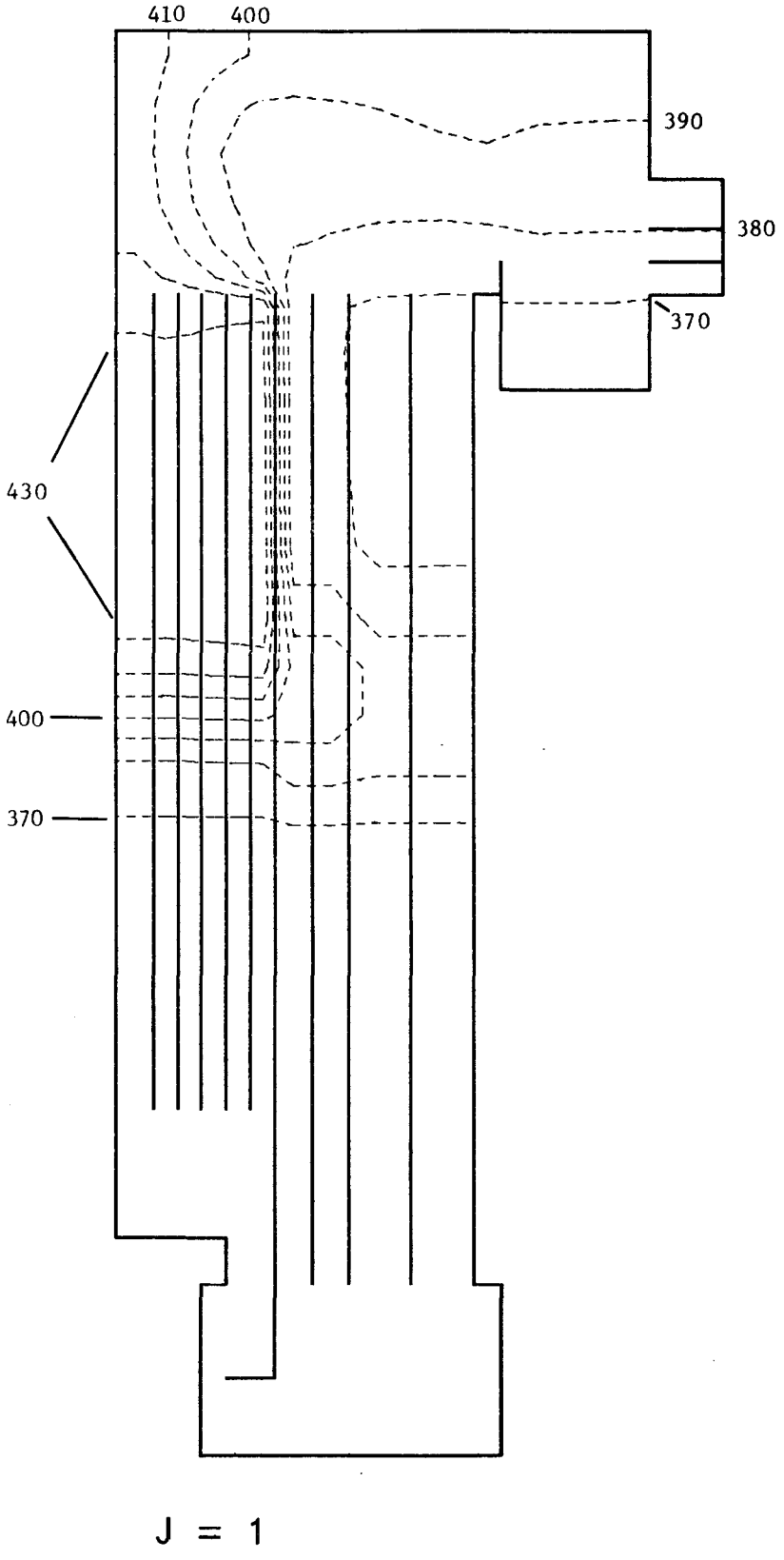

Fig. 61. Temperature Distribution at Time = 200 s

ACKNOWLEDGMENTS

We would like to thank Dr. R. M. Singer for his help by providing detailed information about the EBR-II design and evaluation of the EBR-II natural-circulation test data. We are indebted to Drs. R. T. Curtis, C. N. Kelber, and Mr. P. M. Wood of the United States Nuclear Regulatory Commission for their support, without which this work would not have been possible. The effort used by Mrs. S. A. Moll and Miss B. D. Wright in typing this report is also gratefully appreciated.

REFERENCES

1. EBR-II System Design Descriptions, Vol. II, Primary System, Chapter 2, Reactor (June 1971).

2. R. M. Singer, D. Mohr, and J. L. Gillette, "Transition from Forced to Natural Convection Flow in an LMFBR under Adverse Thermal Conditions," Proc. 7th International Heat Transfer Conference, München, BRD, Paper NR-24 (Sept. 6-10, 1982).

3. W. T. Sha, et al., "COMMIX-1: A Three-Dimensional Transient Single-Phase Component Computer Program for Thermal Hydraulic Analysis," NUREG/CR-0875, ANL-77-96 (Sept. 1978).

4. H. M. Domanus, W. T. Sha, and R. C. Schmitt, "COMMIX-1A: A Three-Dimensional Transient Single-Phase Computer Program for Thermal Hydraulic Analysis of Single and Multi-Component Systems," Draft Report, NUREG/CR-2896, ANL-82-25 (to be published).

5. A. Gopalakrishnan and J. L. Gillette, "EBRFLOW: A Computer Program for Predicting the Coolant Flow Distribution in EBR-II," Nucl. Technol. 17, 205 (1973).

6. K. Rehme, "Pressure Drop Correlations for Fuel Element Spacers," Nucl. Technol. 17, 15-23 (1973).

7. A. Y. Gunter and W. A. Shaw, "A General Correlation of Friction Factors for Various Types of Surfaces in Crossflow," ASME Trans. 67, 643-660 (1945).

8. Donald R. Olander, "Fundamental Aspects of Nuclear Reactor Fuel Elements," Energy Research and Development Administration, TID-26711-P1 (1976).

9. M. R. Granziera and M. S. Kazimi, "A Two-Dimensional, Two-Fluid Model for Sodium Boiling in LMFBR Fuel Assemblies," Energy Laboratory Report No. MIT-EL-80-011 (1980).

DO NOT MICROFILM

Distribution for NUREG/CR-2821 (ANL-82-66)

Internal:

E. S. Beckjord
C. E. Till
R. S. Zeno
P. R. Huebotter
G. S. Rosenberg
W. L. Baumann
B. C. Chen
F. F. Chen
T. H. Chien
H. M. Domanus
C. C. Miao
R. C. Schmitt
W. T. Sha (2)
V. L. Shah
J. E Sullivan
M. Weber
C. I. Yang
P. B. Abramson
F. E. Dunn
D. R. Ferguson
H. H. Hummel
D. Mohr
R. M. Singer
ANL Contract File
ANL Libraries (2)
TIS Files (6)
ANL Patent Dept.

External:

USNRC, for distribution per R7 (275)
USDOE-TIC (2)
Manager, Chicago Operations Office, DOE
Components Technology Division Review Committee:
A. A. Bishop, U. of Pittsburgh, Pittsburgh, Pa. 15261
F. W. Buckman, Consumers Power Co., 1945 Parnall Rd., Jackson, Mich. 49201
R. Cohen, Purdue U., West Lafayette Indiana 47907
R. A. Greenkorn, Purdue U., West Lafayette, Indiana 47907
W. M. Jacobi, Westinghouse Electric Corp., Pittsburgh, Pa. 15230
E. E. Ungar, Bolt, Beranek and Newman, Inc., Cambridge, Mass. 02138
J. Weisman, U. of Cincinnati, Cincinnati, Ohio 45221
K. Absher, Richland Operations Office, USDOE, Richland, Wash. 99352
S. S. Chang, Hanford Engineering Development Lab., P. O. Box 1970, Richland, Wash. 99352
M. H. Cooper, Westinghouse Advanced Reactors Div., P. O. Box 158, Madison, Pa. 15663
A. E. Dubberley, General Electric Co., c/o Argonne National Lab.
G. Drucker, Atomics International, 8900 DeSoto Ave., Canoga Park, CA 91303
F. X. Gavigan, Office of Reactor Research and Technology, USDOE, Washington
H. Alter, Office of Reactor Research and Technology, USDOE, Washington
C. E. Ockert, Office of Reactor Research and Technology, USDOE, Washington
E. L. Gluekler, General Electric Co., 310 DeGuigne Dr., Sunnyvale, CA 94086
J. Mangus, Westinghouse Advanced Reactors Div., P. O. Box 158, Madison, Pa. 15663
J. C. Mills, Atomics International, 8900 DeSoto Ave., Canoga Park, CA 91303
E. Moody, Atomics International, 8900 DeSoto Ave., Canoga Park, CA 91303
E. H. Novendstern, Westinghouse Advanced Reactors Div., P. O. Box 158, Madison, Pa. 15663
S. C. Rose, General Electric Co., 310 DeGuigne Dr., Sunnyvale, CA 94086
R. L. Stover, Hanford Engineering Development Lab., P. O. Box 1970, Richland, Wash. 99352
J. L. Wantland, Oak Ridge National Lab., P. O. Box Y, Oak Ridge, Tenn. 37830